PH. D. DISSERTATION

Investigations of Low Dielectric Constant SiOC(-H) Thin Films for Inter-layer Dielectrics in Cu/Low-*k* Microelectronic Device Applications

Department of Physics
Graduate School
Cheju National University

Chang Sil Yang

December, 2005

Cu/Low-*k* 전자소자 적용 층간 절연 SiOC(-H) 박막에 관한 연구

지도교수 : 최 치 규

양 창 실

이 논문을 이학 박사학위 논문으로 제출함.

2005년 12월

양창실의 이학 박사학위 논문을 인준함.

심사위원장 _____

위 원 _____

위 원 _____

위 원 _____

위 원 _____

제주대학교 대학원

2005년 12월

Investigations of Low Dielectric Constant SiOC(-H) Thin Films for Inter-layer Dielectrics in Cu/Low-*k* Microelectronic Device Applications

Chang Sil Yang
(Supervised by professor Chi Kyu Choi)

A thesis submitted in partial fulfillment of the requirement for the degree of Doctor of Science.

2005. 12.

This thesis has been examined and approved.

_____

_____

_____

_____

_____

_____

Department of Physics
GRADUATE SCHOOL
CHEJU NATIONAL UNIVERSITY

Contents

List of Figures

Abstract

The quest to improve the high performance in ultra large scale integrated (ULSI) circuits is driving the search for new materials with low dielectric constant for interconnection structures. This dissertation discuss about SiOC(-H) films with low dielectric constant are deposited on *p*-type Si(100) substrate by PECVD and UV-assisted PECVD using BTMSM, MTMS, and TMS as precursors. The fundamental properties of SiOC(-H) film such as bonding structure, hardness, elastic modulus, plasma parameters, leakage current density, and dielectric constant were investigated.

The bonding structure of SiOC(-H) film composite of Si-O-Si(C), Si-CH_n, CH_n and OH related bonds and the main peak of FTIR is clearly separated Si-O-Si and Si-O-C bonds and the Si-O-C bonds consist of three kind of links such as ring, open and cage link in the annealed SiOC(-H) film. The highest and lowest dielectric constant of SiOC(-H) film were measured as 3.0 and 2.1 at BTMSM flow rate 85 % for the annealing temperature of 400 ^{o}C. In this case, the concentration of cage link were calculated to be 18.3 and 33.2 % and the electronic polarizability decreased from 4.78 to 4.41 Farad·m^2, From these results, we know that this variation due to the incorporation of CH_3 groups breaks the continuity of Si-O-Si networks and form the nano-pores by the aloof force between CH_3 group and other part of Si-O-Si structure. The elastic modulus of SiOC(-H) films varied from 7.42 to 3.98 GPa for the annealed SiOC(-H) films as a function of BTMSM flow rate

ratios. Therefore, the electronic polarizability of the SiOC(-H) composite film can be decrease due to the incorporation of the CH_x species. The mechanical behavior is depending on the porosity existing in SiOC(-H) film.

The plasma properties have been carefully observed during the deposition of SiOC(-H) film by UV-assisted PECVD. It was that the electron temperature of the plasma with the BTMSM+O_2 mixture decreased from 1.7 to 1.2 eV and electron density increased from 2.8×10^{9} cm^{-3} to 9.9×10^{9} cm^{-3} as a rf power increased without UV irradiation. The deposition rate of the SiOC(-H) film with UV irradiation is higher than without UV irradiated SiOC(-H) film. The deposition rate was measured to be 112 nm/min without UV irradiation whereas it was measured to be 135 nm/min with UV irradiation for MTMS precursor. From these results, we know that the increasing of ionization with excited precursors by UV irradiation because that the electrons in the plasma gain energy from UV light and the excited electrons collide with radicals and energy transfer takes place.

The relative area of the Si-O-C cage-link bond in the SiOC(-H) films with UV irradiation was higher than that in the films without UV irradiation. The relative area of the Si-O-C open-link bonds of the film with UV irradiation decreased from 8 to 4 % in the films without UV irradiation. When the flow rate ratio of MTMS was 100%, Dielectric constant of the UV-irradiated samples was lower than that of films without UV irradiation. The dielectric constant of the SiOC(-H) films decreased consistently from 2.4±0.11 (without UV irradiation) to the lowest value of 2.3±0.11 (with UV

irradiation). From these results, we can infer that the increase in peak intensity for the Si-C cage link and Si-O-C ring link with UV irradiation is due to the abundance of radicals such as Si*, CH_n* etc, within UV-plasma.

The integration problems of SiOC(-H) film such as electrical unstability by the damage from oxygen plasma ashing and its solution were also investigated. The leakage current density of SiOC(-H) film was measured to be 7.3×10^{-5} A/cm^2, it is increased from 7.3×10^{-5} A/cm^2 to 1.8×10^{-3} A/cm^2 as a function of oxygen plasma ashing time. In the case of CH_4 plasma treated SiOC(-H) film, the variation of the leakage current density at 1 MV/cm^2 increased from 2.6×10^{-9} A/cm^2 to 2.02×10^{-8} A/cm^2 during as a function of oxygen plasma ashing time. The dielectric constant of samples without CH_4 plasma treatment increased from 2.9 to 3.6 as oxygen plasma ashing time, and the dielectric constant of samples with CH_4 plasma treatment slightly increased from 2.9 to 3.3 as oxygen plasma ashing time. From these results, the carbon radical contributed to be reacted with the dangling bonds on the surface of SiOC(-H) film. The hydrogen radical broken bonds and the recombination of C and H atoms on the SiOC(-H) film is attributed to a structural change due to the formation of Si-H and Si-C bonds by the CH_4 plasma treatment on SiOC(-H) film. Therefore, the low-*k* dielectric property of SiOC(-H) film is significantly enhanced by CH_4 plasma treatment. In this study, we can infer that the SiOC(-H) film deposited by UV-assisted PECVD is a good candidate for low dielectric materials for the inter-metal dielectric layer of the ULSI.

Chapter I. Introduction

1. Current development of low dielectric materials

As on-chip device densities increase and active device dimensions are reduced, the signal delay and noise also increase due to capacitive coupling and cross-talk between the metal interconnections [1-3, 14]. Since the delay, noise and power consumption all depend critically on the dielectric constant (k) of the separating insulator, much attention has recently been focused on replacing the standard silicon dioxide with new inter-metal dielectric materials that have considerably lower dielectric constant than thermal silicon dioxide films (k=3.9~4.2) [1-3]. The fabrication technology of low-k materials for Cu/Low-k chips is very essential for the next-generation DRAM in which the low-k films with nano-pore structure is used for the inter-layer (ILD) or the inter-metal dielectrics (IMD). The technology includes the high density plasma chemical vapor deposition (HDPCVD) method, the HDPCVD method of a inter-metal barrier for integrating process, a various electrical, chemical and physical analysis methods for characterizing the fabricated dielectrics. Because low-k films with nano-pore structure for the next-generation DRAM memory device of about 60 nm or less must be fabricated by a series HDPCVD technologies. The first point of low-k technology is the realization of low-k materials and process approximating $\varepsilon_r < 2.3$ on the basis of now immature

SiOC(-H) film with nano-pore structure for the low-*k* CVD technologies [15-24].

Excluding the incumbent silicon dioxide and FSG(Fluorine doped silica glass) and HSQ(hydrogen-silsesquioxane), there are three main contenders in the sub-3.0 low-*k* range: SiLK^{TM} of Dow Chemical Co., Flare^{TM} of AlliedSignal Co., and Black Diamond^{TM} of Applied Material Inc. Almost all semiconductor companies interviewed were working on some combination of these materials. It is designed for copper damascene processing and is not for conventional aluminum gap fill technology. The *k* value of Black Diamond^{TM} is 2.7; according to Applied Materials Inc., this may be extended to the 2.4 to 2.2 range in the future by modifying the material's nanoporous structure. The company is using the material to address the extendibility and processing integration issues faced by the semiconductor industry. Flare^{TM} of AlliedSignal Co. is a non-fluorinated, organic, spin-on dielectric material with a dielectric constant of 2.8. Flare^{TM} is one of three products provided by AlliedSignal Co. and is aimed at 0.18 μm or finer generations. It is applied by a spin coater and reportedly has good thermal stability, up to 450 °C, and superior crack resistance. In addition to Flare^{TM}, AlliedSignal Co. has two other materials that have a $k < SiO_2$. One is Nanoglass^{TM} with a *k* of 1.3 to 2.5, and the other is Accuspin T-23 LOSP^{TM} with a *k* of 2.8 to 3.0. These three materials are targeted at high-performance IC devices with different dielectric constants. AlliedSignal Co. has recently established a low-*k* integration facility in California to assist in low-*k* material implementation and processing

integration. SiLK^{TM} of Dow Co. is a non-fluorinated, highly aromatic, organic spin-on polymer with a reported isotropic *k* of 2.65 and very high temperature

YEAR / TECHNOLOGY NODE	1999 180 nm	2000	2001	2002 150 nm	2003	2004	2005 100 nm
MPU ½ pitch	230	210	180	160	145	130	115
MPU gate length (nm)	140	120	100	90	80	70	65
Minimum global wiring pitch (nm)	1050	945	850	765	680	620	560
Global wiring A/R (Al)	2	2.1	2.2	2.3	2.4	**	**
Global wiring dual damascene A/R (Cu wire/via)	2.2/2.4	2.3/2.6	2.4/2.7	2.5/2.7	2.6/2.8	2.7/2.8	2.7/2.8
Cu thinning global wiring due to dishing and erosion (nm), 10% × height, 80% areal density, 15 micron wide wire	116	109	102	95	90	84	76
Cu global wiring dishing (nm), 15 micron wide wire, 10% × height	116	109	102	95	90	84	76
Cu thinning global wiring due to dishing (nm), 100 micron wide feature	80	72	65	59	53	48	43
Conductor effective resistivity (μΩ cm) Al wiring	3.3	3.3	3.3	3.3	3.3	**	**
Conductor effective resistivity (μΩ cm) Cu wiring*	2.2	2.2	2.2	2.2	2.2	2.2	2.2
Barrier/cladding thickness (for Cu wiring) (nm)***	17	16	14	13	12	11	10
Interlevel metal insulator — effective dielectric constant (κ)	3.5–4.0	3.5–4.0	2.7–3.5	2.7–3.5	2.2–2.7	2.2–2.7	1.8–2.2
Interlevel metal insulator — effective dielectric constant (κ)	3.5 4.0	3.5 4.0	2.9 3.5	2.9 3.5	2.2 2.9	2.2 2.9	1.8 2.2
Interlevel metal insulator (minimum expected) — bulk dielectric constant (κ)	2.9	2.9	2.7	2.7	2.0	2.0	1.3

* Assumes a conformal barrier/nucleation layer
** This technology is not expected to extend to this node
*** Calculated for a conformal layer in local wiring to meet minimum effective conductor resistivity

Solutions Exist Solutions Being Pursued No Known Solutions

Fig. 1. International Roadmap for semiconductor.

stability in excess of 450° C. SiLK^{TM} is offered in addition to CYCLOTENE^{TM} benzocyclobutene (BCB) of Dow Co. which is the current material in production for GaAs ILD applications. SiLK^{TM} formulations fit both

copper/damascene and Al/W applications. Dow Corp. has recently built and starteda new world-scale manufacturing facility dedicated to producing SiLK™ with the capacity to supply more than a dozen IC fab's in full production. Extendibility is claimed through the introduction of engineered porosity. Dow Co. is the lead partner with IBM Corp. in a NIST-sponsored advanced technology program designed to develop and commercialize an optimized porous ILD system with k < 2.0. The development of spin-on, organic, low-k materials formulated for both aluminum gap fill and copper damascene processing has been ongoing for several years. For example, Sematech Inc., and IMEC have recently demonstrated integration with SiLK™ in copper damascene and aluminum/tungsten subtractive schemes in two-level structures.

2. Fundamental interconnect issues

2.1. RC delay time

For a MOS (metal-oxide-semiconductor) circuit, the RC delay is defined in terms of the circuit response which is given by

$$V_{out} = V_{in}[1 - \exp(\frac{-t}{RC})], \quad (1)$$

where V_{out} and V_{in} are the output and input voltage of the circuit and t is

the time R and C are lumped total of all the resistance and capacitance of the circuit respectively [1-14]. Thus R and C are, respectively, considered as the effective total resistance of the interconnection and capacitance associated with the dielectric. One can approximate the RC delay, also sometime called as RC time constant, by multiplying R with a simple plate capacitance leading to an expression

$$RC = \frac{\rho}{t_M} \frac{L^2 \epsilon_{ILD}}{t_{ILD}}, \tag{2}$$

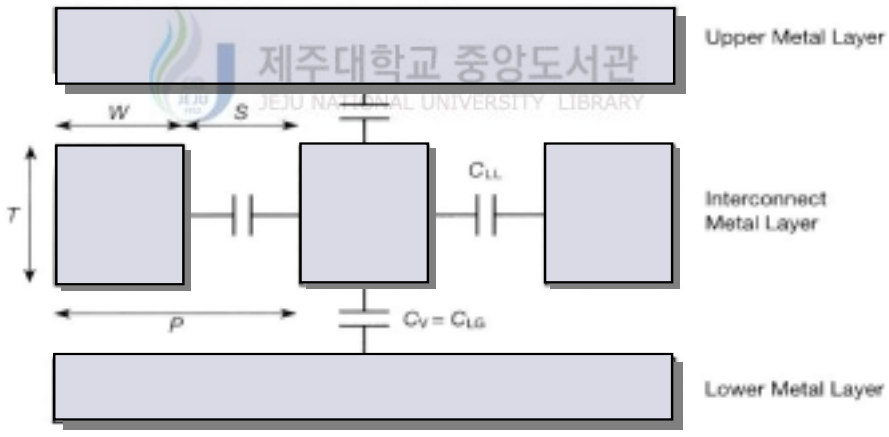

Schematic diagram of an interconnect system, where P is the metal pitch, W the metal width, S the space between metals, T the metal thickness, C_{LL} the lateral line-to-line capacitance, C_V the vertical layer-to-layer capacitance, and C_{LG} the line-to-ground capacitance.

Fig. 2. Schematic diagram of an interconnect system and capacitance of the lateral line to line and the vertical layer to layer as function of feature size.

where ρ, t_M, L, ϵ_{ILD} and t_{ILD}, respectively, are the resistivity, thickness, and length of the interconnection and interlayer dielectric (ILD) permittivity and thickness. To address the RC delay problem, the semiconductor industry recognized the need to implement low-*k* dielectric materials and high conductive metals to meet the requirement for future devices [1-5]. Therefore, the RC delay can be successfully controlled by two material parameters; one is resistivity(ρ) of the interconnect metal and the other is the dielectric constant(ϵ_r) of the interlayer dielectric material.

2.2. Power dissipation

The power dissipation in the integrated circuit was calculated as given by

$$P = \alpha C V^2 f, \tag{3}$$

where, C is total capacitance, V is the supply voltage, f is the operational frequency, and α is the wire activity. Although accurate estimate of power must include all types of circuits on a chip, the higher f, the higher is the power dissipation [2-6]. Figure 3 clearly show that the lower dielectric ϵ and lower resistivity interconnects not only decrease the CPU cycle time, they can also lower the number of wiring levels, in the metal-level interconnect scheme, to maintain a given performance. Thus to reduce power dissipation,

while maintaining high f, C and V must be reduced for the high performance circuit. The using low dielectric constant as a interlayer dielectric, higher performance can be achieved [15-18].

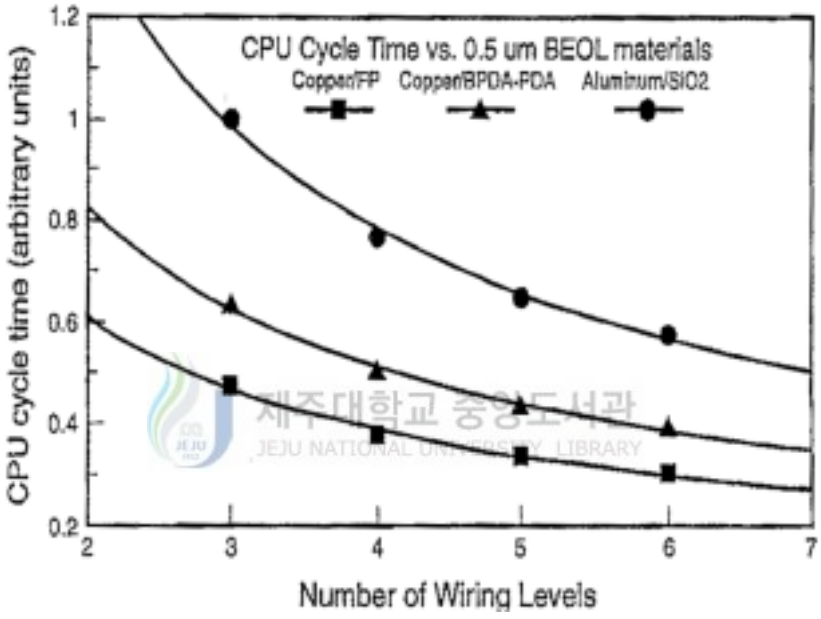

Fig. 3. Calculated cycle time with function of dielectric materials and wiring levels.

2.3. Cross-talk noise

When integrated circuits work more than 100 MHz, the electrical signals through the interconnect lines, the electromagnetic coupling can force significant undesired voltages on the neighboring unpowered lines. During the rise and fall

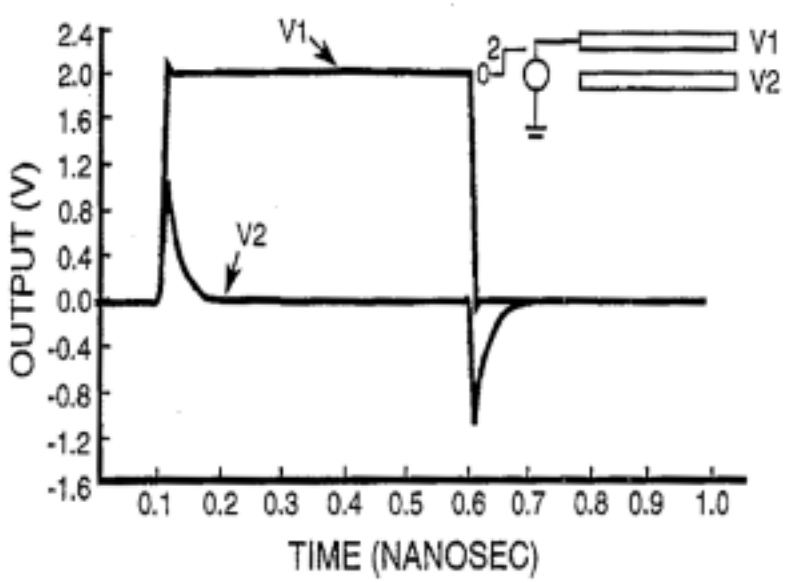

Fig. 4. Cross-talk noise.

of the waveform on the drive line, a substantial unwanted voltage (~50 % of V_1) will be generated on the undriven line [1-8] (Fig. 4).

3. Research Goals

Silicon oxide-based low-*k* materials, like SiOC containing alkyl groups, have attracted attention as they have greater thermal and mechanical stability than many organic materials. Nevertheless, the detailed chemical structure of SiOC(-H) films, including the nano-pore structures, which depend on the PECVD deposition conditions and post-annealing effects, is still unclear.

Moreover, the chemical structure is directly related to the dielectric property of the resulting films. In this study, the chemical structural evolution during hybrid type SiOC(-H) film deposition and post-annealing procedures was investigated, electrical properties such as the dielectric constant was also discussed for the influence according to the chemical structure change from ring to open links. The reason why SiOC(-H) film has a low dielectric constant is a decrease in SiOC(-H) film density, which results from the replacement of Si-O bonds with Si-CH_3 (alkyl group) bonds. However, studies on the influence of carbon contents in the SiOC(-H) film as yet insufficient.

In this study, we first investigated Si-O-Si and Si-O-C bonding structure that can be changed by relative carbon contents in the film. Dependence of dielectric constant on the relative carbon contents in SiOC(-H)film was analyzed ; porosity for the obtained dielectric constants in the films was also calculated. The induced dipole moment and the dielectric constant was investigated, the contribution of electronic, ionic, and oriental components and their relation to the bonding angle and the carbon contents in SiOC(-H) film. The quality of SiOC(-H) film is degraded by the damage from oxygen plasma and hygroscopic behavior during photo-resist stripping. In this thesis, the effect of CH_4 plasma post-treatment on the stability of the SiOC(-H) films was investigated with low dielectric constant for the ashing process.

Recently, the concept of a plasma-processing apparatus with a high-density plasma and low electron temperature at low pressure has received much attention for processing large-diameter wafers with 60 nm patterning. Since a

UV-source can be controlled optimally, radical and ion production is improved by adjusting the energy of the UV irradiation. In this study, we investigated the influence of UV irradiation the plasma parameters and the bonding structure of SiOC(-H) films deposited using UV-assisted PECVD. In addition, the effect of adding He gas to the BTMSM/O_2 mixture on the plasma-phase composition and the properties of the SiOC(-H) film were studied.

This thesis is organized as follows. In chapter III, the bonding structure of SiOC(-H) films were investigated using by FTIR and XPS with flow rate ratio of BTMSM and MTMS. In addition, chapter III refer to electrical properties, mechanical properties, and influence carbon contents by thermal treatment. Chapter IV show that the effect of plasma treatment such as the leakage current density and the dielectric constant of CH_4 plasma treated SiOC(-H) film are more stable than the non-treated SiOC(-H) film after O_2 plasma ashing process. In chapter V, the bonding structure of SiOC(-H) films were investigated using by FTIR and XPS with flow rate ratio of BTMSM, MTMS, and TMS using UV-assisted PECVD. The characteristics of UV-assisted plasma was referred to chapter V. In chapter VI show that the some results and discussion from results of chapter III, IV, and V. Conclusions will be presented in the last chapter.

Chapter II. Experiments and Analyses

1. System and Deposition Condition

SiOC(-H) composite films were deposited on *p*-type Si(100) using bis-trimethylsilylmethane (BTMSM: H_9C_3-Si-CH_2-Si-C_3H_9), tri-methylsilane ($Si(CH_3)_3$, TMS), methyltrimethoxysilane (MTMS : $CH_3Si(OCH_3)_3$), and oxygen mixture gases in a chamber. Figure 5 shows the photograph of the UV-assisted PECVD system used in this study. The plasma was discharge between the upper electrode connected to the 13.56 MHz power supply and the grounded lower electrode. A base pressure of 10^{-3} Torr was maintained for each deposition.

Figure 6 shows the precursors of BTMSM, TMS, and MTMS. The BTMSM and MTMS precursors are a nontoxic, colorless liquid with boiling points of 137 ℃, 101 ℃ at standard atmospheric pressure and the molecular weight of TMS is 74.2 and boiling point is 6.7 °C at standard atmospheric pressure. It was vaporized and carried by inert argon gas from a thermostatic bubbler (maintained at 40 ℃) to the reaction chamber. To prevent re-condensation of precursors, all of the gas delivery lines were heated and kept at a constant temperature of 40 ℃. The wafers were kept in a floating potential and were not intentionally heated. The wafers were cleaned by a standard cleaning procedure before loading them into the reaction chamber.

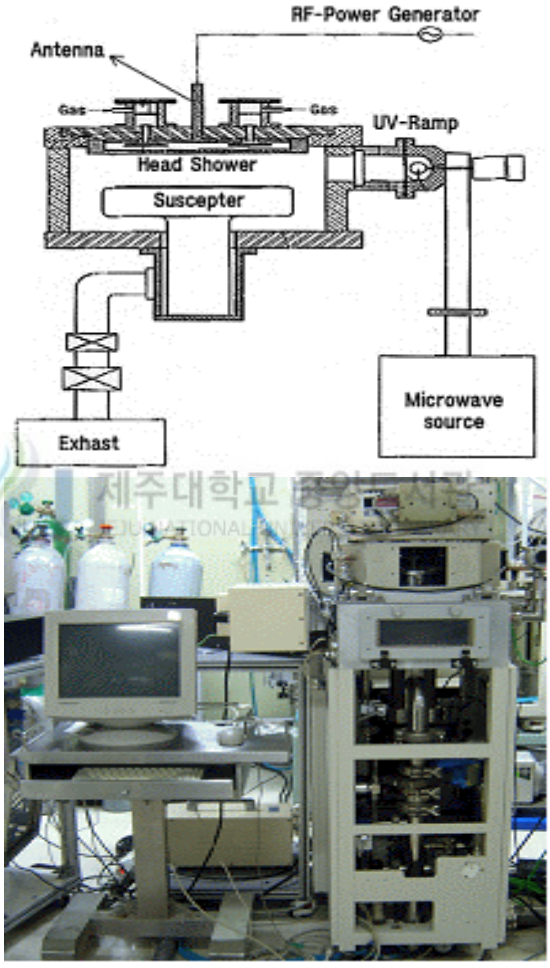

Fig. 5. The UV-assisted PECVD system.

The flow rate ratios as R(%)= [Precursor/(Precursor+O_2)]×100 was varied from 100 to 50% and the total gas of flow rates are kept at a constant of 100 sccm. The films were deposited at room temperature, and the annealing process was performed at 100 ~ 400 ℃ for 30 minutes in a vacuum. A UV light source (Hg lamp; 225 nm < λ < 500 nm, illumination density = 0.6 mW/cm^2), which has a wavelength peak at around 365 nm and a power consumption of 400 W, was installed to illuminate the plasma in the reaction chamber. The electron density and temperature were measured using a fast injection Langmuir probe and calibrated using a microwave interferometer.

Table 1. Experimental Condition.

Plasma Source	**CCP**
rf power (W)	**200 ~ 800 W**
Total flow rate	**100 sccm**
O_2, He, N_2 gas flow rate	**10 ~ 100 sccm**
BTMSM, TMS, MTMS gas flow rate	**10 ~ 100 sccm**
UV wavelength	**225 ~ 500 nm**
Initial pressure	**~ 10^{-3} Torr**
Working pressure	**100 ~ 1000 mTorr**
Deposition time	**10 min.**
Annealing Temp.	**100 ~ 500 ^oC**
Wafer	***p*-type Si(100)**

BTMSM (Bis-trimethylsilylmethane)

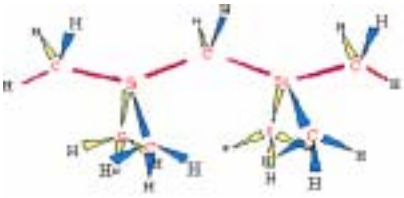

$[(CH_3)_3Si]_2CH_2$

TMS (Trimethylsilane)

$(CH_3)_3SiH$

MTMS

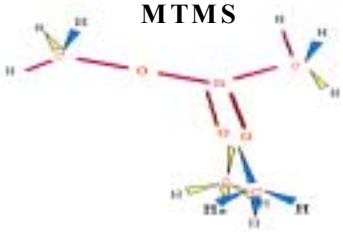

$Si(OCH_3)_3CH_3$

Fig.6. Schematic diagram of BTMSM, TMS, and MTMS.

2. Analysis of SiOC(-H) Films

2.1 Ellipsometer

The film thickness and refractive index of the deposited SiOC(-H) films were measured by using an ellipsometer, at a wavelength of 632.8 nm (GAERTNER, L116D).

2.2 Fourier transform infrared spectroscopy

Fourier transform infrared (FTIR) spectroscopy, performed in absorbance mode with a model Bruker, IFS-120HR/FRA-106 spectrometer, was used to determine the related Si-O-Si(-C) and Si-CH_3 bonding configurations in the film.

2.3 X-ray photoelectron spectroscopy

The X-ray photoelectron spectroscopy (XPS) performed in ESCA Lab. 2000, was used to investigate the various chemical bonding and composition in the film.

2.4 Measurement of Electrical properties

The electric properties including capacitance-voltage (C-V) and current-voltage (I-V) characteristics were investigated using a metal-insulator-semiconductor structure (MIS, Al/SiOC(-H)/Si). The dielectric constant at 1 MHz and current-voltage (I-V) properties were measured by a HP4280 A, HP4140 B meter.

2.5 Nano-indentation

The mechanical properties such as Hardness (H) and elastic modulus (E) were measured by the nano-indentation (Berkovich diamond indenter, 0.4 nm, 50 nN) method.

Chapter III. Results and Discussion

1. Bonding structure of SiOC(-H) films

1.1. FTIR Analysis

Figure 7 shows the FTIR spectra of as-deposited SiOC(-H) composite films, which were deposited at room temperature with [BTMSM/(BTMSM+O_2)] flow rates of 15%, 50% and 85%. The spectra are generally broadened and overlapped due to the complex stoichiometry and the amorphous nature of the films. It is known that there are Si-CH_3 (889 cm^{-1}, 1276 cm^{-1}), Si-O-Si(C) (from 1000 to 1250 cm^{-1}), CH_n (n=1,2,3) (740 cm^{-1}, 2970 cm^{-1}), and OH-related (1420 cm^{-1}, 3720 cm^{-1}) bonds in the film [24, 34, 45]. generally broadened and overlapped due to the complex stoichiometry and the amorphous nature of the films. It is known that there are Si-CH_3 (889 cm^{-1}, The peaks near 1260 cm^{-1} and 2990 cm^{-1} are identified as the Si-CH_3 and CH_3 bonding modes, respectively. In the range from 1000 cm^{-1} to 1250 cm^{-1}, the bonding mode at around 1030 cm^{-1} corresponds to the Si-O-Si asymmetric stretching mode, and the bonding mode near 1063 cm^{-1} is the ring-link form of the Si-O-C asymmetric stretching mode and the bonding mode near 1109 cm^{-1} is the open-link form of the Si-O-C asymmetric stretching mode [34, 45]. The bonding mode near 1171 cm^{-1} and near 1276

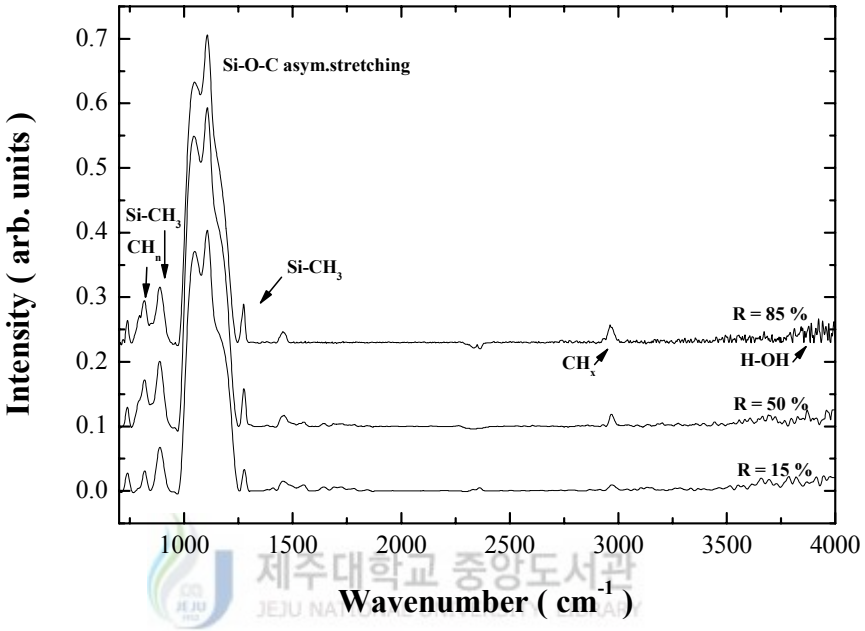

Fig. 7. FTIR spectra of the as-deposited SiOC(-H) films prepared with different [BTMSM+(BTMSM/O_2)] flow rate ratio.

cm^{-1} are due to the Si-C cage-like stretching and Si-CH_3 bonding modes, respectively. When compared with the relative intensities of the related bonding modes, these peak intensities of the Si-CH_3 and CH_3 bonding modes increased as increasing of BTMSM flow rate. The shoulder at the higher wavenumber of the 1109 cm^{-1} absorption peak indicates the existence of a cage type Si-C bond structure. In this case, the peaks at the wavenumber range from 1000 to 1250 cm^{-1} correspond to several substructure bonds such

as the cage-link, the open-link and the ring-linked Si-O-C bonds. There are not only main skeleton atomic Si-O-Si or Si-O-C groups, also there are many other groups such OH and CH_x modes [24]. Figure 8 shows the FTIR spectra of the annealed samples with various temperatures for a flow rate ratio of 85%. The bonding structure is similar to that of Fig. 6. When the annealing temperature is increased from 100 ℃ and higher, the intensity of H-OH bond also decreased and it disappears totally at 400 ℃. The intensity

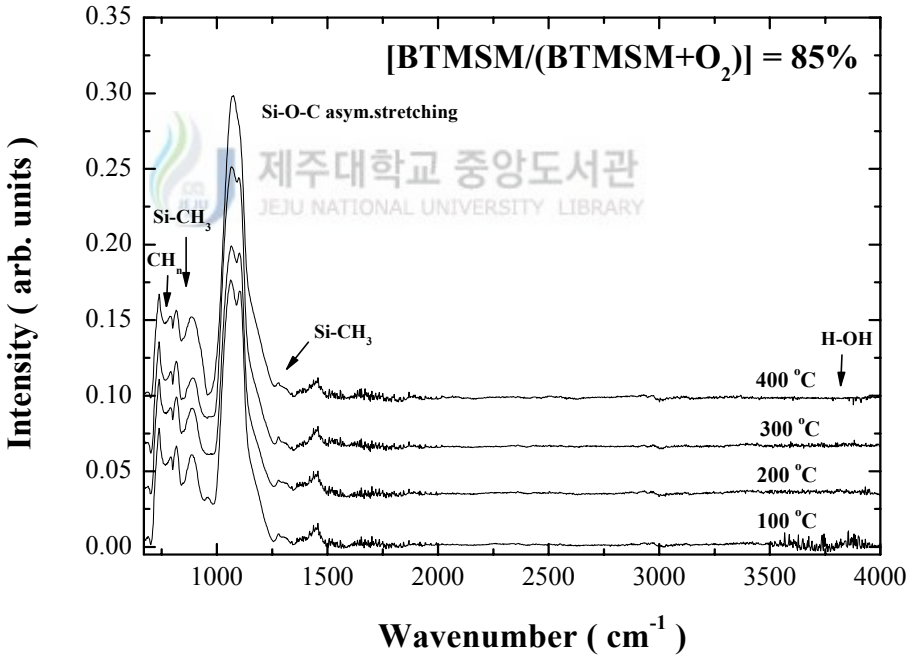

Fig. 8. FTIR spectra of the SiOC(-H) films prepared with various annealing temperatures for [BTMSM+(BTMSM/O_2)] flow rate ratio of 85%.

of the open linked Si-O-C bond is decreased than that of as-deposited samples, but the intensity of the ring-linked Si-O-C bond is increased.

Figure 9 shows the FTIR spectra of as-deposited SiOC(-H) composite films, which were deposited at room temperature with [MTMS/(MTMS+O_2)] flow rates of 50 to 100 %. The bonding structures of the SiOC(-H) composite films are similar to Fig. 7. It is known that there are Si-CH_3 (889 cm^{-1}, 1276 cm^{-1}), Si-O-Si(C) (from 1000 to 1250 cm^{-1}), CH_n (n=1,2,3) (740 cm^{-1},

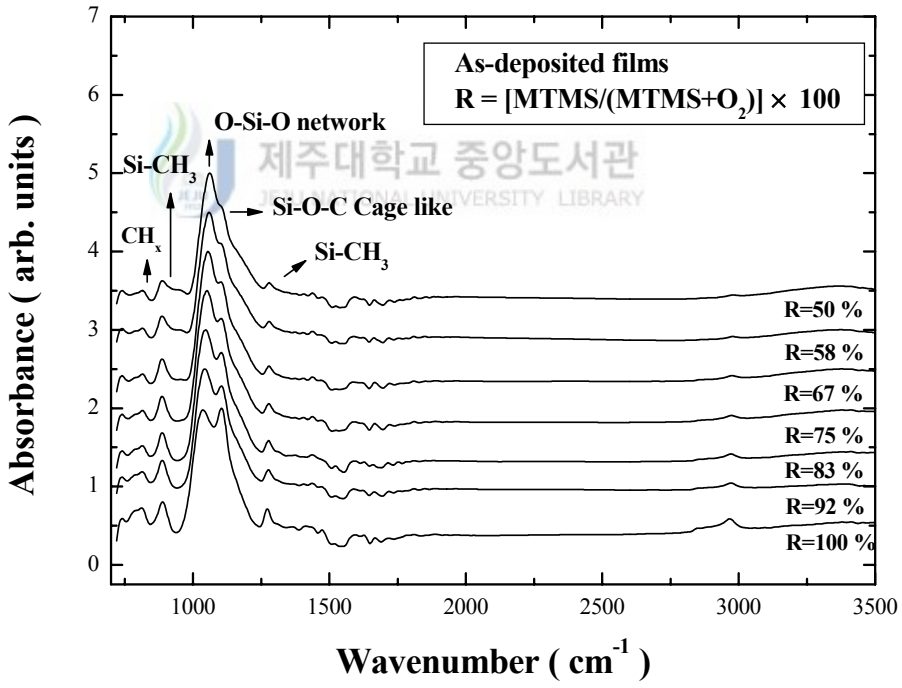

Fig. 9. FTIR spectra of the as-deposited SiOC(-H) films prepared with different [MTMS+(MTMS/O_2)] flow rate ratio.

2970 cm^{-1}), and OH-related (1420 cm^{-1} , 3720 cm^{-1}) bonds in the film [24, 62]. The peak position of Si-O-C open link bond for the sample with the MTMS/(MTMS+O_2) flow rate ratio of 100% shifted to a lower (red shift) wavenumber than that of the sample with the MTMS/(MTMS+O_2) flow rate ratioof 50 %, but the peak position of Si-O-C mode shifted to a higher (blue shift) wavenumber. These frequency shifts in the IR spectra are related to the change in the bonding characteristics, such as bonding angle and bond length [15]

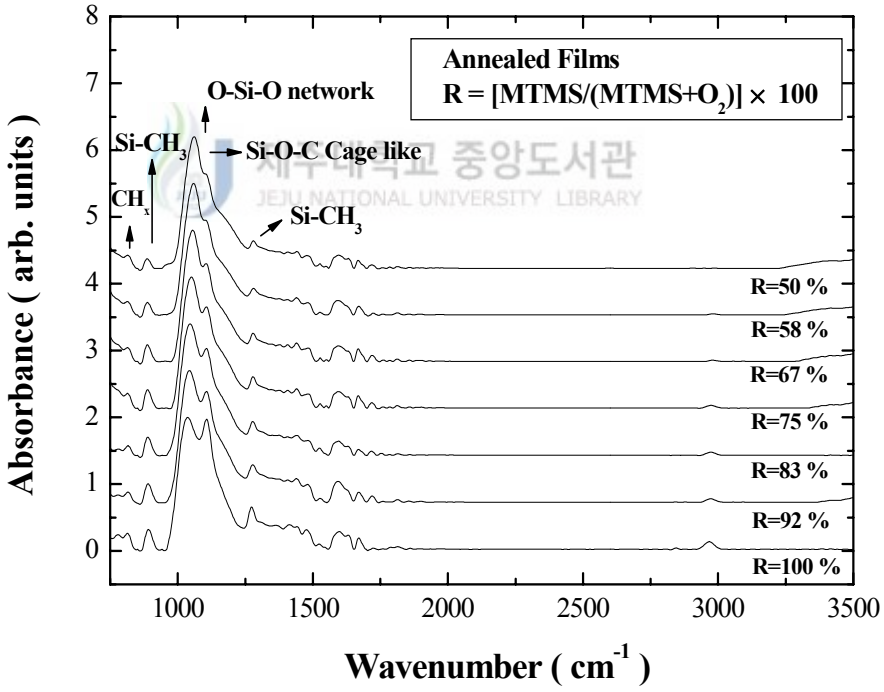

Fig. 10. FTIR spectra of the SiOC(-H) films prepared with different [MTMS+(MTMS/O_2)] flow rate ratios annealed at 400 ℃.

length[15]. These peaks reflect the enhanced porosity of the film. Because some of the Si-O-Si open links may change into ring links in which CH_3 organic groups are attached. The repulsive force between Si-O and Si-C bonds increased in accordance with the increase of carbon content. Figure 10 shows the FTIR spectra of the annealed samples with various MTMS flow rate ratios. The bonding structure is similar to that of Fig. 8. The intensities of $Si-CH_3$ and CH_n bond groups are lower than that of as-deposited films. This result indicates that some CH_n species are removed from the bulk of the film due to the annealing process, and it can cause the formation of nano-pores in Si-O-C composite film. Chang et al. reported that the annealed ultra low-*k* films had significantly higher C and H concentrations than the pure SiOC(-H) film, indicating the incorporation of significant amounts of CH_3 fragments in the structure of annealed films [32]. The intensity of the open linked Si-O-C bond is decreased than that of as-deposited samples, but the intensity of the ring-linked Si-O-C bond is increased. Therefore, we can infer that post annealing would induce the rearrangement of the chemical bonds in SiOC(-H) film.

To confirm the variation of the integrated absorption area of ring link, open link and cage links of Si-O-C and Si-O-Si bonds according to [BTMSM/(BTMSM+O_2)] and [MTMS/(MTMS+O_2)] flow rate ratio and annealing temperature, we deconvoluted the spectra in the range from 900 to could be attributed to Si-O-Si asymmetric stretching mode at 1016 cm^{-1}, Si-O-C (ring link) at 1054 cm^{-1}, Si-O-C (open link) at 1106 cm^{-1} and Si-C

(cage link) at 1158 cm^{-1} for as-deposited film (see Figs. 7, 9). Figure 11 shows the deconvoluted peaks of annealed samples using BTMSM precursor. In this case, the four peaks are assigned to Si-O-Si asymmetric stretching mode at 1025 cm^{-1}, Si-O-C (ring link) at 1064 cm^{-1}, Si-O-C (open link) at 1103 cm^{-1} and Si-C (cage link) at 1145 cm^{-1}. Figure 12 shows the deconvoluted peaks of the annealed samples using MTMS precursor. In this case, the four peaks are assigned to Si-O-Si asymmetric stretching mode at 1025 cm^{-1}, Si-O-C (ring link) at 1064 cm^{-1}, Si-O-C (open link) at 1103 cm^{-1} and Si-C (cage link) at 1145 cm^{-1}. The peak position of Si-O-C open link bond for the sample with the [BTMSM/(BTMSM+O_2)] flow rate ratio of 85 % is shifted to lower (red shift) wavenumber than that of the sample with the [BTMSM/(BTMSM+O_2)] flow rate ratio of 15 % , but the peak position of Si-O-C (ring link) mode is shifted to a higher (blue shift) wavenumber. In the case of MTMS precursor, the four peaks are assigned to Si-O-Si asymmetric stretching mode at 1025 cm^{-1}, Si-O-C (ring link) at 1064 cm^{-1}, Si-O-C (open link) at 1103 cm^{-1} and Si-C (cage link) at 1145 cm^{-1}. These peaks reflect the enhanced porosity of the film. Some of the Si-O-C open linked bond will change into ring link in which the C atoms have been incorporated. Because the transformation of open-linked to ring-linked substructure may have something to do with the reduction of -OH groups. The chain of the Si-O-Si links is broken. Therefore, the void can be formed, and void can be filled easily by other open links[24, 43, 46, 56].

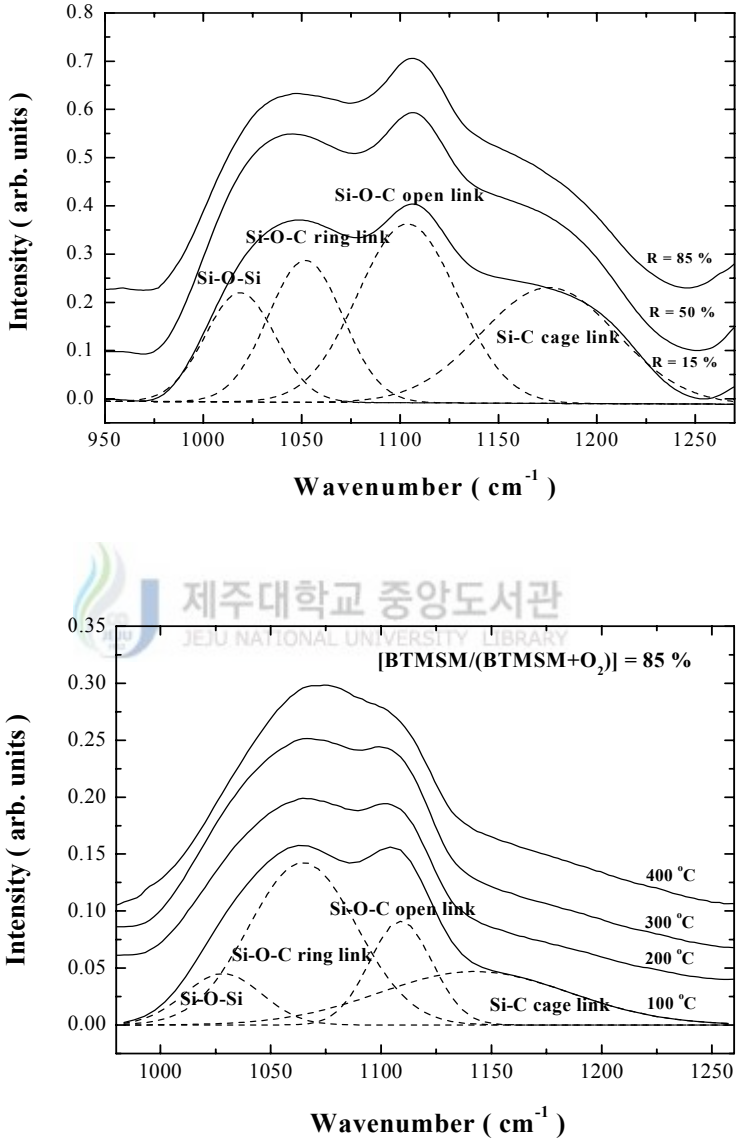

Fig. 11. Deconvolution of Si-O-C bonding mode in the wavenumber range from 1000 to 1250 cm^{-1} of the as-deposited SiOC(-H) films prepared with various annealing temperatures.

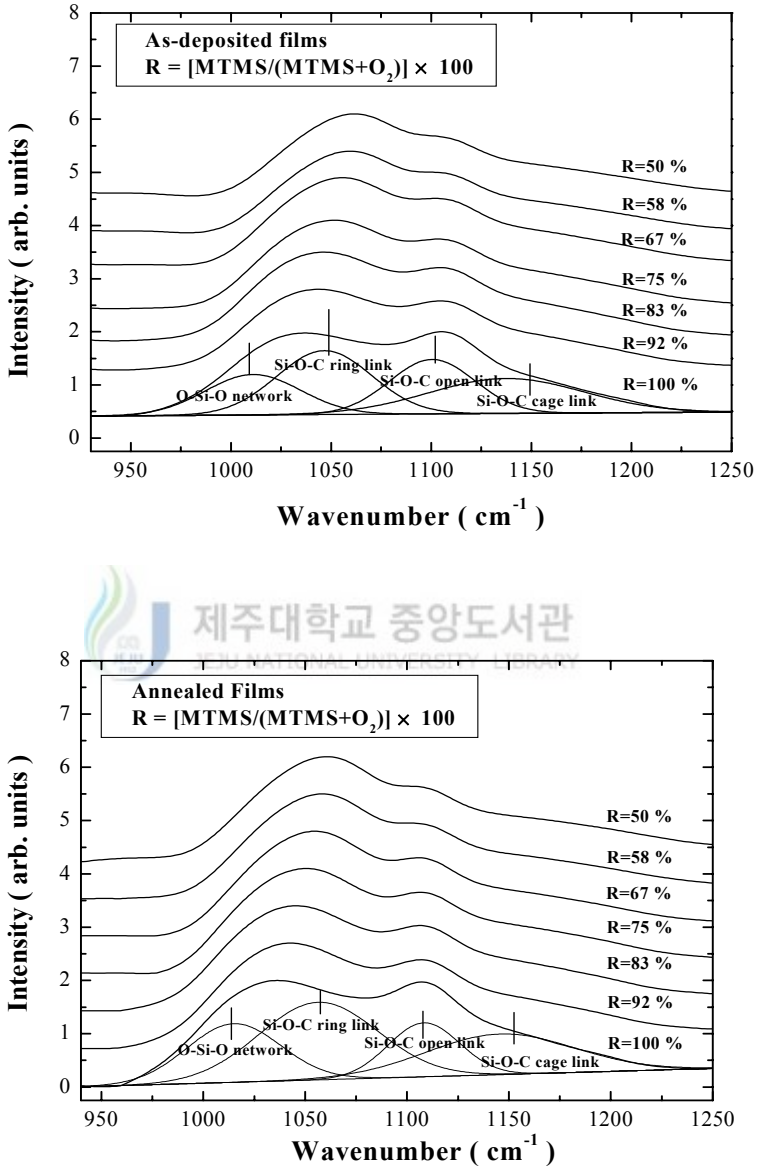

Fig. 12. Deconvolution of Si-O-C bonding mode in the wavenumber range from 1000 to 1250 cm^{-1} of the as-deposited and annealed SiOC(-H) films prepared with different [MTMS+(MTMS/O_2)] flow rate ratios.

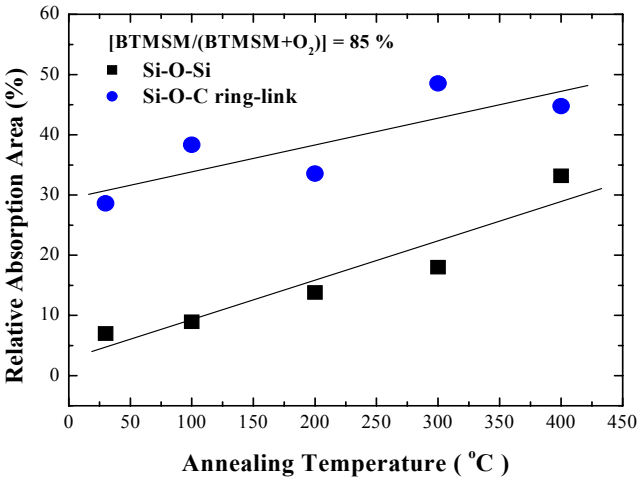

Fig. 13. Relative absorption areas of the Si-O-Si and Si-O-C ring link mode of the SiOC(-H) films prepared with various annealing temperatures for [BTMSM(BTMSM/O_2)] flow rate ratio of 85 %.

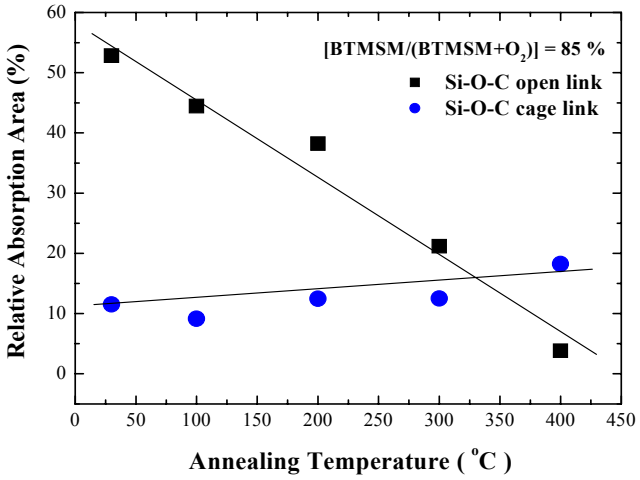

Fig. 14. Relative absorption areas of the Si-O-C open link and Si-O-C cage link mode of the SiOC(-H) films prepared with various annealing temperatures for [BTMSM(BTMSM/O_2)] flow rate ratio of 85 %.

Figures 13 and 14 show the evolution of relative integrated absorption areas (peak area/total area of the spectrum from 1000 to 1250 cm^{-1}) of Si-O-Si asymmetric stretching mode, ring link, open link and cage links of Si-O-C bond for the samples with the BTMSM flow rate ratio of 85 % as a function of annealing temperature for the resultant fitted peaks from Fig. 13. When the annealing temperature is increased the relative absorption areas of Si-O-Si and Si-O-C (ring link) increase. But from Fig. 14, we can see that the relative absorption area of Si-O-C (open link) decreases with increase of annealing temperature, while that of Si-O-C (cage link) area is constant till 300 ℃ and increases slightly when the annealing temperature is 400 ℃.

Figure 15 shows the evolution of relative integrated absorption areas (total area of the spectrum from 1000 to 1250 cm^{-1}) of Si-O-Si asymmetric stretching mode, ring link, open link and cage links of Si-O-C bond for the samples with the annealing temperature as a function of MTMS flow rate ratio for the resultant fitted peaks from Fig. 12. When the annealing temperature is increased the relative absorption areas of Si-O-Si and Si-O-C (ring link) increase ing the left side figure. But from right side figure, we can see that the relative absorption area of Si-O-C (open link) decreases with increase of MTMS flow rate and annealing.

From these results, we known that the Si-O-C open-linked substructure was unstable during post-annealing procedure as the O_2 gas flow rate increases, some of them could be transformed to ring-linked substructure. While SiOC(-H) film may contain ring link or open link of Si-O-C bonds,

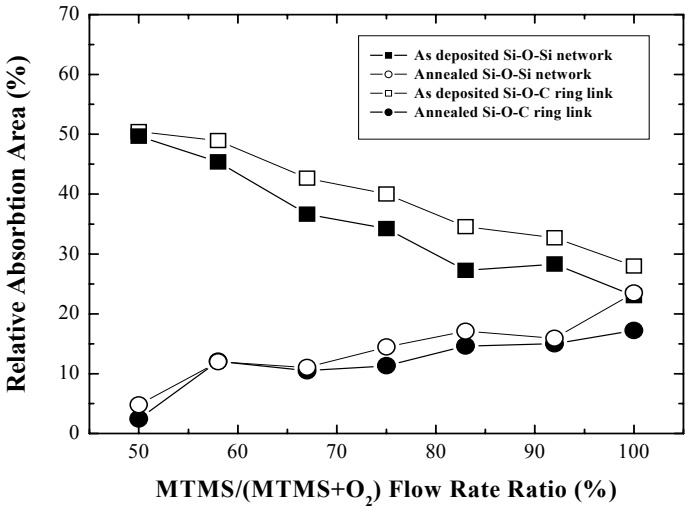

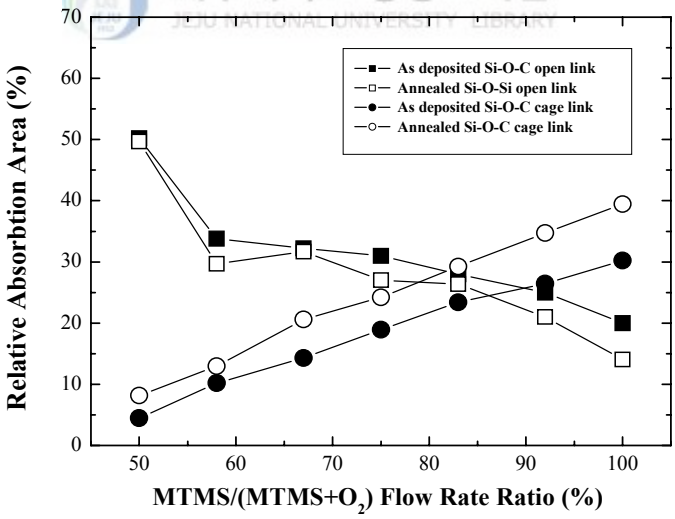

Fig. 15. Relative absorption areas of the Si-O-Si, Si-O-C ring link, Si-O-C open link and Si-O-C cage link mode of the as-deposited and annealed SiOC(-H) films prepared with different [MTMS+(MTMS/O_2)] flow rate ratio.

any contributions to the absorptions from 1000 to 1200 cm^{-1} from Si-O-C asymmetric stretching vibrations cannot be identified because they overlap with the Si-O-Si asymmetric stretching band. Some of the open linked Si-O-C bond may change to ring link in which CH_3 or organic groups are attached. Because there is aloof force between the CH_3 group and other parts of the Si-O-Si links, which resulted in formation of voids In the case of open links, voids are filled easily by other open links. Therefore, we can infer that the formation of Si-O-C ring links by attaching CH_3 groups to Si-O-Si voids in the film. The dielectric constant of the Si-O-C film is reduced due Si-O-Si asymmetric stretching band is responsible for the generation of nano-sized to the decreased film density, which resulted from the replacement of Si-O bonds with Si-CH_3 (Si-R) bonds [24, 59, 61].

Figure 16 shows the carbon concentration and the Si-O-C bonding angle with BTMSM/(BTMSM+O_2) = 85 % as a function of annealing temperature. The carbon concentration increases as annealing temperature is increased, which is increased from 22% to 31% when the annealing temperature increases in steps from 100 °C to 400 °C. The Si-O-C bonding angle increases from 144.4 ^{o} to 152.3 ^{o} as a function of annealing temperature. The bonding angle between Si-O and Si-C bonds increases as the carbon content increases. The reason of angle variation is due to the incorporation of CH_3 groups breaks the continuity of Si-O-Si networks and form the nano-pores by the aloof force between CH_3 group and other part of Si-O-Si links. Because the repulsive force between Si-O and Si-C bonds is smaller than those between

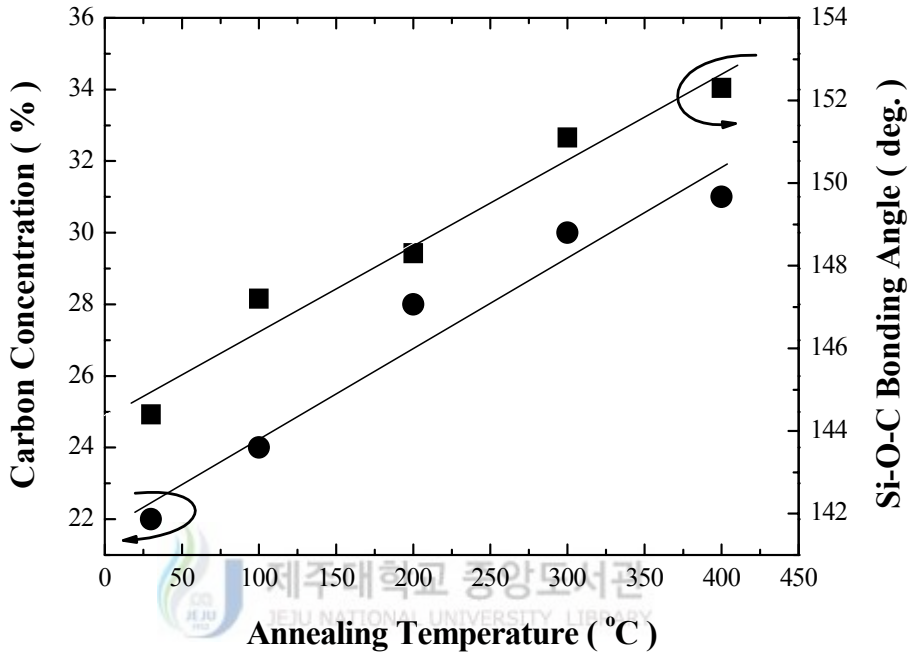

Fig. 16. Relative carbon atomic concentration and the Si-O-C bonding angle of SiOC(-H) films prepared with various annealing temperatures for [BTMSM+(BTMSM/O_2)] flow rate ratio of 85 %.

Si-O and Si-C bonds in [SiO_3C] tetrahedron due to electro-negativity of carbon atom (2.5), which is lower than that of oxygen atom (3.5).

Figure 17 shows the carbon concentration and the Si-O-C bonding angle with annealing as a function of MTMS flow rate ratio. The carbon concentration increases as MTMS flow rate increased, which is increased from 24 to 36 % when the MTMS flow rate increases in steps from 50 to 100%. The Si-O-C bonding angle increases from 144.4 ^{o} to 154.6 ^{o} as a

function of MTMS flow rate. The bonding angle between Si-O and Si-C bonds increases as the carbon content increases. The reduced ionic contribution might be a consequence of the decrease in Si-O bonds in the film, which have strong ionic polarization. The decrease in the ionic polarization plays a great role in decreasing the dielectric constant of SiOC(-H) film [24].

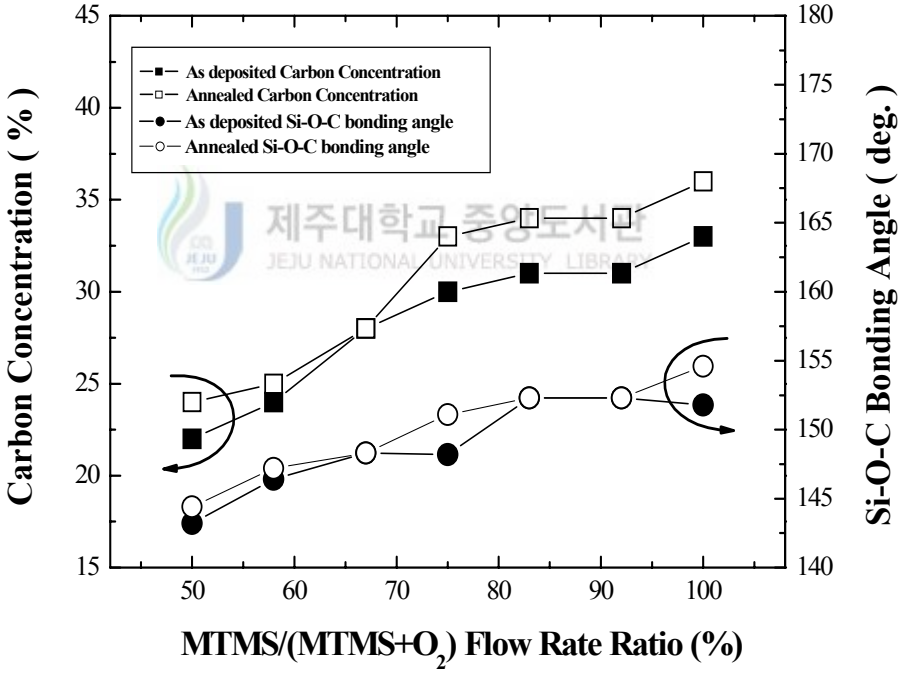

Fig. 17. Relative carbon atomic concentration and the Si-O-C bonding angle of as-deposited and annealed SiOC(-H) films prepared with different [MTMS+(MTMS/O_2)] flow rate ratios.

1.2. XPS Analysis

To further elucidate this re-arrangement from FTIR analysis, the XPS narrow scanning spectra of Si 2p of as-deposited and annealed samples prepared with different [MTMS+(MTMS/O_2)] flow rate of 85 % were collected and deconvoluted using Gaussian peaks, as shown in Fig. 18. Only two kinds of Si chemical moieties could be identified in the as-deposited SiOC(-H) films, Si-O_4 with binding energy of 103.41 eV, and C_2-Si-O_2 with

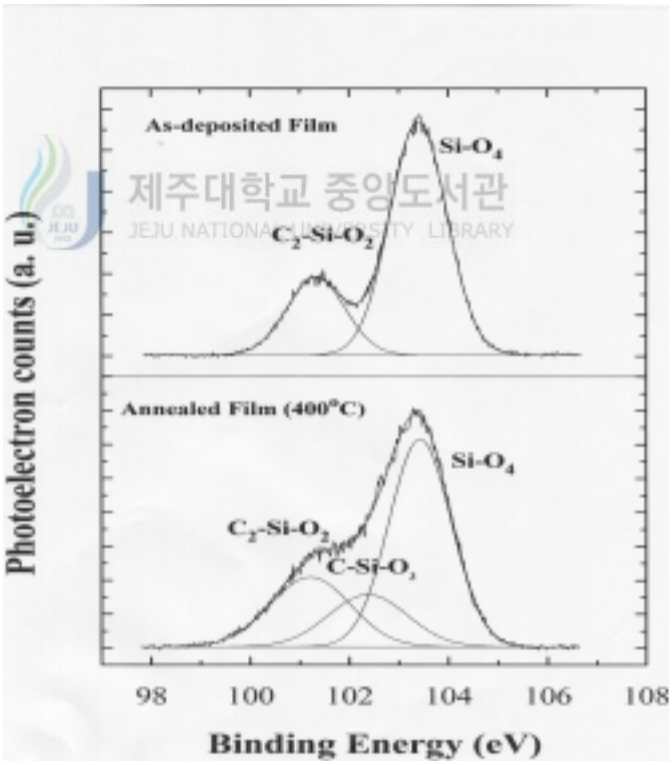

Fig. 18. Si 2p XPS spectra of SiOC(-H) films : (a) as-deposited, and (b) annealed.

binding energy of 101.24 eV [5, 14], the full widths at half maximum (FWHM) are 1.35 eV and 1.37 eV, respectively. The relative areas of $Si\text{-}O_4$ and $C_2\text{-}Si\text{-}O_2$ bond moieties are 75 % and 25 %, respectively. There appeared a new peak at the binding energy of 102.37 eV with the FWHM of 1.88 eV in annealed SiOC(-H) films as indicated in Fig. 18, which could be attributed to $C\text{-}Si\text{-}O_3$ moiety [5, 14]. The relative areas of $Si\text{-}O_4$, $C_2\text{-}Si\text{-}O_2$ and $C\text{-}Si\text{-}O_3$ bond moieties are 57 %, 25 %, and 18 %, respectively. The relative area of $C_2\text{-}Si\text{-}O_2$ bond is the same (25 %) in as-deposited and annealed SiOC(-H) films indicates that it has high thermal stability, considering the thermal stability of Si-O-C cage-link structure, it can be concluded that $C_2\text{-}Si\text{-}O_2$ bond corresponds to Si-O-C cage-link structure. From the decrease of the $Si\text{-}O_4$ bonds (from 75 % to 57 %) and the appearance of $C\text{-}Si\text{-}O_3$ bonds in annealed SiOC(-H) films we can infer that some O atoms in $Si\text{-}O_4$ bond are replaced by the C atoms or CH_3 groups during annealing process. It is reported that the replacement of O atom may be caused by the reaction between OH and H in $Si\text{-}CH_3$ groups[4], and the total elimination of OH related groups by annealing, as shown in Fig. 8, demonstrates this interpretation. As a result of this reaction, more nano-pores could be formed in annealed SiOC(-H) film, which in turn could decrease its dielectric constant [44, 68].

Figure 19 shows the high resolution XPS C 1s electron orbital spectra of as-deposited and annealed SiOC(-H) films prepared with [MTMS+(MTMS/O_2)] flow rate ratio of 50 %. Each spectral region was deconvoluted into individual

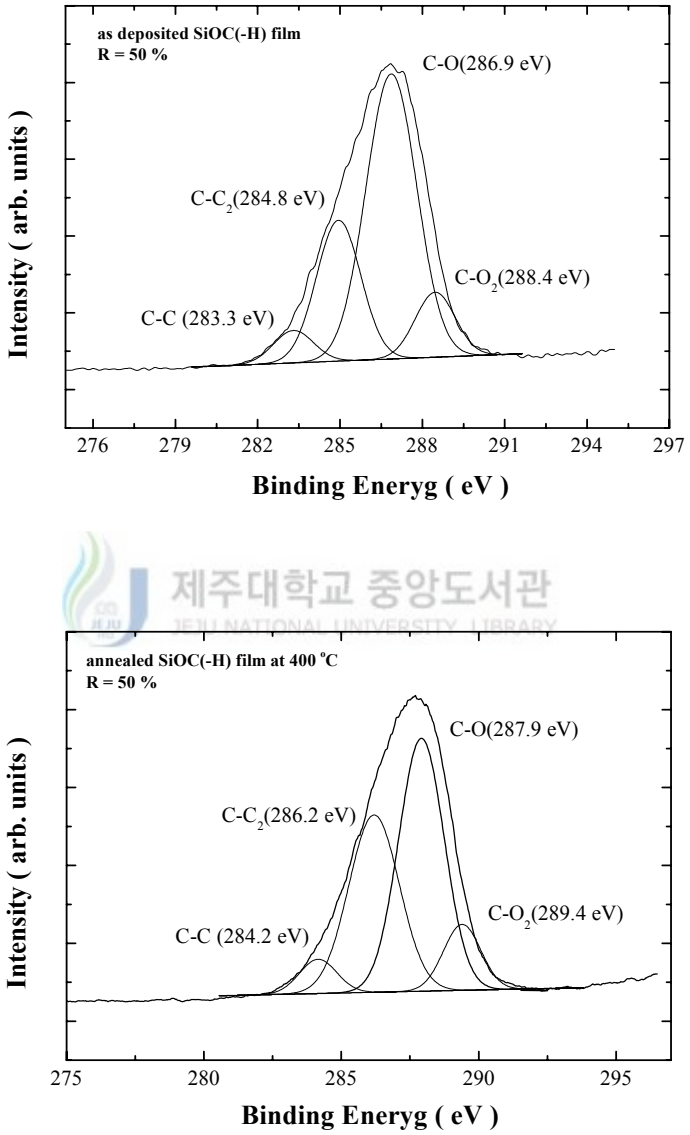

Fig. 19. The XPS (C 1s) orbital spectrum of the as-deposited and annealed SiOC(-H) films prepared with [MTMS+(MTMS/O_2)] flow rate ratio of 50 %.

peak assuming all peaks to be perfectly Gaussian. The fitted results for the SiOC(-H) films show that C 1s spectra consist of four peaks. A Gaussian decomposition of this spectrum gives peak at 284.2, 286.2, 287.9 and 289.4 eV in the case of as-deposited SiOC(-H) film. These include the sp^3 (tetrahedral, C-O), sp^2 (trigonal C=O), sp^3 (tetrahedral, C-C) and sp^2 (trigonal C=C) bonds. According to assignment, the lowest C 1s peak at 285 eV is assigned to C-C bonds; this position is at an intermediary value between the two position of the C 1s peak attributed to C-C sp^2 bond in graphite-like and C-C sp^3 bonds in diamond-like amorphous carbon [14]. In the case of annealed SiOC(-H) film, all of the peaks are chemically shifted to lower binding energy as 1.0 eV. A Gaussian decomposition of this spectrum gives peak at 283.3 (C-C), 284.2 ($C-C_2$), 286.9 (C-O) and 288.4 eV ($C-O_2$). Since the major reaction during annealing process are decreasing related oxygen elements and increasing carbon element after annealing process, such binding energy changes can be easily explained by the carbon atoms. The electro negativity of the carbon atom is lower than that of oxygen atom. The carbon element in MTMS precursor is combined with oxygen-generating CC and CC_2 more than CO, CO_2, therefore, the binding energy of C 1s is shifted to higher binding energy [45, 67]. This chemical shift towards lower binding energy is due to the incorporation of abundant carbon atoms in the Si-O-Si chain structure attached CH_n group, which are integrating into Si-O links to form Si-O-C links as more CH_n radicals increase in the bulk plasma.

2. Electrical properties of SiOC(-H) films

2.1. Properties of C-V measurement

Figure 20 shows the measured C-V characteristics of the as-deposited and annealed SiOC(-H) films. The small dip (marked with a circle in Fig. 20) in weak inversion region of C-V curve of as-deposited film indicates the film contains

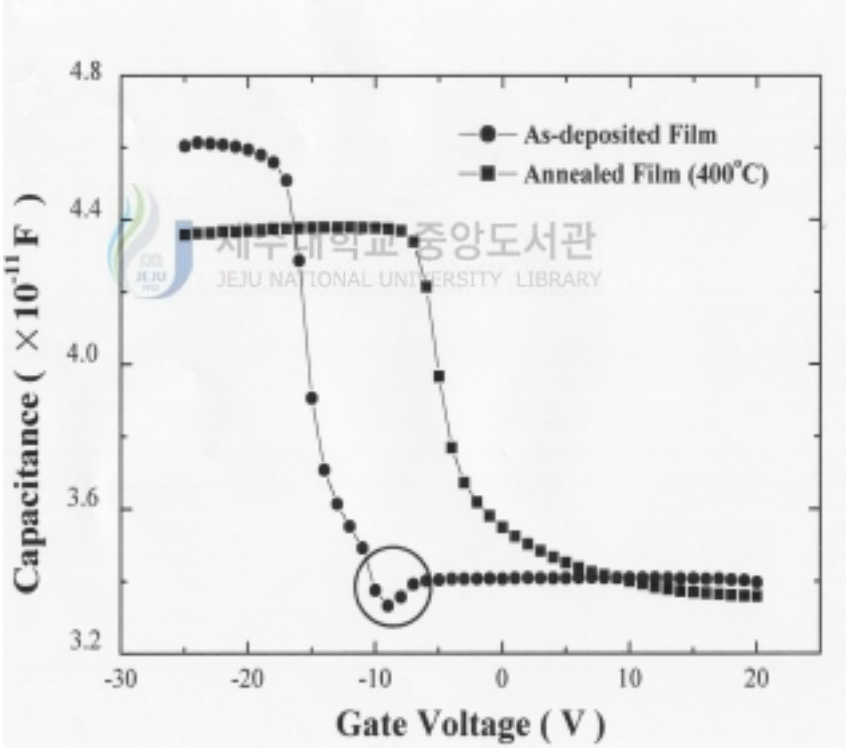

Fig. 20. Capacitance vs. gate voltage for as-deposited and annealed SiOC(-H) films.

either the trapped charges in the interface between the film and substrate silicon wafer or bulk traps in the wafer. But this dip disappears in the C-V curve of annealed film, it suggests the small dip should be caused by the interface trapped charge rather than the bulk traps. The interface charge traps may come from the defects between film and substrate surface, after annealing, these defects could be efficiently removed. Another difference between as-deposited and annealed C-V curves is that the flat voltage of annealed

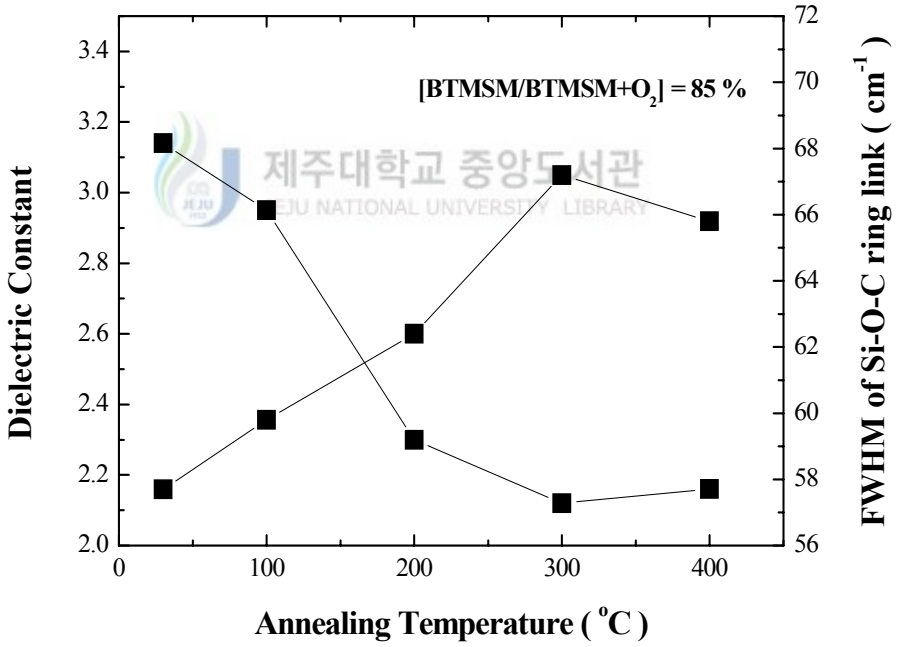

Fig. 21. Dielectric constant and FWHM of ring linked Si-O-C bonding of SiOC(-H) films prepared with various annealing temperatures for [BTMSM(BTMSM/O_2)] flow rate ratio of 85 %.

C-V curve is more shifted toward the gate voltage of 0 V than that of as-deposited film. The flat voltages of as-deposited and annealed SiOC(-H) films are -17 V and -7 V, respectively. This shift is caused by the elimination of OH related groups during an annealing process, as such groups usually act as charge trapping centers in insulators.

Figure 21 shows the dielectric constant and full width half maximum (FWHM) in ring link of FTIR spectra on SiOC(-H) film with BTMSM/O_2 flow ratio of 85 %. The dielectric constant decreases from 3.14 to 2.12 when the annealing temperature is 300 ℃. Further increase of annealing temperature to 400 ℃ results in slight increase of the dielectric constant to 2.25. The FWHM of the Si-O-C ring link increases from 57.5 to 67 cm^{-1} as a function of annealing temperature till 300 ℃. But when the annealing temperature is 400 ℃, the FWHM of ring linked Si-O-C decreases and is found to be 65.8% The FWHM of ring linked Si-O-C bond increases with decreasing dielectric constant.

Figure 22 shows the dielectric constant of SiOC(-H) film with MTMS/O_2 flow ratio from 50 to 100%. The dielectric constant decreases from 3.05 to 2.39 in the as-deposited SiOC(-H) films and for the annealed films the dielectric constant decreases from 3.18 to 2.25.

The possible reason for the decrease in the dielectric constant is due to the incorporation of more CH_3 groups into the films when the flow rate ratio of the gas is increased. The replacement of Si-O by Si-CH_n bonds can also play a role in increasing the porosity, as the Si-CH_n bond can

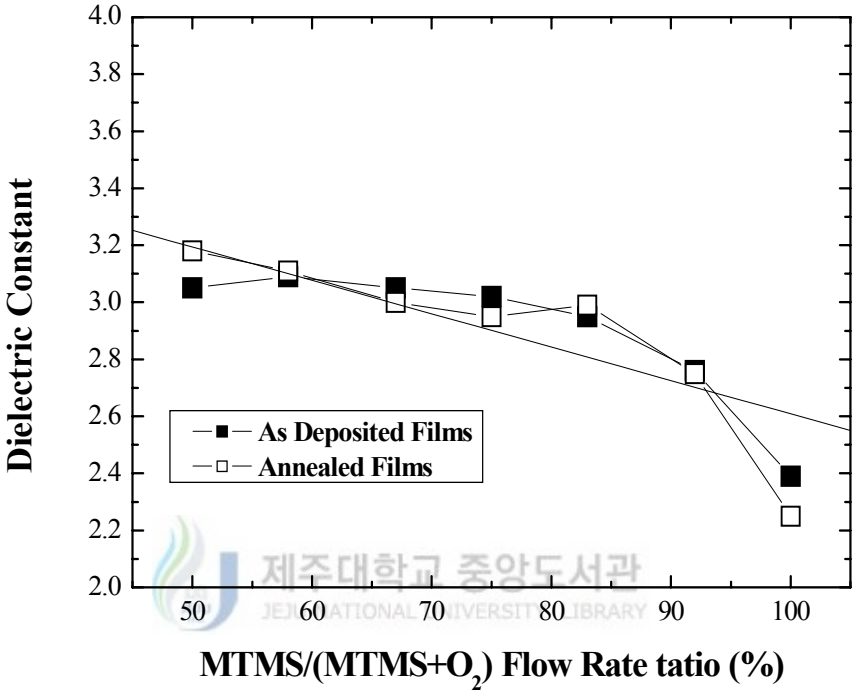

Fig. 22. Dielectric constant of as-deposited and annealed SiOC(-H) films prepared with different [MTMS+(MTMS/O_2)] flow rate ratio.

generate the void. During post annealing, water was removed selectively from the film, without breaking Si-CH_3 bonds. Hence, we assume that voids are formed due to the rearrangement of the bonding configuration in the film.

Hence the annealed films have lower dielectric constant than as deposited films. But, when the temperature is increased to 400 ℃, the increase in dielectric constant is due to the collapse of nano-pores at this temperature, which resulted in the densification of the films.

2.2. Properties of I-V measurement

Figure 23 shows the leakage current density versus electric field in the log J versus $E^{1/2}$ plots for the as-deposited and annealed SiOC(-H) films. The leakage currents of the as-deposited and annealed films are 3.4×10^{-10} A/cm^2 at the applied electric field of 1 MV/cm, this value is significantly lower than that imposed by the requirements for integration of the dielectric in ULSI devices [2].

It is well know that various conduction mechanisms such as Schottky emission and Poole-Frenkel emission can be demonstrated using the MIS structure through *log J* versus square root of electric field curve fitting. The Schottky emission generated by thermo ionic effect is caused by the electron transport across the potential energy barrier via field-assisted lowering at a metal-insulator interface, the Poole-Frenkel emission is due to the field-enhanced thermal excitation of trapped electrons in the insulator into the conduction band [22, 62]. The Schottky and Poole-Frenkel emission mechanisms can be quantified by the following equation (5) and (6), respectively,

$$J_S = A_R T^2 \exp(-q\phi_b/kT)\exp[(q/kT)(qE/4\pi\epsilon_0\epsilon_r)^{1/2}], \quad (5)$$

$$J_P \propto E\exp(-q\phi_b/kT)\exp[(q/kT)(qE/4\pi\epsilon_0\epsilon_r)^{1/2}], \quad (6)$$

where A_R, ϕ_b, T, q, E, ϵ_0, ϵ_r and k are the effective Richardson's constant, the barrier height, the absolute temperature, the electronic charge, the electric field, the dielectric constant of free space, the relative dielectric constant at high frequency and the Boltzmann's constant, respectively. From equation (5) and (6), the relative dielectric constants are given by the following equation (7) and (8), respectively,

$$\epsilon_{rs} = (q^3/4\pi\epsilon_0)(1/kT)^2[(E_1^{1/2} - E_2^{1/2})/(\ln J_1 - \ln J_2)]^2, \quad (7)$$

$$\epsilon_{rp} = 4\epsilon_{rs}, \quad (8)$$

where ϵ_{rs} and ϵ_{rp} are relative dielectric constants given by Schottky and Poole-Frenkel mechanisms, respectively. J_1 and J_2 are leakage current density values at the electric fields E_1 and E_2, respectively.

It is found that the leakage current density is linearly proportional to the square root of the applied electric field for both the as-deposited and annealed SiOC(-H) films when the applied electric field is less than 1.8 MV/cm^2. The relative dielectric constants of the as-deposited and annealed SiOC(-H) films, calculated from equation (7), are 2.21 and 3.32, respectively. These values are very similar to that based on C-V characteristics (2.1 and 3.15, respectively). The similarity demonstrates that the dominant conduction mechanism in as-deposited and annealed SiOC(-H) films is Schottky emission

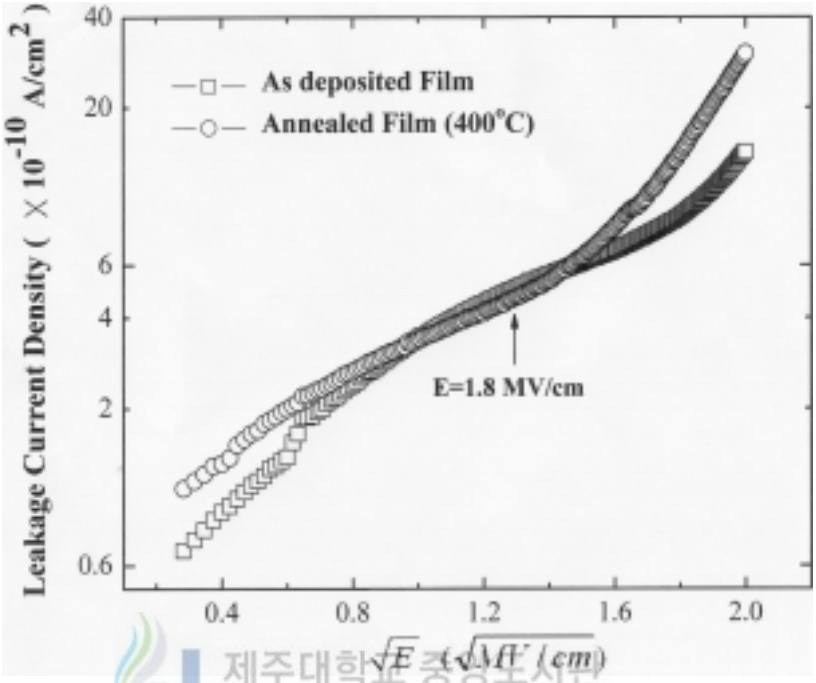

Fig. 23. Leakage current density J, as a function of electric field, in $\log J$ vs. $E^{1/2}$ plot.

at mid electric field. When the electric field is higher than 1.8 MV/cm^2, the relationship between log J and $E^{1/2}$ is still nearly linear for annealed film, but the slope is larger than that of mid electric field. The relative dielectric constant calculated from equation (8) is 2.28, from this value we infer that Poole-Frenkel emission is the dominant conduction mechanism at high electric field for SiOC(-H) film annealed at 400 ℃. The relationship between log J and $E^{1/2}$ is deviated from linearity for as-deposited film at high electric field, as shown in Fig. 23. This deviation may be caused by space-charge limited

conduction mechanism, because OH related groups usually act as the charge trapping centers in as-deposited SiOC(-H) film, as discussed above.

3. Dielectric properties of SiOC(-H) films

3.1. Analysis of three components for the dielectric constant

The dielectric constant is a frequency-dependent, intrinsic materials property. As it is well known, the dielectric constant is composed of three components: electronic (ϵ_{elec}), ionic (ϵ_{ionic}) and orientation (ϵ_{orient}). The dielectric constant, $\epsilon(w)$, can be obtained from the following equation.

$$P(w) = \sum \epsilon(w) E(w), \tag{9}$$

where is a complex number. $P(w)$ is polarization, and $E(w)$ is the electric field. For isolated molecules, the dielectric constant is given by the sum of the three components[22].

$$\epsilon(w) = \epsilon_{elec}(w) + \epsilon_{ionic}(w) + \epsilon_{orient}(w), \tag{10}$$

Hence, all three components must be considered in estimating the dielectric

constant. Here, the key point is to treat materials as collections of oscillators and atoms. The dielectric constant of a material can be calculated from the refractive index, as expressed in

$$\epsilon(w) = n^2(w) + \kappa^2(w), \tag{11}$$

where $\epsilon(w)$ is a relative dielectric constant, $n(w)$ is a real part of a refractive index, $\kappa(w)$ is an imaginary part of a refractive index, and is the frequency of a light source. The pure electronic contribution to the dielectric constant (ϵ_{elec}) was calculated from the refractive index obtained in the visible-ultraviolet region. The contribution of the electronic polarization, $\epsilon_{elec}(w)$, can be written in terms of the electronic polarizability, α_e, as given by :

$$\epsilon_{elec}(w) = 1 + 4\pi N\alpha_e, \tag{12}$$

where N is the number of molecules per unit volume. Since the ionic polarization is based on atomic oscillations, it must be described in terms of the sum of the oscillation strengths, F_j, which in turn is related to the derivative of the dipole moment with respect to a normal coordinate[24],

$$\epsilon_{ionic}(w) = \frac{4\pi N' e^2}{m} \sum \frac{F_j}{w_j^2 - w^2 - i\Gamma_j}, \tag{13}$$

where N' is the number of oscillators per unit volume, e is the charge of an electron, m is the reduced mass of an oscillator, w is the angular frequency (1/s), and Γ_j is the oscillator strength of the j^{th} mode ($\Gamma_j \propto \left| \frac{\partial \mu_j}{\partial q_j} \right|$). Therefore, F_j must be related to the absolute IR intensity of the j^{th} band. Since the orientation polarization is related to the dipole moment, it should exhibit temperature dependence [22, 24],

$$\epsilon_{orient}(w) = N''\mu^2/3kT, \tag{14}$$

where, N'' is the number of dipole moments per unit volume. k is Boltzman's constant, μ is a dipole moment and T is the absolute temperature. The relation between the dielectric constant, $\epsilon(w)$, and polarizability, α , was qualitatively estimated by the Clausius-Mosotti relation as given by [24],

$$\frac{M}{\rho}\frac{\epsilon - 1}{\epsilon + 2} = N_A \frac{\alpha}{3\epsilon_0}, \tag{15}$$

where ρ is the film density, N_A is Avogadro's number, M is the molecular weight, and ϵ_0 is the vacuum dielectric constant.

3.2. Three components for the dielectric constant

The bonding angle and the carbon contents of the Si-O-C composite films were investigated and the bonding angle between Si-O and Si-C bonds and the carbon contents are shown in Fig. 24 as a function of flow rate ratio. The bonding angle, θ, can be calculated from the following simple equation [24].

$$\bar{\nu} = \bar{\nu}_0 \sin(\frac{\theta}{2}), \tag{16}$$

where, θ is the bonding angle between Si-O and Si-C bonds. $\bar{\nu}$ is experimentally obtained as the wavenumber of Si-O-C open link in Fig. 7, and $\bar{\nu}_0$ =1080 cm^{-1} is the wavenumber for the thermal oxide (SiO_2). In this figure, the relative carbon contents is increased as the BTMSM/(O_2+ BTMSM) flow rate ratio increased. The relative concentration of carbon incorporated in the SiOC(-H) films was calculated by relative carbon content (%) = $\{A_C/(A_0 + A_C)\}\times100$ equation normalized to the peak areas of the Si-O-C stretch vibration, where A_0 and A_C are the peak areas of the Si-O-C stretching vibration mode from 1000 to 1250 cm^{-1} and the Si-CH_3 stretching vibration mode at 883 cm^{-1} and 1260 cm^{-1}. The bonding angle between Si-O and Si-C bonds increased as the carbon content increased. Above results indicate that there are at least two methods of incorporation of C atoms into SiOC(-H) films during the deposition. First method is as CH_3

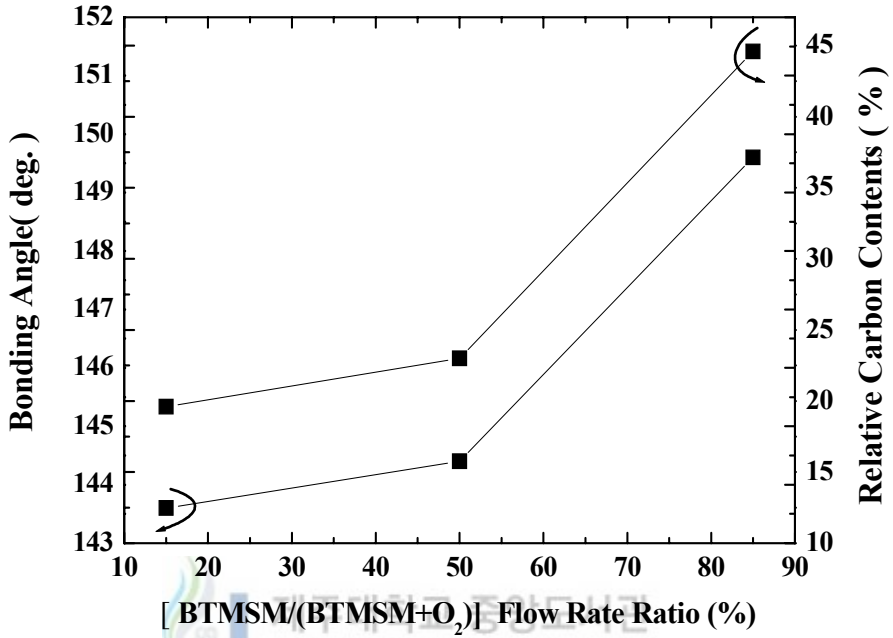

Fig. 24. The bonding angle calculated from Fig. 7 and the relative carbon contents as functions of the [BTMSM/(BTMSM+O_2)] flow rate ratios.

groups attached to Si atoms in Si-O-Si networks, and another method is as Si-O-C structure [16]. The incorporation of CH_3 groups break the continuity of Si-O-Si networks and form the nano-pores by the aloof force between CH_3 group and other part of Si-O-Si links. Because the repulsive force between Si-O and Si-O bonds is smaller than those between Si-O and Si-C bonds in [SiO_3C] tetrahedron due to electro-negativity of carbon atom (2.5) is lower than that of oxygen atom (3.5). Therefore, the bonding angle of O-Si-O is lower than 120^o in [SiO_3C] tetrahedron.

To investigate the dipole moment of the Si-O-C chain structure with a variation in the bonding angle between Si-O and Si-C bonds, we calculated it by the following equation:

$$\mu_{elec} = \mu_{Si-O} + \mu_{Si-C}, \tag{17}$$

where, μ_{elec} is the total induced dipole moment, μ_{Si-O} and μ_{Si-C} are the induced dipole moment of Si-O and Si-C bonding molecules.

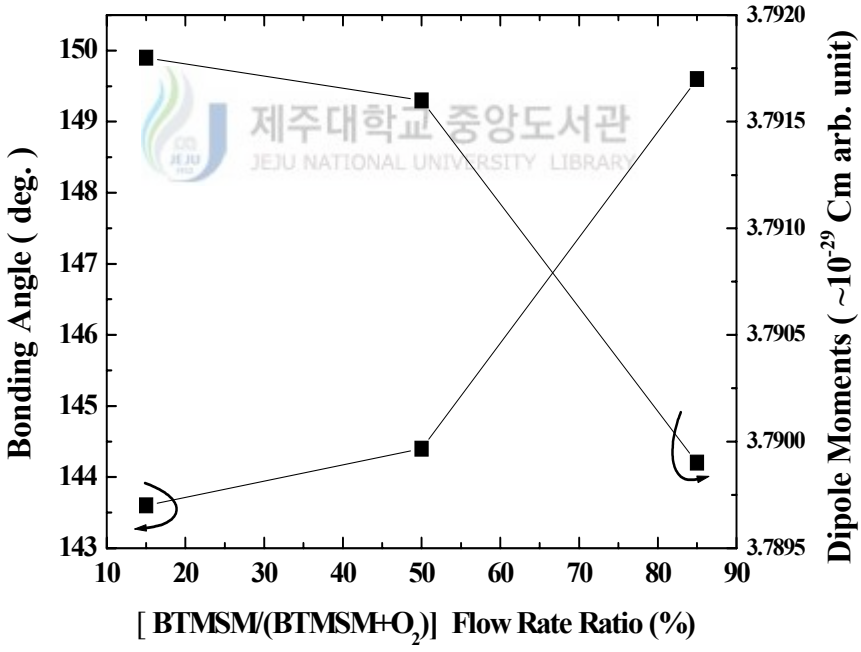

Fig. 25. The dipole moment calculated from Fig. 24 and the bonding angle as functions of the [BTMSM/(BTMSM+O_2)] flow rate ratios.

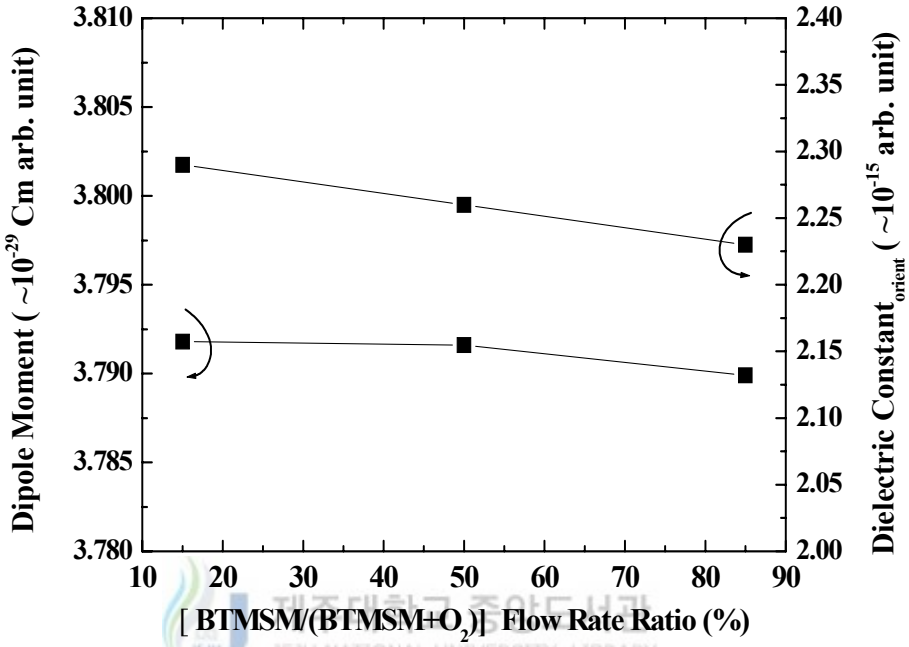

Fig 26. The orientation dielectric constant calculated from Fig. 25 and the dipole moment with different [BTMSM/(BTMSM+O_2)] flow rate ratios.

For BTMSM/(BTMSM+O_2) flow rate ratio of 85%, the total induced dipole moment increasing with carbon content is attributed to the reduction of the dipole moment. The orientation and electronic polarization is affected from the redistribution moment decreased abruptly to about 3.79×10^{-29} Cm, and the bonding angle increased to about 149.9^{o} as shown in Fig. 25. These results are explained by the difference of dipole moment. The dipole moment usually reflects the difference between the electronegativities of the carbon and oxygen atoms, since the dipole moment of Si-O (1.9×10^{-29} Cm) is larger

than that of Si-C (1.8×10^{-29} Cm) at BTMSM/(BTMSM+O_2) flow rate ratio of 85%. The increased number of Si-O bond replacement to Si-C bonds results in the reduction of the sum of dipole moments in the molecular unit. Therefore, the drastic decrease in the orientation polarization of SiOC structure with of charge and structure like bonding angle, when a group of atoms with a net permanent dipole moment reorients itself in space with increasing BTMSM flow rate. In order to investigate the orientation polarizability, we measured the film density by ERD-TOF method which the samples with flow rate ratio of 15, 50 and 85 (%) obtained as 1.88, 1.85 and 1.83 (g/cm^3), respectively. The orientation dielectric constant (ϵ_{orient}), calculated by Eq. (14), decreased slightly with increasing flow rate ratio, as shown in Fig. 26. When the flow rate ratio is 85 %, ϵ_{orient} is about 2.23×10^{-15}. The estimated orientation dielectric constant is much lower than that of the vacuum dielectric constant. It means that the average of orientation dipolar polarizability is nearly zero because the orientation polarizability on the SiOC bonding structure is distributed randomly in the SiOC(-H) film. Therefore, the influence of orientation dielectric constant can be neglected for low-*k* dielectrics, whereas high-*k* dielectrics have dominant orientation polarizability.

We calculated the electronic polarizability by equation (12) and (15). Figure 27 shows the characteristics of the electronic polarizability and the film densities as a function of BTMSM/(BTMSM+O_2) flow rate ratios. The

film density decreased to the value of 1.88 to 1.83 (g/cm^3) when the BTMSM/(BTMSM+O_2) flow rate ratios are changed from 15 to 85 (%). In this case, carbon concentrations was increased from 19.6 to 44.6 (%). The decrease of the film densities were resulted from the termination of the Si-O-C bonding network, which is related to replacing oxygen atoms with hydrocarbon groups such as -CH_n. Also, the extension of the bonding angle between the Si-O and the Si-C bonds in the Si-O-C structure effects to the decreasing the film density. Therefore, the electronic polarizability of the SiOC(H) film can decrease due to the incorporation of the carbon content.

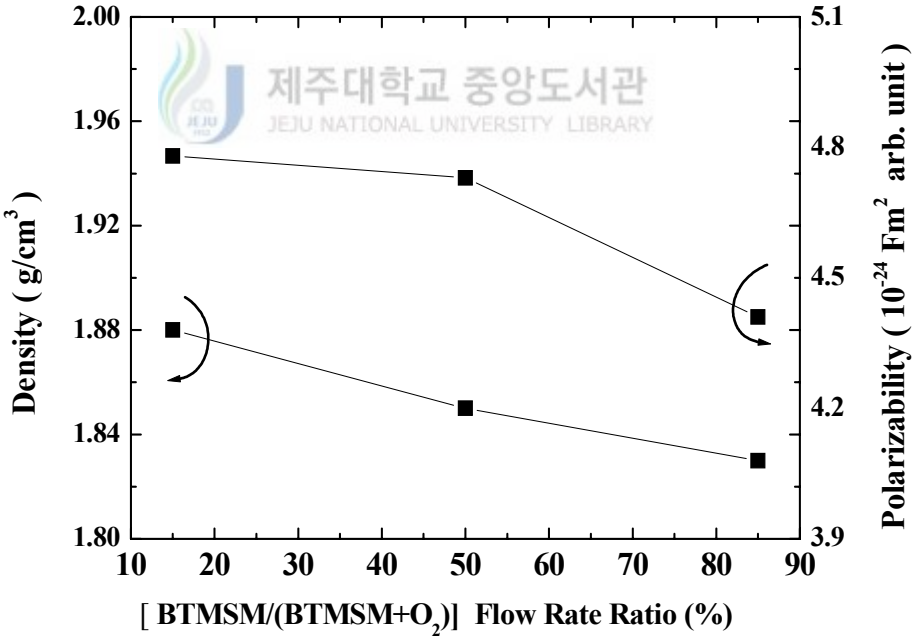

Fig. 27. The calculated electronic polarizability and the film density with different [BTMSM/(BTMSM+O_2)] flow rate ratios.

The electronic polarizability rapidly decreases from 4.78 to 4.41 (Fm^2) with increase of the carbon content as shown in Fig. 24. This result means that the electronic dielectric constant would be reduced.

Figure 28 shows the electronic, ionic, and orientation contributions to the dielectric constant of SiOC(-H) film with the variation of BTMSM/(BTMSM+O_2) flow rate ratios. The dielectric constant measured by C-V method (1 MHz) decreases as BTMSM/(BTMSM/O_2) flow rate ratio increases.

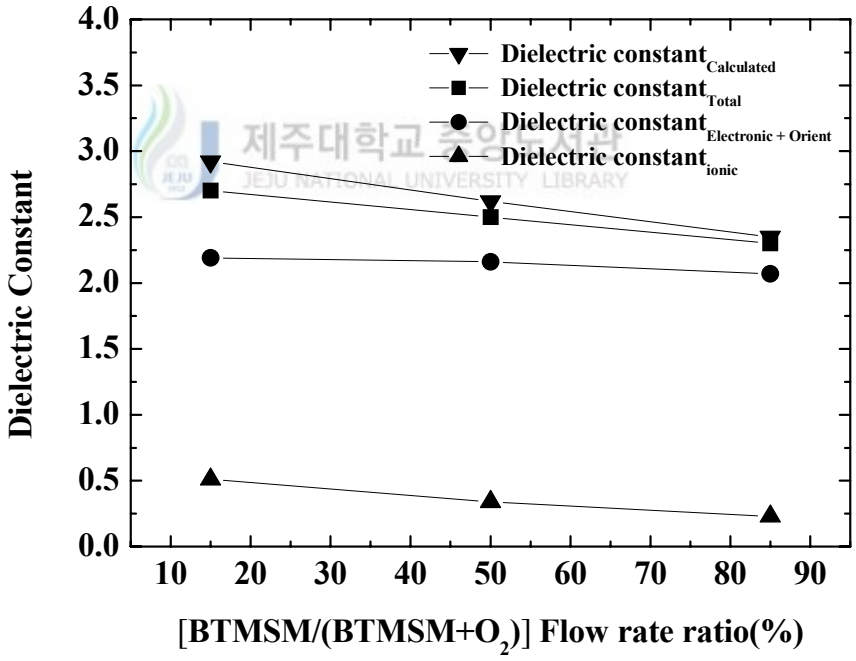

Fig. 28. The orientation, electronic and ionic dielectric constant with different [BTMSM/(BTMSM+O_2)] flow rate ratios.

The lowest relative dielectric constant with flow rate ratio of 85% was 2.3 and the electronic and ionic components (ϵ_{elec} and ϵ_{ionic}) of the dielectric constant have lowest value as 2.01 and 0.23 at this flow rate. The electronic dielectric constant calculated by the Clausius-Mosotti equation is higher than the experimental result by square of refractive index ($\epsilon \approx n^2$, λ= 632.8 nm), and the difference value is 0.28 at BTMSM/(BTMSM/O_2) flow rate ratio of 85%. This result means that the Clausius-Mosotti equation has two components of dielectric properties such as electronic and ionic, whereas obtained

Table 2. The dielectric properties of SiOC(-H) films with different [BTMSM/(BTMSM+O_2)] flow rate ratios.

Carbon Contents (%)	Bonding Angle Between Si-O and Si-C (°)	Dipole Moment ($\times 10^{-29}$ Cm)	Polarizability (10^{-24} Fm^2)	Three components of dielectric constant			ε_{total} (C-V)
				ε_{total} ($\times 10^{15}$)	ε_{ion}	ε_{elec}	
19.6	143.6	3.7918	4.41	2.29	0.51	2.19	2.7
23.0	144.4	3.7916	4.73	2.26	0.34	2.16	2.5
49.6	149.6	3.7899	4.78	2.23	0.23	2.01	2.3

the refractive index has only electronic components dielectric properties at the 632.8 nm. From Eq. (15), we can infer that the ionic dielectric constant was

as 0.23 at BTMSM/(BTMSM+O_2) flow rate ratio of 85%. The dielectric constant of the SiOC(-H) film mainly depends on the electronic contribution, and the reduction of the electronic contribution can be explained by a decrease in the film density.

The carbon contents and the bonding angle, moreover, led to the three components dielectric constant, as summarized in Table 2. The variation of electronic polarizability was caused by the change of O-Si-C bonding angle, which is resulted from the incorporation of carbon contents. The replacement of Si-O by Si-CH_n bonds also plays a role in decreasing the ionic contribution due to the Si-CH_n bond. The higher carbon content corresponds to a lower ionic contribution. The orientation dielectric constant depends on the film structure just like crystal or amorphous [22]. SiOC(-H) composite films were formed amorphous, so that the average dipole moment can be negligible.

4. Mechanical properties of SiOC(-H) films

Figures 29 and 30 show the elastic modulus and hardness of as-deposited SiOC(-H) composite films, which were deposited at room temperature with the [MTMS/(MTMS+O_2)] flow rates. The elastic modulus of as-deposited films decreased from 22.49 to 13.02 GPa when the [MTMS/(MTMS+O_2)] flow rate increased in steps of 10 from 50 to 100% and it was decreased from 9.89 to 7.12 GPa in the annealed SiOC(-H) films. The hardness of as-deposited

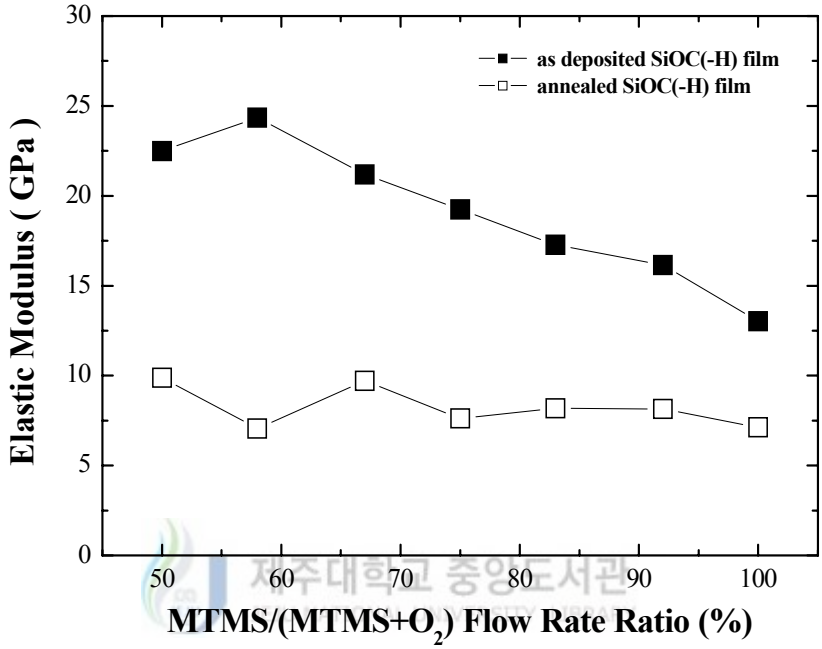

Fig. 29. The elastic modulus of the as-deposited and annealed SiOC(-H) films prepared with different [MTMS+(MTMS/O_2)] flow rate ratios.

films decreased from 22.49 to 13.02 GPa when the MTMS/(MTMS+O_2) flow rate increased in steps from 50 to 100% and it was decreased from 9.89 to 7.12 GPa in the annealed SiOC(-H) films. The reason for this variation is that the incorporation of CH_3 groups breaks the continuity of Si-O-Si networks and forms the nano size voids by the aloof force between CH_3 group and other part of Si-O links. Because the repulsive force between Si-O and Si-C bonds is larger than those between Si-O and Si-C bonds in [SiO_3C]

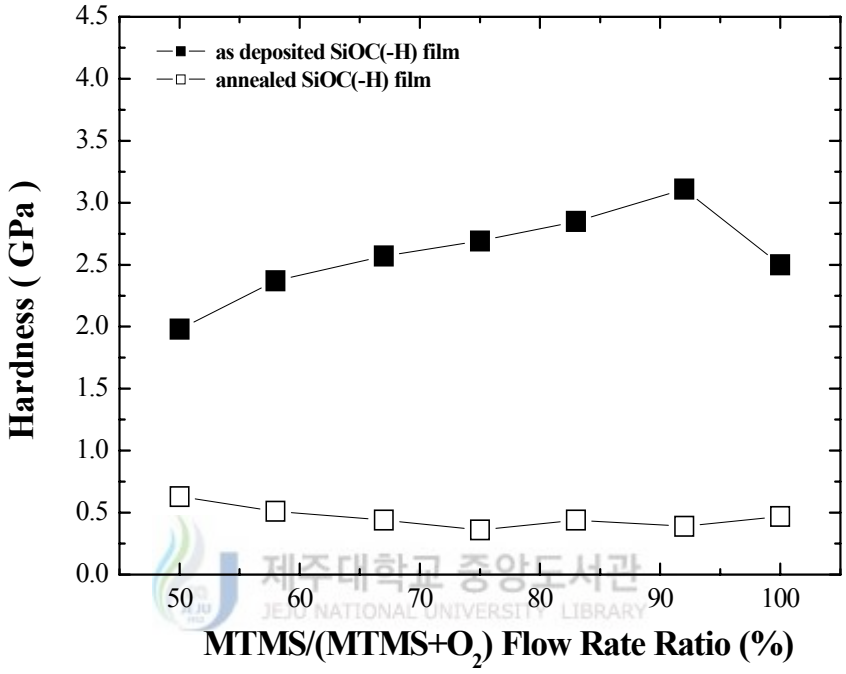

Fig. 30. The hardness of the as-deposited and annealed SiOC(-H) films prepared with different [MTMS+(MTMS/O_2)] flow rate ratios.

tetrahedron due to electro-negativity of carbon atom due to electro-negativity of carbon atom (2.5), which is lower than that of oxygen atom (3.5). The reduced elastic modulus might be the consequence of the decreased in Si-O bonds in a film, which have weak bonding energy and makes the film less dense.

One possible way to extract the elasticity can be via a Johnson analysis for solids of revolution, taking into account the Trecsca criterion, the load (P_y)

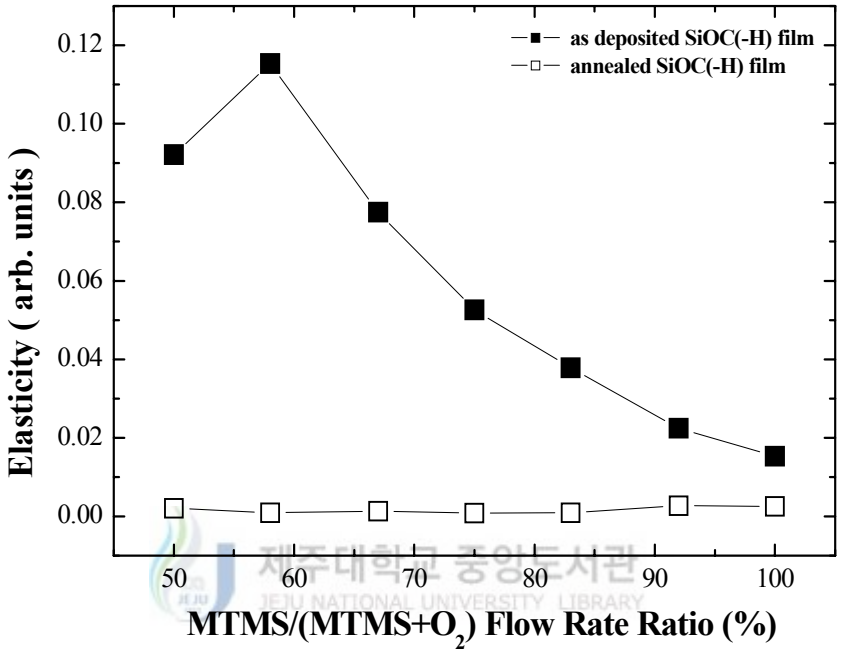

Fig. 31. The elasticity of the as-deposited and annealed SiOC(-H) films prepared with different [MTMS+(MTMS/O_2)] flow rate ratios.

to initial the yield (plastic deformation) is proportional to the term (H^3/E^2); $Py=k(H^3/E^2)$ (where, H is the hardness and E is the elastic modulus). The term H^3/E^2combines the H and E values of a material and sets the amount of elasticity exhibited by the film. In particular, high (low) values of H^3/E^2 means a highly elasticity (H^3/E^2) for the SiOC(-H) films deposited with various MTMS flow rate ratios (see in Fig. 31). The elasticity of as-deposited films decreased as MTMS/(MTMS+O_2) flow rate increased, which is

decreased from 0.11 to 0.01. The elasticity of the annealed SiOC(-H) films changed a little from 0.0009 to 0.002. Since the generation of alkyl group (CO_2) in SiOC(-H) film softens the oxide and make it more polymer like, SiOC(-H) film is more plastic behavior than other films.

This results related with the CH_n components in SiOC(-H) film. To confirm the variation of the area of CO (sp^3) and CO_2 (sp^2) in the C 1s according to [MTMS/(MTMS+O_2)] flow rate ratio and annealing temperature by using Gaussian peak fitting, and the results are shown in Fig. 32 a) and b) for as-deposited and annealed films respectively. The carbon concentrations in the as-deposited film are rapidly increased 16 to 30% when the MTMS/(MTMS+O_2) flow rate increased in steps from 50 to 100%. The concentration of CO(sp^3)/CO_2(sp^2) of as-deposited films decreased from 2.2 to 1.4% when the MTMS/(MTMS+O_2) flow rate increased in steps from 50 to 100%.This result indicates that CH_n group in the MTMS precursor, rapidly combine with oxygen element as increasing oxygen flow rate and the increasing oxygen element generated the CO_2(sp^2) more than CO_2(sp^2) element [16]. The higher portion of alkoxy groups (CO, CO_2) which have relatively poor mechanical property, lead to the higher hardness or elastic modulus[68]. In the case of annealed sample, the concentration of carbon and CO(sp^3)/CO_2(sp^2) were decreased from 14 to 28% and 0.6 to 1.4% respectively. The possible reason for the decreasing of the CO(sp^3)/CO_2(sp^2) concentration is due to the incorporation of more CH_3 groups into the films

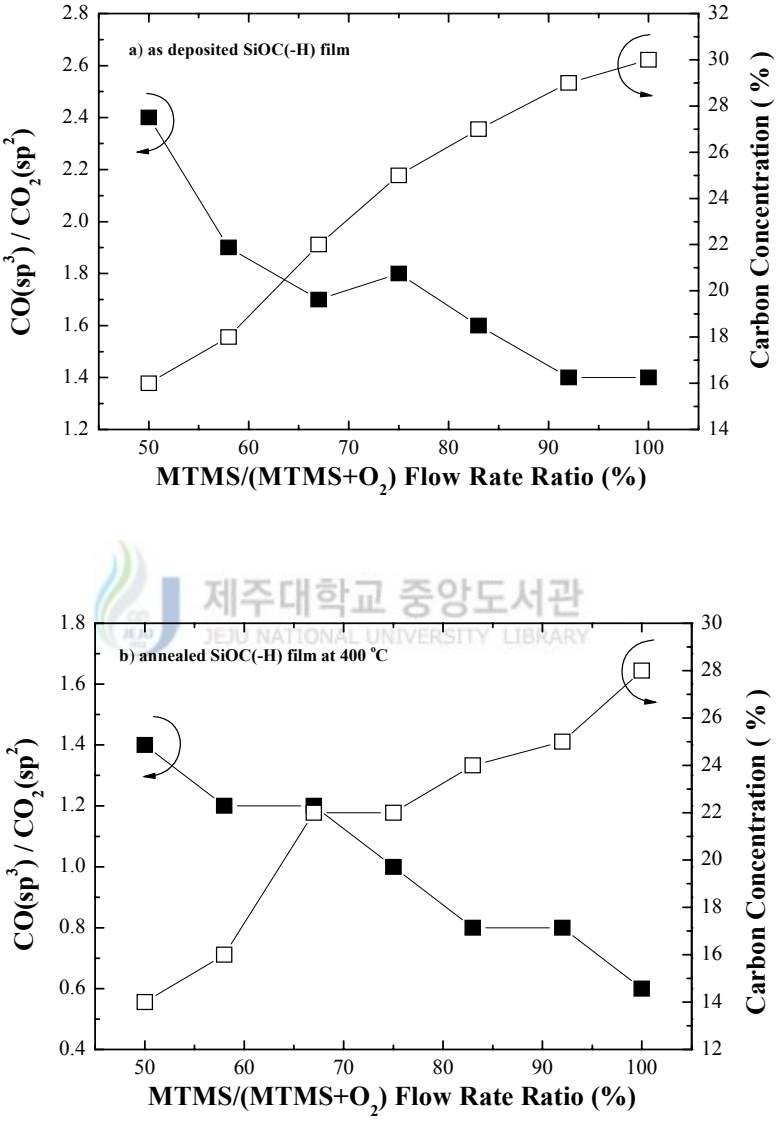

Fig. 32. Relative absorption areas of the $CO(sp^3)/CO_2(sp^2)$ and carbon concentration of a) the as-deposited and b) annealed SiOC(-H) films prepared with different [MTMS+(MTMS/O_2)] flow rate ratios.

when the flow rate ratio of the MTMS precursor is increased. The replacement of Si-O by Si-CH_n bonds can also play a role in increasing the nano-size void. During post annealing, water was removed selectively from the film, without breaking Si-CH_3 bonds. Hence the annealed films have lower dielectric constant than as deposited films. Nevertheless, the nano-size voids affected on the film density, the elastic modulus of the film is proportioned to the film density in general. Therefore, we can infer that the post annealing process would induce the decreasing of the film density or elastic modulus in SiOC(-H) film.

5. Influence of carbon contents by thermal treatment

Figure 33 shows the FTIR spectra of as deposited and annealed SiOC composite films- deposited at room temperature with the O_2/BTMSM flow rates of 3:17 and 17:3 sccm. The spectra are generally broadened and overlapped due to the complex stoichiometry and amorphous nature of the film. It is known that there are Si-CH_3 (889 cm^{-1}, 1276 cm^{-1}), Si-O-Si(C) (from 1000 to 1250 cm^{-1}), CH_n (n=1,2,3) (740 cm^{-1}, 2970 cm^{-1}), and OH-related (1420 cm^{-1}) bonds [24, 26, 32]. The FTIR was taken one month later from the deposition. We obtained the same spectra right after the films were prepared as shown in Fig. 33. From these results, we know that a small amount of un-reacted Si-CH_3 bonds exist in the film, and O-H bonds are formed during the deposition process, because the peak of the O-H bond

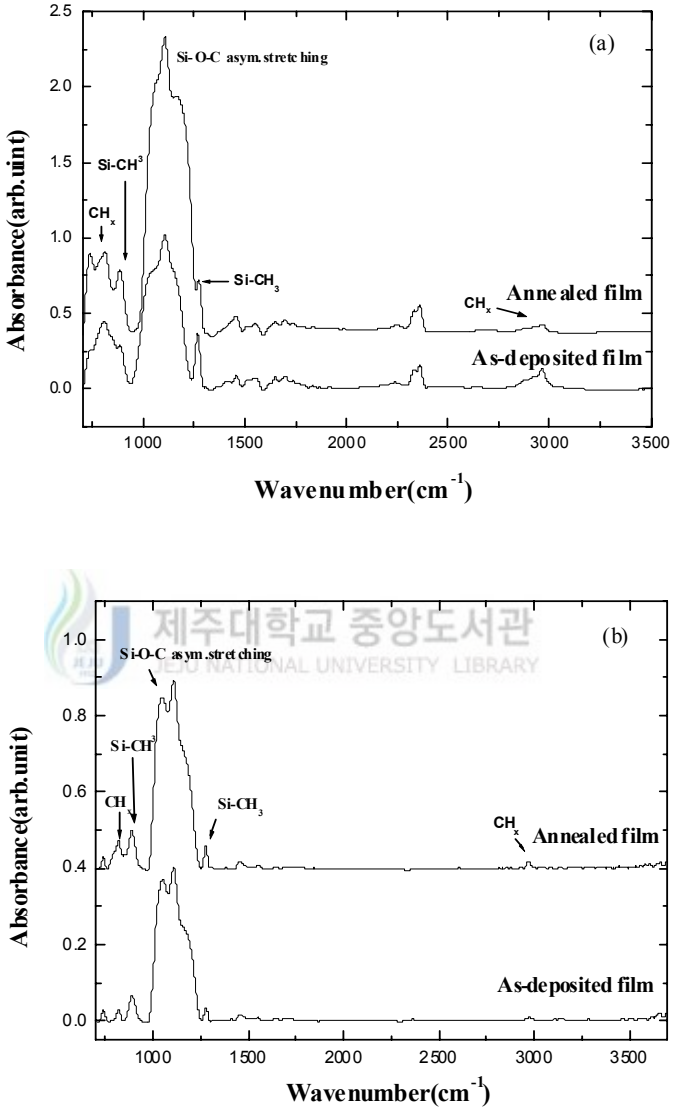

Fig. 33. The FTIR spectra of the as-deposited and annealed SiOC(-H) composite films with the O_2:BTMSM flow rate of (a) 3:17 sccm and (b) 17:3 sccm.

in the annealed film has the same spectra as-deposited film.

In the range from 1000 cm^{-1} to 1250 cm^{-1}, the bonding mode near 1030 cm^{-1} is the Si-O-Si asymmetric stretching mode. The bonding modes near 1104 cm^{-1} and 1180 cm^{-1} are due to Si-O-C asymmetric stretching mode in an open link and Si-C cage-link, respectively. The broad bonding mode at 1171 cm^{-1} and at 1267 cm^{-1} of the as-deposited sample with an O_2/BTMSM flow rate of 3:17 sccm are due to the Si-C cage-like stretching and Si-CH_3 bonding modes, respectively. After annealing, the peaks are shifted to higher wave numbers (blue-shift) of 1197 cm^{-1} and 1277 cm^{-1}, respectively, (to see Fig. 33 (a)). The peak intensity of the Si-CH_3 mode decreases. In the sample with an O_2/BTMSM flow rate of 17:3 (sccm), the peak of Si-O-C asymmetric stretching mode in an open link is shifted to a lower wave number (red shift) [24].

From these results, we can infer that the decrease in peak intensities for the Si-C cage link and Si-CH_3 rocking mode with increased annealing temperature is due to the rearrangement of chemical bonds within the film. Therefore, the peak structure of a clearly separated Si-O-Si and Si-O-C bonds indicates the existence of caged SiC bonds and a reflection of enhanced porosity in the film [43, 45]. As previously mentioned, the voids formed in the film result in a low dielectric constant.

Figure 34 shows the atomic concentrations of the as-deposited and annealed SiOC(-H) film as a function of O_2/BTMSM flow rate ratios. The atomic concentrations of Si, O and C in the as-deposited film are nearly not

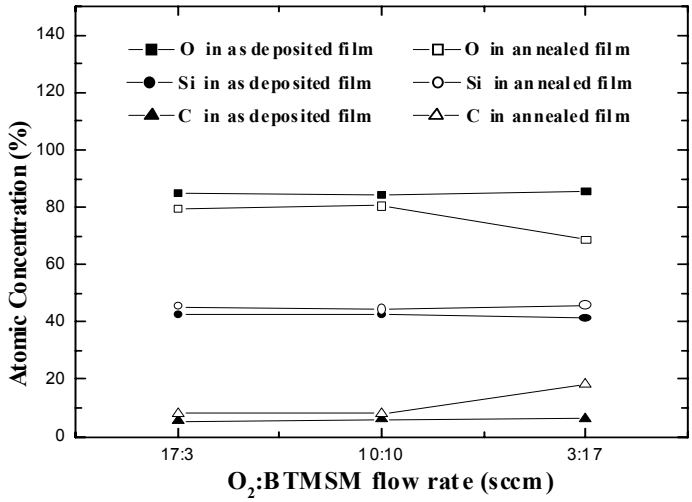

Fig. 34. The Atomic concentration of as-deposited and annealed SiOC(-H) composite films with the various O_2/BTMSM flow rate ratios.

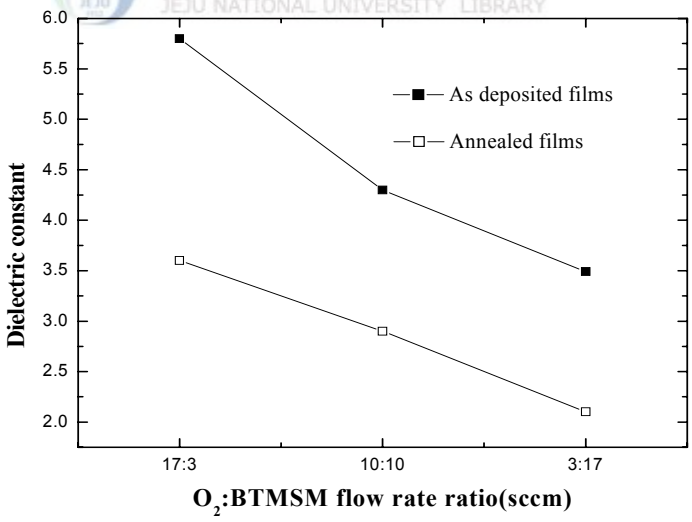

Fig. 35. The Dielectric constants of as-deposited and annealed SiOC(-H) films with the various O_2:BTMSM flow rate ratios.

changed at different gas flow rate ratios. These are composed of about oxygen 70 % , silicon 27 %, and carbon 3 %. In annealed samples, the relative atomic concentration of O decreases, and those of Si and C increase. When the O_2:BTMSM flow rate is 3:17 (sccm), the concentration of O decreases to about 54 %, and those of Si and C increase to about 31 % and 15 %, respectively. These are the same result as FTIR. These results indicate that some CH_x species are removed from the bulk of film due to the annealing process, and it can cause the formation of nano-pores in SiOC(-H) composite film.

The dielectric constants of as-deposited and post-annealing films with various O_2/BTMSM flow rate ratios are shown in Fig. 35. In this figure, the dielectric constants of post-annealed films are lower than those of as-deposited films. The dielectric constant decreases as O_2/BTMSM flow rate ratio decreases; the lowest relative dielectric constant of annealed film with O_2/BTMSM flow rate as 3:17 (sccm) is obtained as approximately 2.1. From these results, we suggest that the dielectric constant of SiOC composite film depends on the relative carbon content. Pore density of the SiOC(-H) film is closely related to film density. The effect of porosity on dielectric constants can be predicted using a simple model such as the Bruggeman effective medium approximation as given by [24] :

$$f_1 \frac{k_1 - k_e}{k_1 + 2k_e} + f_2 \frac{k_2 - k_e}{k_2 + 2k_e} = 0 , \qquad (1)$$

where f_1 and f_2 represent the fraction of the two components, k_1 and k_2 are the dielectric constants of the components, and k_e is the effective dielectric constant of the material. The model assumes two components to the film such as the solid wall materials and voids. Figure 36 shows the dielectric constant as a function of porosity predicted by the model for SiO_2 (k=4.0) and SiOC(-H) (k=3.4) wall material. The solid and dotted lines indicate SiO_2 and annealed SiOC(-H) films. Figure 36 demonstrates that to obtain a given value, significantly less porosity would have to be incorporated into the SiOC(-H) film with lower k than SiO_2. From the results of Fig. 36 using equation (1), the relative porosity of annealed samples with a low dielectric constant of 2.1, 2.9 and 3.6 are 68 %, 35 % and 13 %, respectively. Since a high percentage of porosity in the film can be expected to give a rise in reliability concerns. These results indicate that SiOC(-H) films with higher carbon concentrations obtain greater porosity, which means that pore density depends on the carbon concentration within the film as shown in Fig. 7 and Fig. 36. The CH_3 fragment can also contribute to the formation of a less dense structure in the films. In general, the reason for the lower dielectric constant of the annealed SiOC(-H) films can be interpreted as a change of polarization, which depends on the bonding length between atoms. The bonding length of Si-Cis shorter than the bonding length of Si-O in general because carbon atoms have smaller radius than oxygen atom. Therefore, we know that the ultra low-k values of SiOC film may be related to the porosity and carbon concentrations.

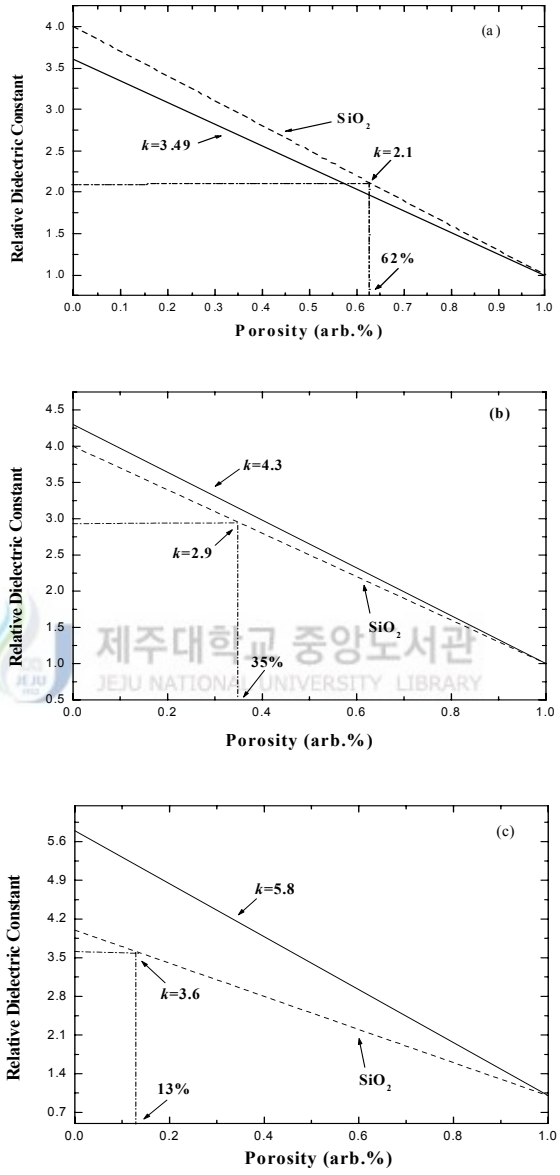

Fig. 36. The relative porosity calculated for annealed films with different dielectric constants. (a) O_2:BTMSM=3:17 sccm (b) O_2:BTMSM=10:10 sccm (c) O_2:BTMSM=3:17 sccm.

Figure 37 shows the cross-sectional transmission electron microscopy (TEM) image of the as-deposited and annealed SiOC(-H) films at 400 ℃ for 30 minutes in a vacuum with O_2/BTMSM=3:17 sccm. In the as-deposited sample, nano size pores were locally formed within the film and do not have uniformity as shown Fig. 33 (a). The annealed sample has many nano-pores, the diameters of which are about 2 nm, regularly distributed from the interface of the SiOC(-H)/Si(100) structure to the surface of the SiOC(H) film. A thin layer clearly seen at the Si-O-C/Si interface is native oxide (to see Fig. 33 (b)). In general, the nano size pore in Si-O-C film deposited using O_2/BTMSM precursors is formed due to the post annealing and deposition temperature. In our as-deposited sample, we infer that the formation of the

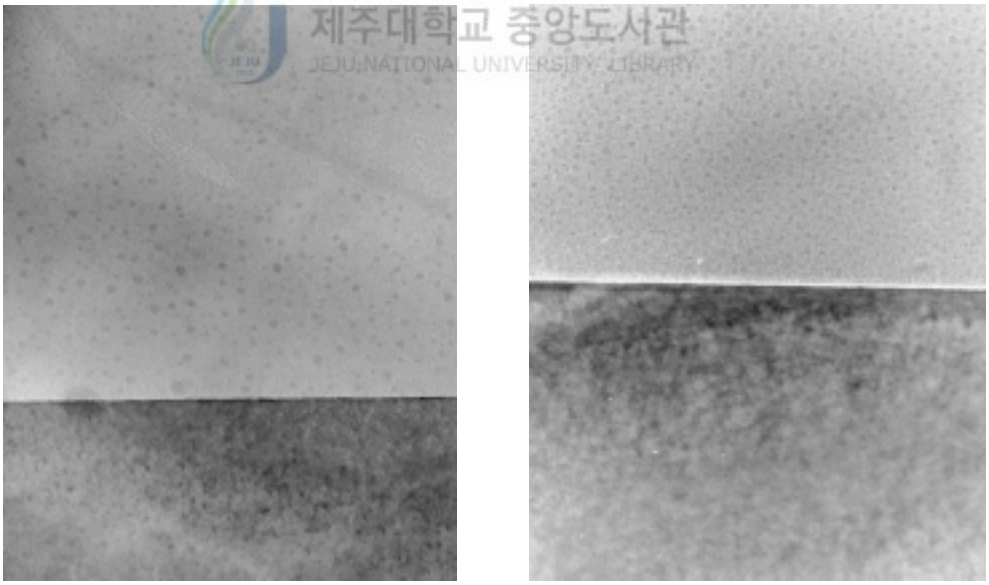

Fig. 37. The cross-sectional TEM image of as-deposited and the annealed SiOC(-H) films with O_2:BTMSM flow rate of 3:17 sccm, (a) as-deposited film and (b) the annealed film at 400 ℃ for 30 minutes in a vacuum.

nano-pore within the film is due to the deposition temperature, which is originated from the substrate heating by plasma during the deposition process. We know that this TEM image can establish the FTIR result. Therefore, it was expected that the dielectric constant of the post-annealed film would decrease to a lower value than that of the deposited film.

6. Plasma Treatment of SiOC(-H) Films

6.1. O_2 plasma ashing

Figure 38 shows the FTIR spectra of as-deposited and annealed SiOC(-H) composite film. The film was deposited at room temperature with a flow rate ratio, [TMS/(TMS+O_2)], of 85% and was annealed at 400 ℃ for 30 min in a vacuum. The spectra are generally broadened and overlapped due to the complex stoichiometry and amorphous nature of the film. Si-CH_3 (914 cm^{-1}), Si-O-Si(C) (from 1000 to 1250 cm^{-1}), and Si-H_2 (740 cm^{-1}) bonds are known to exist. The peaks near 950 cm^{-1} and 1450 cm^{-1} are identified as the Si-CH_3 and CH_3 bonding modes, respectively. The transformation of an open-linked substructure to a ring-linked one may relate to the reduction in OH groups and to the formation of empty space (pore). Moreover, these pores are not filled easily because the number of open links, which readily link with other molecules and fill the void, has decreased.

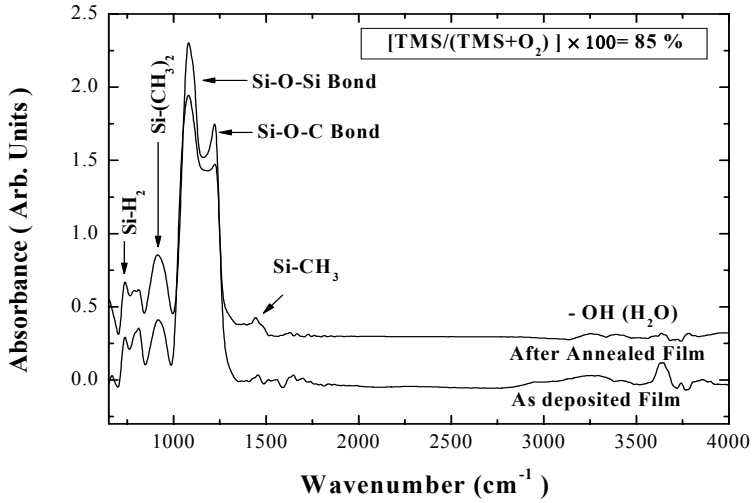

Fig. 38. The FTIR spectra of as-deposited and annealed SiOC(-H) composite films deposited with a flow rate ratio of [TMS/(TMS+O_2)]=85% and after annealing at 400 ℃ for 30 min in a vacuum.

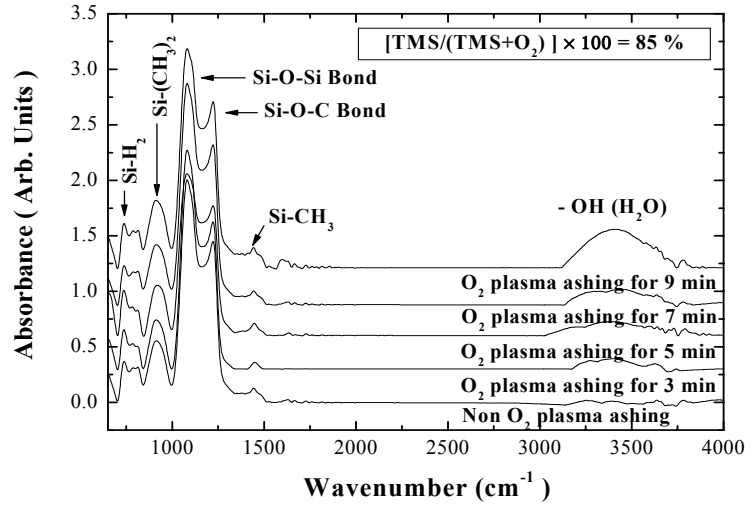

Fig. 39. The FTIR spectra of the same annealed sample with O_2 plasma ashing for 3 to 9 min.

In the integrated process, the photo-resist stripping was implemented conventionally by utilizing O_2 plasma ashing to remove organic elements. Therefore, the impact of O_2 plasma on the quality of SiOC(-H) composite film as the inter-metal dielectric layer is significant. Figure 39 shows the FTIR spectra of the same annealed sample as in Fig. 38 with O_2 plasma ashing for 3 to 9 min. The peak position and area of the Si-O-Si cage like bond, Si-O-C open like bond and related $Si-CH_3$ bond had almost no change, but the intensity of OH-related (from 3200 to 3700 cm^{-1}) bond dramatically increased after O_2 plasma ashing for 7 to 9 min. This result indicates that oxygen radicals, during O_2 plasma ashing, deeply diffuse into the porous inner structure of the SiOC(-H) film to break the Si-C bonds in the SiOC(-H) film. The increase of the Si-OH bond peak intensity has two possible causes [62]. One is that when the oxygen radical break the Si-C bond in the SiOC(-H) film, the SiOC(-H) film can absorb oxygen radicals and $Si-CH_3$ bonds convert into Si-OH bonds. The other is that the defect sites (or dangling bonds surface of the SiOC(-H) film) absorb oxygen radical when the SiOC(-H) film is exposed to the O_2 plasma. The dangling bonds may be easily converted into Si-OH bonds when the dangling bonds are exposed to the environment[51]. The Si-OH bonds in damaged SiOC(-H) films often lead to moisture uptake and as a result the peaks for Si-OH bonds and H_2O appear in the FTIR spectra. Figure 40 shows the leakage current density of the same sample as in Fig. 39 as a function of the electric field strength. The leakage current density increases with increasing duration of the O_2

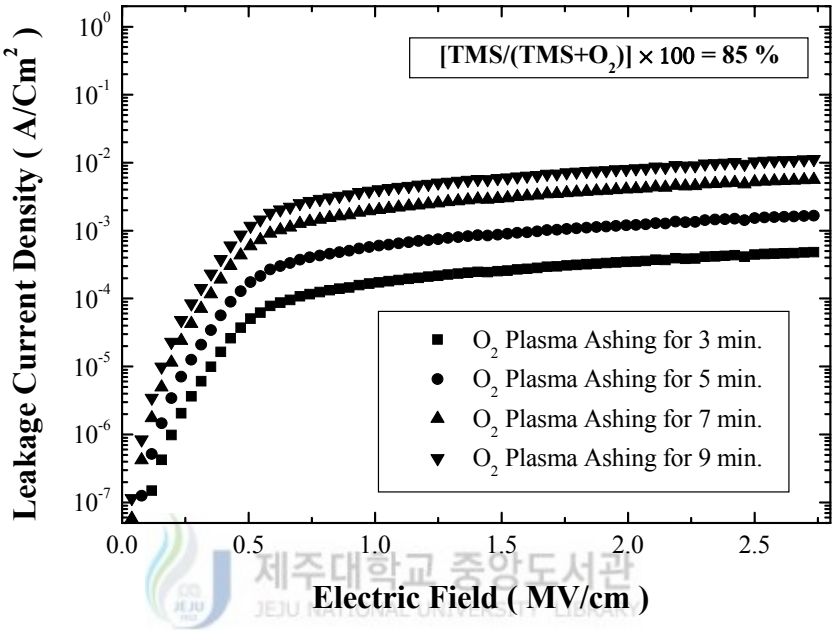

Fig. 40. The leakage current density of the same sample as in Fig. 39 with various electric field strength.

plasma treatment, and the leakage current density at 1 MV/cm^2 increased from 7.3×10^{-5} A/cm^2 to 1.8×10^{-3} A/cm^2 as a function of O_2 plasma treatment time.

6.2. CH_4 Plasma Treatment

The effect of CH_4 plasma post-treatment on SiOC(-H) composite film was investigated. The films, which were deposited at room temperature with a

flow rate ratio of 85% [TMS/(TMS+O_2)] and annealed at 400 ℃ for 30 min in a vacuum, were treated by CH_4 plasma from 3 min to 9 min. Figure 41 shows the FTIR spectra of the SiOC(-H) films after 3 to 9 minutes O_2 plasma ashing. The bonding structures of the SiOC(-H) composite films are similar to Fig. 39. But the intensity of OH-related bond, Si-CH_3 and Si-OH bonds decreased a little bit compared to Fig. 39. These results mean that C and H radicals, in CH_4 plasma state, are reacted with the dangling bonds in

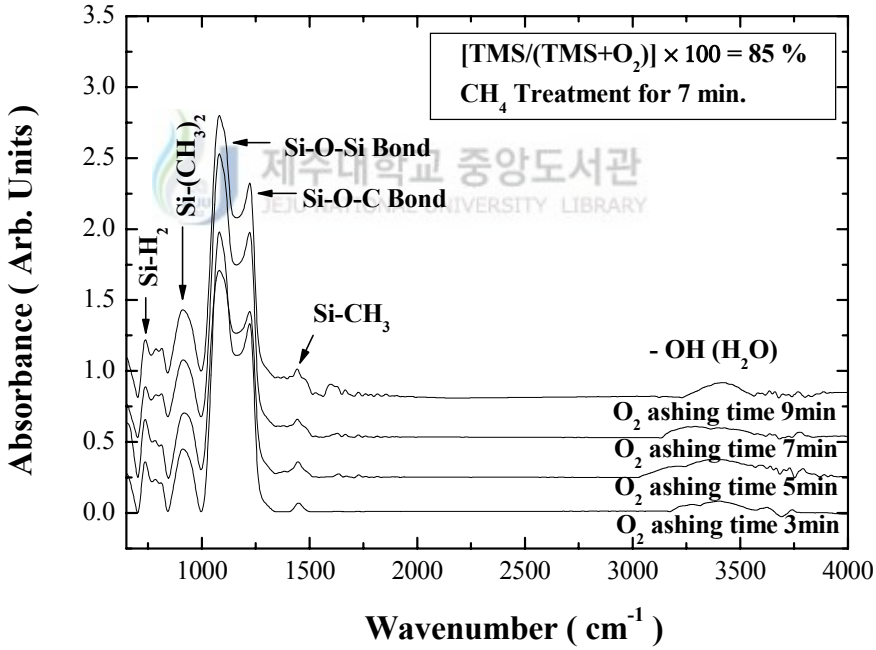

Fig. 41. The FTIR spectra of the SiOC(-H) film with O_2 plasma ashing for 3 to 9 min., which was deposited at room temperature with a flow rate ratio of 85% [TMS/(TMS+O_2)] and after annealing at 400 ℃ for 30 min in a vacuum and treated by CH_4 plasma treatment for 3 to 9 min.

the SiOC(-H) film. Therefore, the Si-OH bonds not only decreased to repair the damaged SiOC(-H) films, but also react with C and H atoms to form Si-O-Si and Si-O-C chain structures. So the $Si-CH_3$ bonds are hydrophobic that surface of the SiOC(-H) film can be more hydrophobic by CH_4 plasma treatment. The hydrophobic surface will reduce the moisture uptake. To confirm the variation of the integrated absorption area of Si-O-C, Si-O-Si and $Si-CH_3$ bonds according to O_2 plasma ashing time from the results of Figs. 39 and 40. We deconvoluted the spectra in the range from 900 to 1500 cm^{-1} by using several Gaussian peaks, and the relative area ratio (%) of Si-O-C, Si-O-Si and $Si-CH_3$ bonds is shown in Fig. 42. The relative area of the $Si-CH_3$ bond decreased slightly during O_2 plasma The relative area of the $Si-CH_3$ bond decreased slightly during O_2 plasma ashing, which the sample with CH_4 plasma treatment decreased from 0.76 to 0.72 %, and the non-treatment sample decreased from 0.76 % to 0.65 % (see Fig. 42 (a)). Figure 42 (b) show that the relative area ratio (%) of Si-O-C and, Si-O-Si bonds with CH_4 plasma treatment and non-treatment samples as a function of O_2 plasma ashing time. The variation of the relative area ratio (%) of Si-O-C bond developed a similar tendency as $Si-CH_3$ bond, but the relative area ratio (%) of Si-O-Si bond increased during O_2 plasma ashing. From these results, we know that the variation of the relative area ratio (%) of SiOC(-H) film with CH_4 plasma treatment are a little bit smaller than that of non-treatment SiOC(-H) film. Therefore, CH_4 plasma treatment on SiOC(-H) film suggests that the carbon radical contributed to be react Si dangling bonds in SiOC(-H)

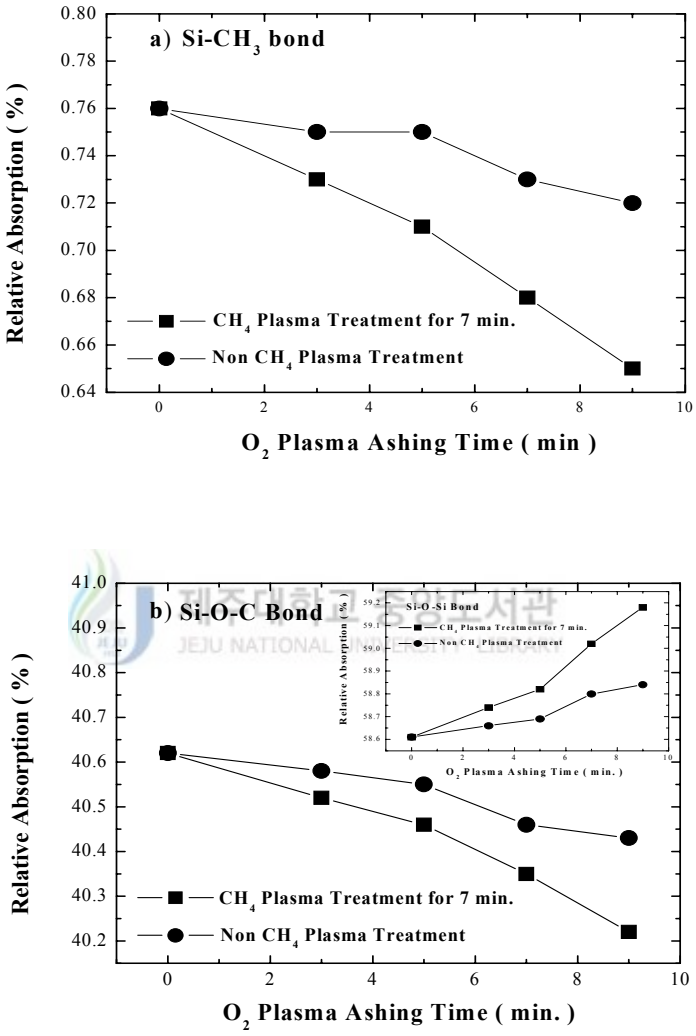

Fig. 42. a) The relative area ratio (%) of the Si-CH_3 bonds (peak area/total area of spectrum between 900 to 1500 cm^{-1}) for the results fitted Figs. 40. b) The relative area ratio (%) of the Si-O-C and Si-O-Si bonds (peak area/total area of spectrum between 900 to 1500 cm^{-1}) for the results fitted Figs. 39 and 41.

and the hydrogen radical broken bonds, and the recombination of C and H atoms on the SiOC(-H) film is attributed to a structural change due to the formation of Si-H and Si-C bonds.

Figure 43 shows the leakage current density of the same sample as in Fig. 41 as a function of the electric field strength. The variation of the leakage current density during O_2 plasma ashing developed a similar tendency as shown in result of Fig. 43. The leakage current density at 1 MV/cm^2 increased from 2.6×10^{-9} A/cm^2 to 2.02×10^{-8} A/cm^2 during as a function of O_2

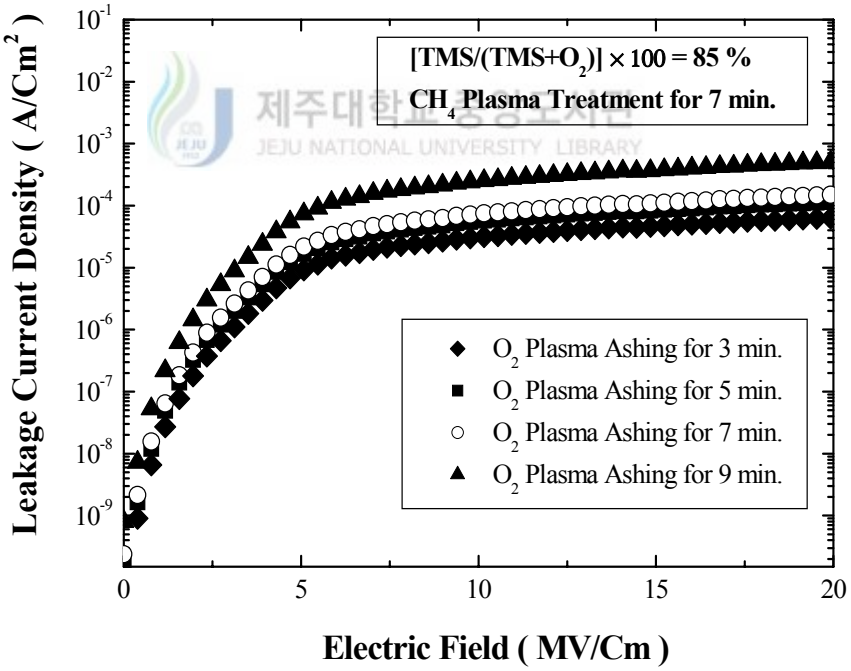

Fig. 43. The leakage current density of the same sample as in Fig. 41 with various electric field strength.

plasma treatment time. From Figs. 40 and 42 results, we know that the leakage current density at 1 MV/cm^2 of CH_4 plasma treatment samples was a lower of the order of 4 and 5 than that of non-treatment samples. These results can infer that CH_4 plasma can repair the damaged structure in the SiOC(-H) film and reduce both the leakage current density after the photo-resist removal process.

The dielectric constant of CH_4 plasma treatment and non-treatment samples of O_2 plasma ashing time were shown in Fig. 44. The dielectric constant

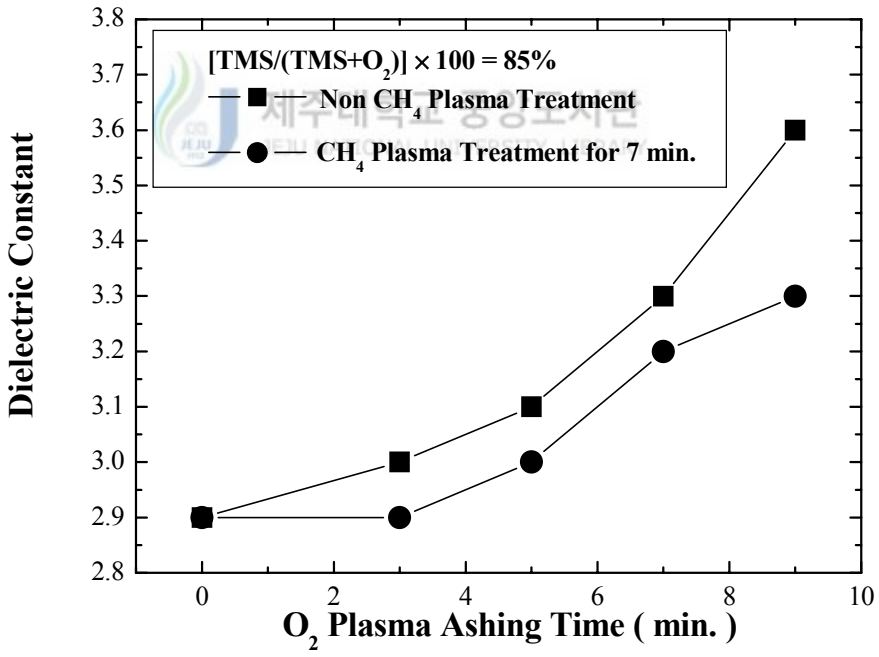

Fig. 44. The dielectric constant of CH_4 plasma treatment and non-treatment samples with various O_2 plasma treatment time.

constant of samples without CH_4 plasma treatment increased from 2.9 to 3.6 as O_2 plasma treatment time, and the dielectric constant of samples with CH_4 plasma treatment slightly increased from 2.9 to 3.3. In non-treatment CH_4 plasma sample, the increase of the dielectric constant of 3.6 in O_2 ashing time at 9 min are due to conversion of $Si-CH_3$ bonds into Si-OH bonds when O_2 plasma is applied to SiOC(-H) film. Because the OH-related bonds are increased the dielectric constant of SiOC(-H) film. This result is in accord with FTIR spectra in Fig. 39 and Fig. 41. Therefore, we know that the electrical properties of the SiOC(-H) film becomes unstable after O_2 plasma ashing process [45]. The dielectric constant variation of the SiOC(-H) films with CH_4 plasma treatment during O_2 plasma ashing process are lower than that of films samples with non-treated CH_4 plasma. This high resistance of the post-treated SiOC(-H) films to an oxygen plasma might result from an blocking the diffusion of oxygen elements. This indicates that the CH_4 plasma can resist the surface of SiOC(-H) film by O_2 plasma and reduce both the leakage current density and dielectric constant after the photo-resist removal process.

7. Characteristics of SiOC(-H) Films using UV-assisted PECVD

7.1. Characteristics of UV-assisted plasma

7.1.1. Electrical properties of UV-assisted plasma

In general, low pressure rf discharge plasma shows non-equilibrium conditions. Thus, they shows an essential departure from a Maxwellian energy distribution. Single Langmuir probe diagnostics methods are ideally suitable for plasma parameters measurement in low pressure gas discharge. A modification of this method, known as the Druyvesteyn method, where the EEPF is inferred from the second derivative of the probe current-voltage (I-V) characteristics is used to measure EEPFs in low pressure gas discharge plasma. It is well known that the Langmuir probe method and validity fo the Druyvesteyn formula are assumptions of a small probe and a collisionless probe sheath. For a cylindrical probe used in common practice this means; $a[\ln(l/2a)] \ll \lambda_e$, and $\lambda_D \ll \lambda_e$, where a is the probe radius, l is probe length, λ_e is the electron mean free path and λ_D is the electron Debye length. Measuring probe I-V properties, we can get electron energy distribution function (EEDF) using as given by :

$$g_e(V) = \frac{2m}{e^2 A}\left(\frac{2eV}{m}\right)^{1/2}\frac{d^2 I_e}{dV^2}, \tag{18}$$

where A is probe area, m is electron mass and $V(V_p - V_b)$ is differential between plasma potentials and probe bias potential. The electron energy

probability function, $g_p(\epsilon) = \epsilon^{-\frac{1}{2}} g_e(\epsilon)$ is sometimes introduced instead. We can calculate electron density (n_e) and effective electron temperature (T_{eff}) from the EEPF.

$$n_e = \int g_e(\epsilon)\, d\epsilon, \tag{19}$$

$$T_{eff} = \frac{3}{2}\frac{1}{n_e}\int \epsilon g_e(\epsilon)\, d\epsilon, \tag{20}$$

Figure 45 shows probe current-voltage characteristics and EEPF with and without UV irradiation for Ar gas. The distribution is characterized by the high-temperature low-energy electron group and the low-temperature high-electron group. As the UV irradiate, the low-energy high-temperature electron group reduced. This result shows that the electrons gain the energy from UV light and the excited electrons collided with ion or radical and transfer the energy each other. The energetic electrons are lost to the electron energy cause inelastic collision with excited radicals. This result means that the electron collided with ion or radical on the energy transfer each other.

The electron densities of various mixed gases for different rf power are shown in Fig. 46. The plasma density remains an approximately constant ~10^9 cm^{-3}, until rf power increase up to 300 W. When the non-UV light

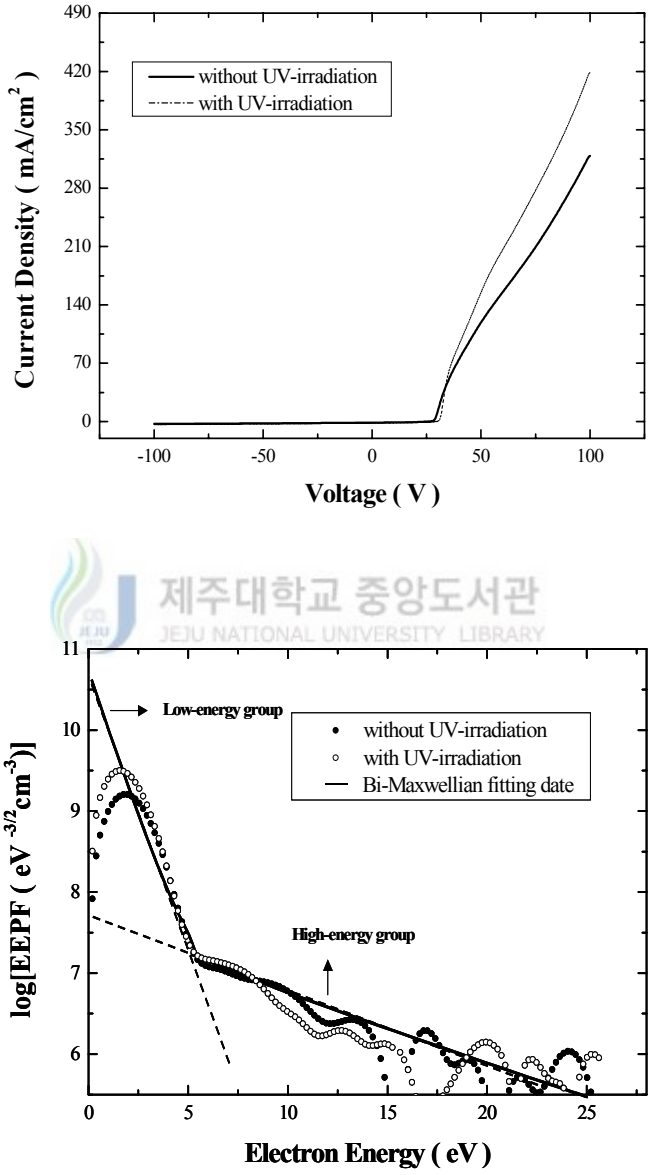

Fig. 45. I-V , EEPF curve for Ar plasma with and without UV irradiation.

irradiate, the electron density rapidly increase using mixed He gas than others gases. The electron density varied 4.45×10^{-9} cm^{-3} to 9.4×10^{-9} cm^{-3} with various mixed gases. The important point for a high degree of ionization is

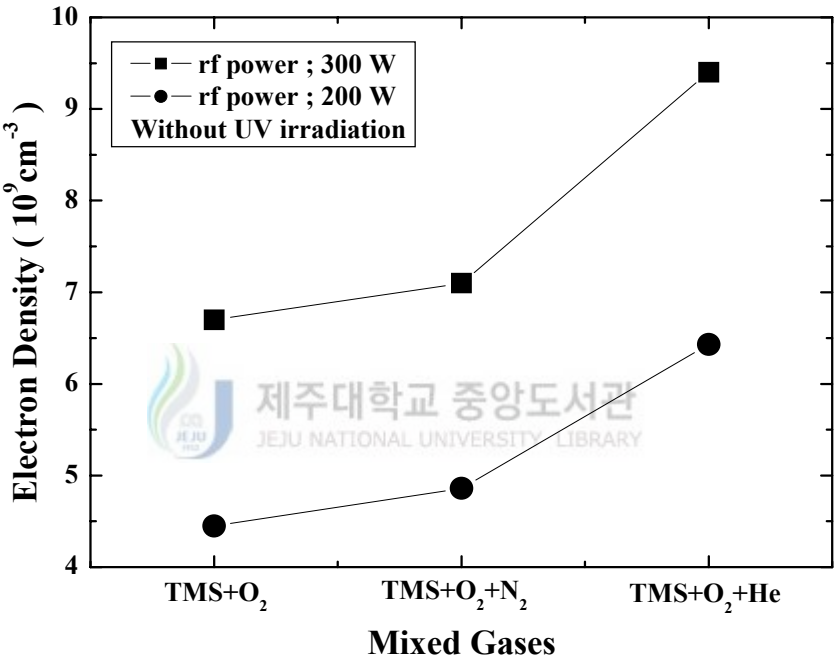

Fig. 46. Electron density of the plasmas without UV irradiation for several gas mixtures and various rf power.

efficient production and preservation of energetic electrons. In this case, the increase in the electron density with a mixing ratio is mainly due to the large inelastic cross section of mixed He gas. Figure 47 shows the electron densities of various mixed gases for different rf power with UV irradiation. At

UV irradiation with rf power using He mixed gas, the electron density has maximum value about ~10^{10} cm^{-3}. This is also explained by the fact that the large inelastic cross section of mixed He gas than N_2 mixed gas. Moreover, the dissociation cross section is larger than the ionization cross section. Thus,

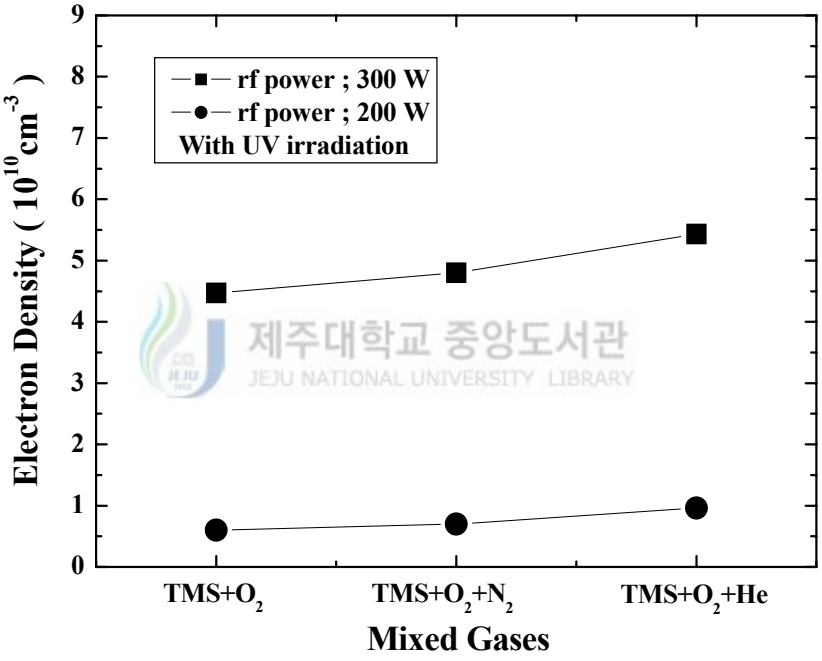

Fig. 47. Electron density of the plasmas with UV irradiation for several gas mixtures and various rf power.

increasing rf power or mixed He gas effected increasing the electron density.

Figure 48 shows the electron temperature of plasmas with and without UV light irradiation for several gas mixtures. The electron temperature varied

from 7.9 eV to 3.21 eV with various mixture gases such as N_2 and He in TMS/O_2 precursor. When an UV irradiation with He mixture gas, the electron temperature dramatically decrease than other method such as N_2 mixture gas and the non UV irradiation. The electron temperature is lowest with He mixture

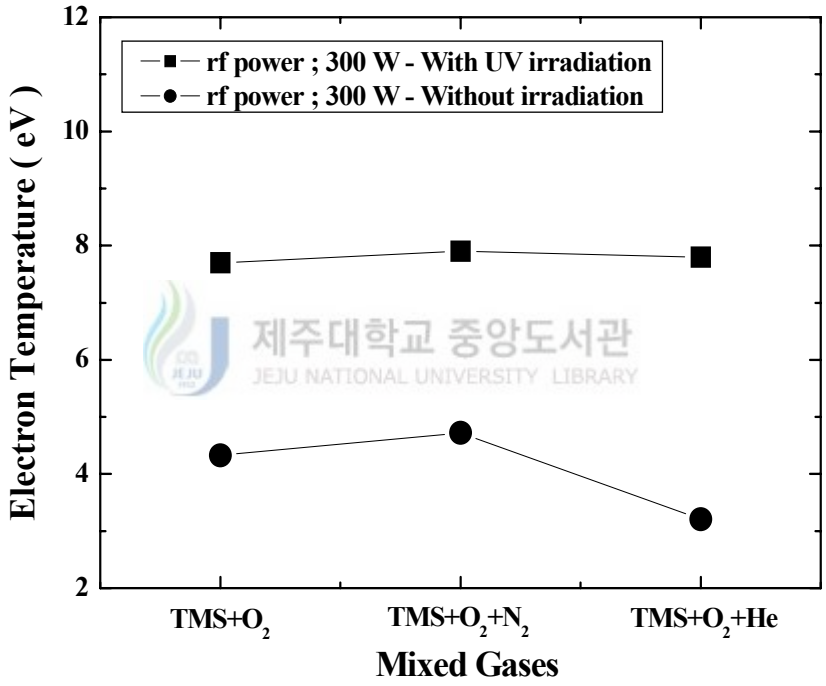

Fig. 48. Electron temperature of the plasmas with and without UV irradiation for several gas mixtures and various rf power.

gas (about 3.21 eV) and highest in N_2 mixture gas (about 7.8 eV). The effective ionization threshold energies is the function of the electron temperature. It means that the high electron temperature of N_2 plasma is due

to the high ionization threshold energy of N_2 mixture gas than He mixture gas. This result shows that the electrons gain the energy from UV light and the excited electrons collided with ion or radical and transfer the energy each other. The energetic electrons are lost to the electron energy cause inelastic collision with excited radicals. This result means that the electron collided with ion or radical on the energy transfer each other. The electron density increases when the gases, especially He, are added to the mixture of TMS and oxygen.

Figure 49 shows the electron density of the plasmas without and with UV light irradiation for various gas mixtures such as BTMSM+O_2 and BTMSM+O_2+He when the discharge power is 500, 600 and 700 W. The electron densities were about ~10^9 cm^{-3} and increased very slightly with the rf power. The electron density of plasma generated from the precursor mixture including He gas was greater than that without He. At an rf power of 700 W, the electron density of plasma with the BTMSM+O_2 mixture was 2.8×10^9 cm^{-3}, while that with the BTMSM+O_2+He mixture was 5.2×10^9 cm^{-3}. The increased electron density with He is mainly due to the large inelastic cross-section of He gas [65]. Therefore, we can infer that the efficient production and preservation of energetic electrons is important for a high degree of precursor ionization. The electron density of the plasma had a maximum value of 9.8×10^9 cm^{-3} with UV irradiation with an rf power of 700 W with the He mixture. The result in Fig. 49 shows that the electron density of the plasma with UV irradiation was higher than that without UV

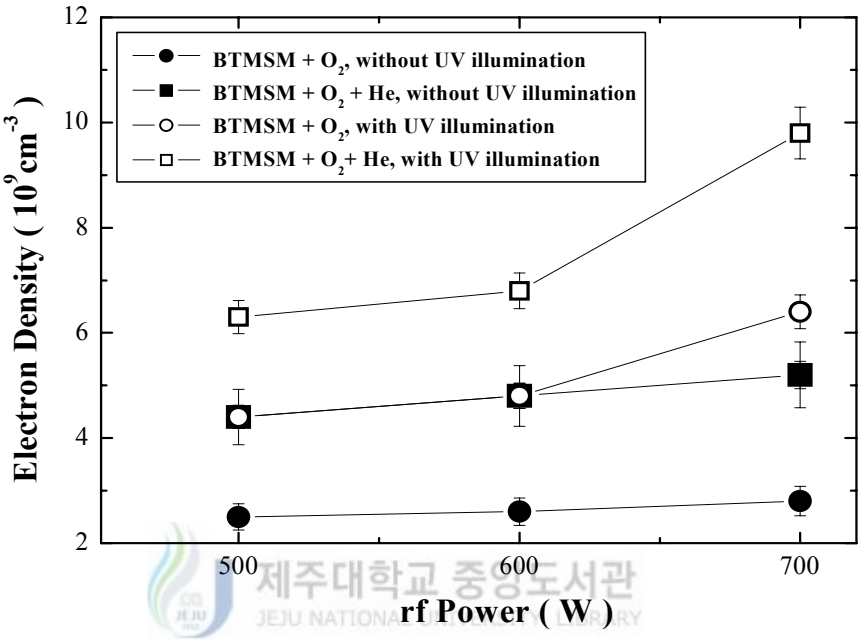

Fig. 49. Electron density of the plasma without and with UV light irradiation for the BTMSM+O_2 and BTMSM+O_2+He mixtures at rf powers of 500, 600 and 700 W.

irradiation. This occurs because UV photons can excite the energy states of the precursors, increasing the number of radicals, including silane (SiH_4) and methyl (CH_n) groups with dissociative electrically excited states; abundant radicals and ions were generated in the presence of UV irradiation. Therefore, more radicals form with UV irradiation. Figure 50 shows the electron temperature of the plasmas with and without UV irradiation for different gas mixtures, and the rf discharge was set up at 500, 600, and 700 W. When

the rf power was 700 W, the electron temperature of the plasma was lower than that at 500 and 600 W. The electron temperature of the plasma was much lower with He gas than without He. In the unirradiated plasma, the electron temperature of the plasma with the BTMSM+O_2 mixture decreased from 7.0 to 6.4 eV as the rf power increased, while the electron temperature of the plasma with BTMSM+O_2+He was 1.98 eV at 700 W. The electron temperature of the plasma with UV irradiation of BTMSM+O_2+He decreased

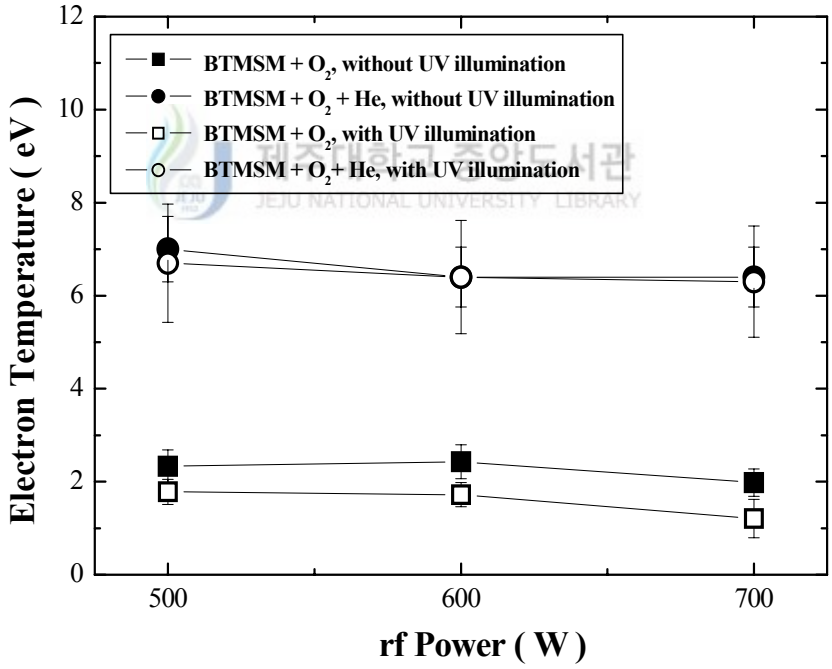

Fig. 50. Electron temperature of the plasma without and with UV irradiation for the BTMSM+O_2 and BTMSM+O_2+He mixtures at rf powers of 500, 600 and 700 W.

from 1.7 to 1.2 eV as the rf power increased, and was about 1.2 eV at an rf power of 700 W. This electron temperature was much lower than that of conventional PECVD. Generally, the effective ionization threshold energy is a function of the electron temperature. From Fig. 50, the high electron temperature of O_2 plasma is due to the high ionization threshold energy of O_2 gas, rather than He gas. This means that the electrons gain energy from UV light and the excited electrons collide with ions or radicals and energy transfer takes place. Electron energy involves inelastic collisions with excited radicals. Therefore, the electron density increases when gases such as He are added to the mixture of BTMSM and oxygen (see Fig. 49).

7.1.2. Optical properties of UV-assisted plasma

As mentioned in Section 1, UV irradiation is responsible for the dissociation of Low-*k* precursor molecular. The emission intensity of OES for with and without UV irradiation are shown in Fig. 51 using MTMS precursor. It is known that there are CO^{+2} (402 nm), OH (430 nm), CH_n (n=1,2,3) (477 nm), CO (515 nm) and O-related (654 nm) species. When the with UV irradiate, the intensity of CO^{+2}, CH_n, CO species rapidly increase than that of without UV irradiation. In Fig. 51, the ratio of the CH species and CO intensities is shown as a function of the UV irradiation. The CH species is the origin ion of either the molecule $Si(CH_3)_3$ or the radical CH_3Si.

A clear enhancement of the species is seen, when the UV irradiated, indicating

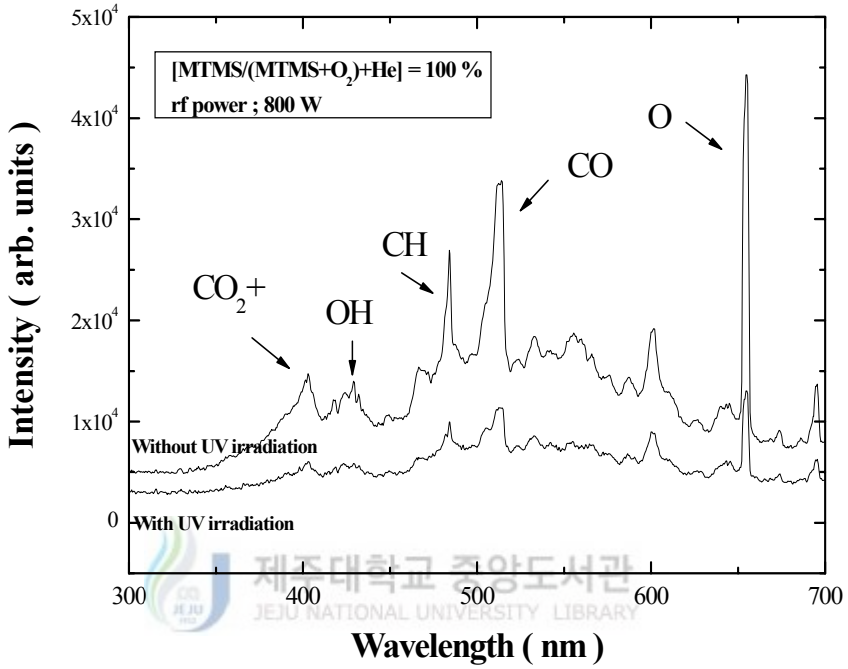

Fig. 51. Emission intensity of the plasma without and with UV irradiation for the MTMS+O_2+He mixtures at rf powers of 800 W.

that $[Si(CH_3)_3]^+$ or $[CH_3Si]^+$ are more generated than that of without UV irradiation. Figure 52 shows the integrated emission intensity of the plasma without and with UV irradiation as a function of rf power as given by :

$$I \propto k[n_e A], \tag{21}$$

where, I is the emission intensity, k is a proportional factor, n_e is the plasma density and A is the density of ion or radical species. When compared

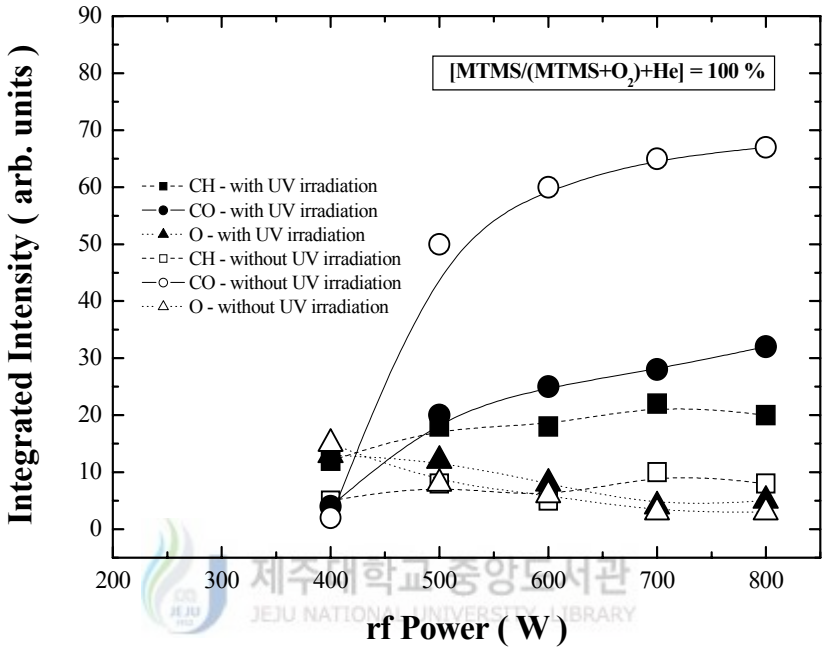

Fig. 52. The integrated emission intensity of the plasma without and with UV irradiation as a function of rf power.

with the relative intensities of the related ion species, the peak intensities of the CH and CO fragments increased as UV irradiation, but the intensity of the O species decreased. From these results, we can infer that the increase in peak intensity for the CH and CO fragments with UV irradiation is due to the abundance of radicals such as CO*, CH_n* etc, within UV assisted plasma. It means that the UV irradiation can selectively produce Si-C* or Si-O* radicals. Figure 53 shows the integrated emission intensity of the plasma without and with UV irradiation as a function of MTMS flow rate ratios.

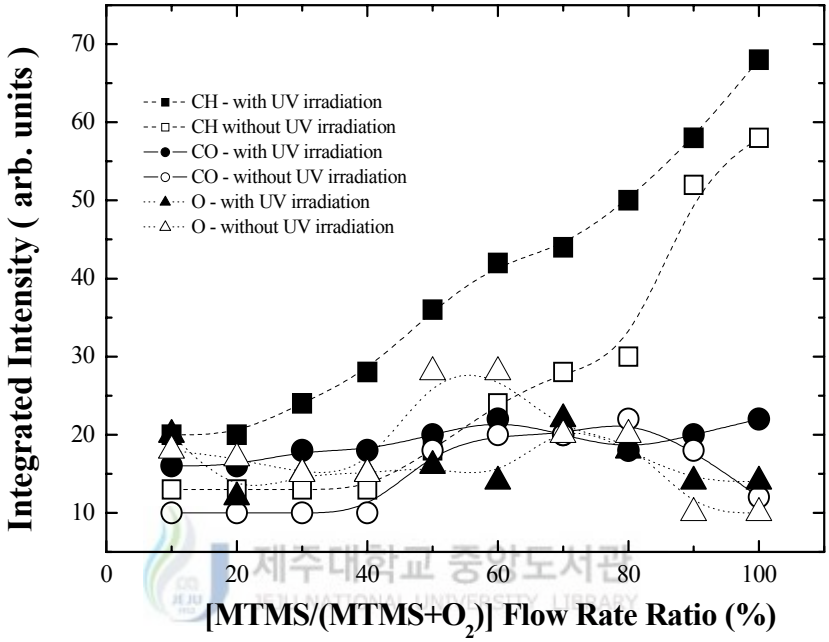

Fig. 53. The integrated emission intensity of the plasma without and with UV irradiation as a function of MTMS flow rate ratios.

The relative emission intensity is similar to that of Fig. 52. The peak intensities of the CH and CO fragments increased as UV irradiation and increasing of MTMS flow rate, but the intensity of the O species decreased. It is means that the UV irradiation can selectively produce Si-C* or Si-O* radicals. However, the peak structure for clearly increased Si-O-C asymmetric stretching mode indicates the existence of caged Si-C bonds and is a reflection of enhanced porosity in the film. Therefore, when the film surface

is irradiated with UV light suggests that the carbon radical increased than non-UV plasma, and the more combination of C and H atoms on the SiOC(-H) film is attributed to a structural change due to the formation of Si-H and Si-C bonds.

From this result, the reaction in Scheme 1 show the possible dissociation of MTMS molecules in the expanding thermal plasma : a charge exchange occurs between the He+ and the MTMS molecules can dissociate at the Si-O, Si-C or C-H bond. The Si-O bond of the MTMS molecules is broken preferably, at least in conditions for which [He+] + UV $\leqq$ [MTMS]. The cleavage of the Si-O bond in the gas phase is not desirable as this bond represents the 'mechanical strong' backbone for the deposition of scratch-resistance $SiO_xC_yH_z$ films.

$$CH_3Si(OCH_3)_3 + He + UV \rightarrow CH_3Si(OCH_3)_3 + He^+ + UV$$

$$CH_3Si(OCH_3)_3 + He^+ + UV \rightarrow [CH_3Si(OCH_3)_3]^+ + He$$

$$[CH_3Si(OCH_3)_3]^+ + e^- \rightarrow \begin{cases} CH_3SiO + SiO_2(CH_3)_3 \rightarrow CH_3 + SiO + O_2Si(CH_3)_3 \\ CH_3SiOSiCH_3 + (CO)_2 + CH_3 \\ CH_3SiOSiCH_3 + CO_2 + OH + (CH)_2 \end{cases}$$

Scheme 1. The possible dissociation route of MTMS with UV irradiation.

7.2. Characteristics of SiOC(-H) Film by UV-assisted PECVD

7.2.1. Deposition rate of UV-assisted PECVD

Figure 54 shows the deposition rate of SiOC(-H) films and electron temperature of the plasmas for three kinds of mixed precursors with UV irradiation and non-UV irradiation at 300 W rf power. The deposition rate is 310 nm/min for the mixture of TMS and O_2, and it is increased to 320 nm/min

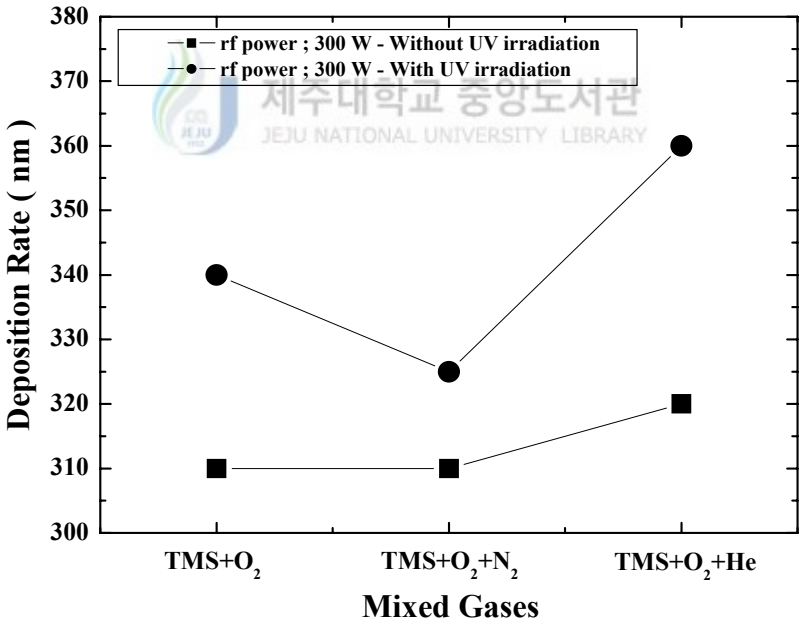

Fig. 54. The deposition rates of SiOC(-H) with and without UV light irradiation for several gas mixture.

for the mixture of TMS/O_2 and He without UV irradiation. In this case, the deposition rate is almost proportional to the electron density and it is increased about 10 % with He addition. This is caused by the results as shown the Fig. 47, it means that the increase in the deposition rate with a mixing ratio is mainly due to the large inelastic cross section of mixed He gas. The deposition rate for the mixture of TMS/O_2, TMS/O_2/N_2 and TMS/O_2/N_2 are 340 nm/min, 325 nm/min and 360 nm/min, respectively, when the film surface is irradiated with UV light produced by a Hg lamp (225 nm < λ < 500 nm,

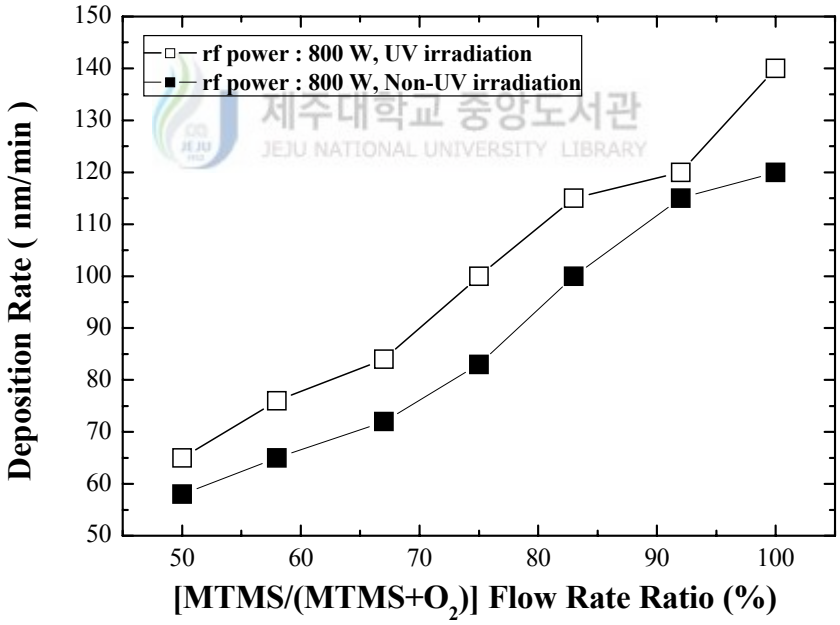

Fig. 55. The deposition rate of SiOC(-H)film with and without UV irradiation as a function of [MTMS/(MTMS+O_2)] flow rate ratios.

irradiation density = 0.6 mW/cm^2). The deposition rate for the mixture of TMS, O_2 and N_2 is slightly less than that of TMS and O_2 in spite of the increased electron density. By the UV irradiation, the deposition rate increases about 10 to 15 %. Figure 55 shows the deposition rate of SiOC(-H) films for [MTMS/(MTMS+O_2)] flow rate ratio with and without UV irradiation. The deposition rate of the SiOC(-H) film increased proportionally as a function of flow rate ratios. The deposition rate of the films with UV irradiation is higher about 10 to 15 % than that of films without UV irradiation. In general, the thickness of the SiOC(-H) film deposited using PECVD method depends on the plasma density and the electron temperature. From this result, we can infer that the electron density increase and more radicals are produced when the UV light irradiates the bulk plasma. The silane (SiH_4) and methoxy (OCH_n) groups exist as dissociative electronically excited states and the UV irradiation generated abundant radicals and ions. The UV photon can excite the energy states of the precursors and the increase of radicals can occur. It means that the silane (SiH_4) and methyl group (CH_n) show dissociative electronically excited states and the abundant radicals and ions were generated UV irradiation.

7.2.2. FTIR analysis

Figure 56 shows FTIR spectra of without UV irradiation and UV TMS/O_2 irradiation SiOC(-H) composite films deposited at room temperature with

TMS/O_2 flow rate of 50 %. The spectra are generally broadened and overlapping due to the complex stoichiometry and amorphous nature of the film. It is known that there are $Si-CH_3$ (889 and 1276 cm^{-1}), Si-O-Si(C) (from 1000 to 1250 cm^{-1}), CH_n (n=1,2,3) (740 and 2970 cm^{-1}) and OH-related bonds. In the range from 1000 to 1250 cm^{-1}, the bonding mode near 1030 cm^{-1} is the Si-O-Si asymmetric stretching mode. Figures 57 and 58 shows the FTIR spectra of the SiOC(-H) films without and with UV irradiation, which is deposited with $BTMSM+O_2$ and $BTMSM+O_2$+He mixture gases at rf powers of 500, 600, and 700 W. The films contain

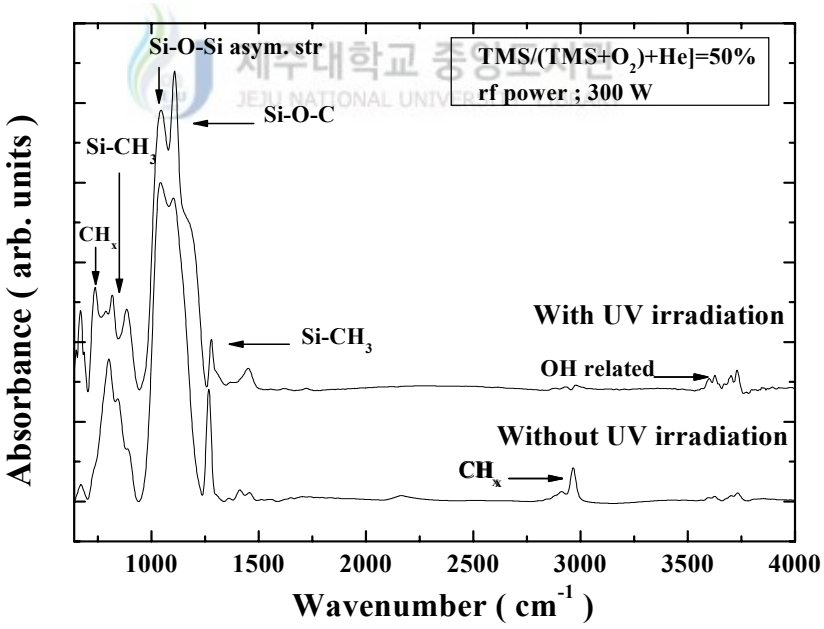

Fig. 56. FT-IR spectra of the as-deposited SiOC(-H) films prepared with and without UV irradiation.

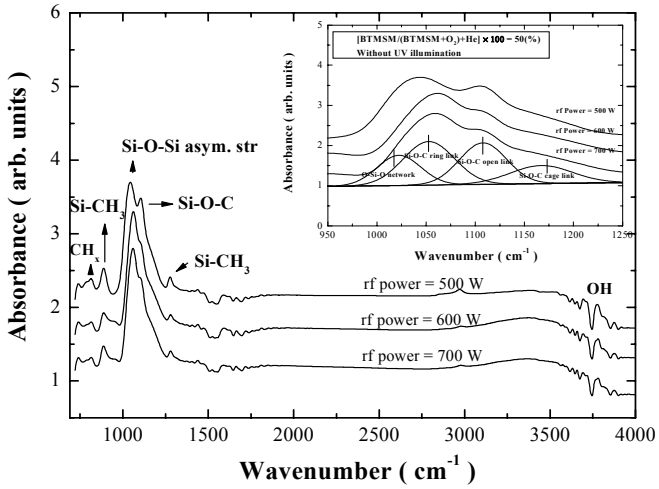

Fig. 57. FTIR spectra of SiOC(-H) films prepared without UV irradiation using the BTMSM+O_2+He mixture at rf powers of 500, 600 and 700 W.

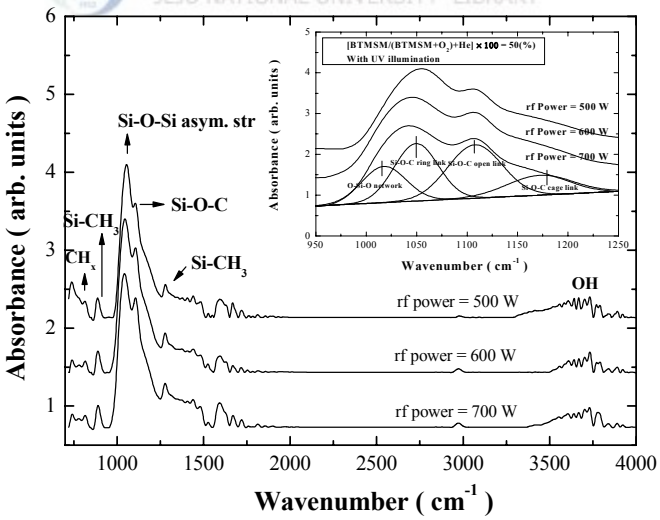

Fig. 58. FTIR spectra of SiOC(-H) films prepared with UV irradiation using the BTMSM+O_2+He mixture at rf powers of 500, 600 and 700 W.

$Si-CH_3$ (889 and 1276 cm^{-1}), Si-O-Si(C) (from 1000 to 1250 cm^{-1}), CH_n (n=1,2,3) (810 and 2970 cm^{-1}), and OH-related bonds. In the range from 1000 to 1250 cm^{-1}, the bonding mode near 1030 cm^{-1} is the Si-O-Si asymmetric stretching mode. The bonding modes near 1104 and 1180 cm^{-1} are due to Si-O-C asymmetric stretching modes in open link and Si-C cage link, respectively [43]. The shoulder at the higher wavenumber of the 1109 cm^{-1} absorption peak indicates the existence of a caged Si-O-C bond structure. The intensity of the Si-O-C open link increased with the rf power. The peak

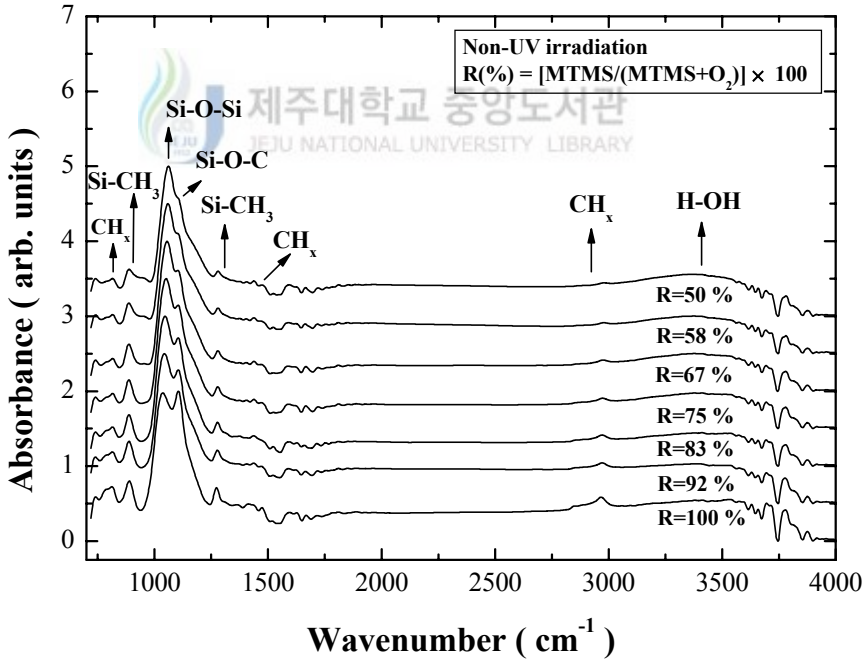

Fig. 59. FTIR spectra of the SiOC(-H) films prepared without UV irradiation as a function of [MTMS/(MTMS+O_2)] flow rate ratios.

stretching mode and the bonding modes near 1165, 1104 and 1180 cm^{-1} position of the O-Si-O open link bond for the sample with an rf power of 500 W shifted to a lower (red shift) wavenumber than that of the sample with the rf power of 700 W, but the peak position of Si-O-C mode shifted to a higher (blue shift) wavenumber. These frequency shifts in the IR spectra are related to the change in the bonding characteristics, such as bonding angle and bond length [69]. SiOC(H) film consists of four kinds of bonding mode: the Si-O-Si network, and the ring, open, and cage links of the Si-O-C bonding (see the inserts in Figs. 57 and 56). Figures 59 and 60 show the FTIR spectra of SiOC(-H) films without and with UV irradiation which were deposited with various flow rate ratios. There were $Si-CH_3$ (889 and 1276 cm^{-1}), Si-O-Si(C) (from 1000 to 1250 cm^{-1}), CH_n (n=1,2,3) (740 and 2970 cm^{-1}) and OH-related bonds in the film. In the range from 1000 to 1250 cm^{-1}, the bonding mode near 1030 cm^{-1} was the Si-O-Si asymmetric resulted from Si-O-C asymmetric stretching modes in ring, open, and cage links, respectively. The peak position of Si-O-Si and the Si-O-C bonding mode was shifted to a higher (blue shift) wavenumber as a function of flow rate ratio. When compared with the relative intensities of the related bonding modes, the peak intensities of the Si-O-C asymmetric stretching of the SiOC(-H) films was greater with UV irradiation than without UV irradiation, while the OH-related bonds decreased and the intensity of the $Si-CH_3$ group was not changed. This result indicates that the SiOC(-H) film with UV irradiation had a more cross-linked structure with chained Si-O-Si and

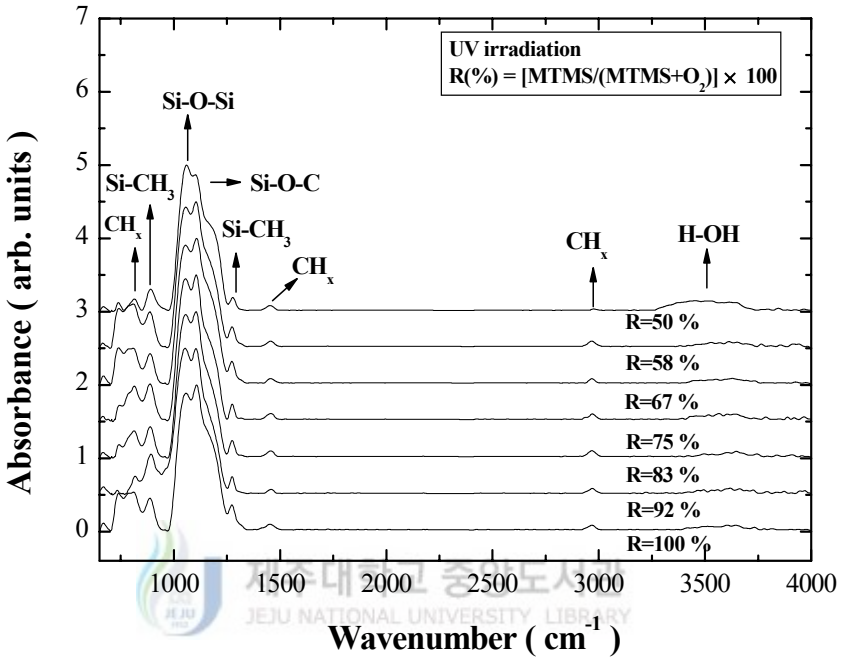

Fig. 60. FTIR spectra of the SiOC(-H) films prepared with UV irradiation as a function of [MTMS/(MTMS+O_2)] flow rate ratios.

$O\text{-}Si\text{-}CH_n$ bonds, in which the incorporation of CH_3 groups broke the continuity of -Si-O-Si- network. To examine the variation in the integrated absorption area of the Si-O-Si, open, ring, and cage links of the Si-O-C bonding mode with and without UV irradiation, the spectra in the range from 900 to 1250 cm^{-1} were deconvoluted using several Gaussian peaks, as shown in Fig. 61. The relative area of the Si-O-C cage link decreased when UV irradiation. The variation of the relative area ratio (%) of Si-O-C ring link increased with a similar tendency as Si-O-C open link, but the relative area ratio (%)

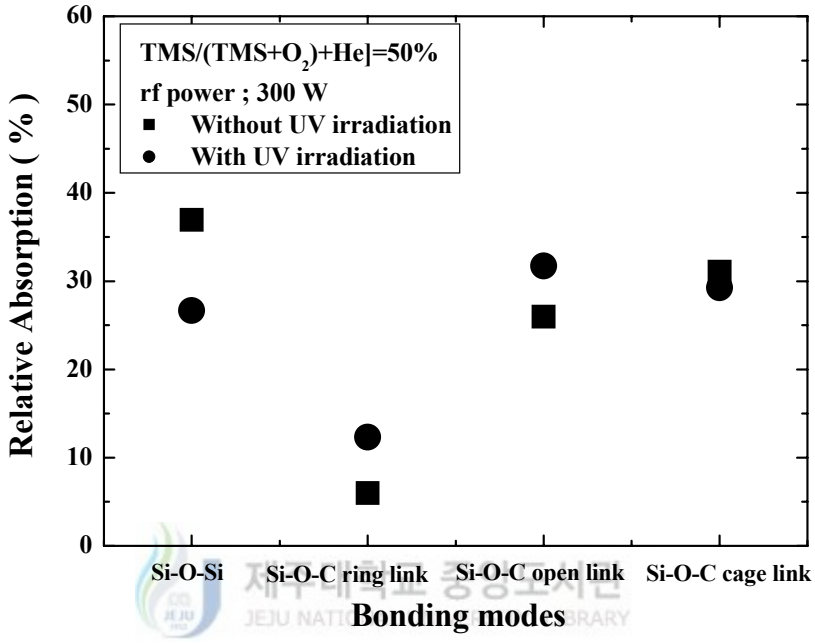

Fig. 61. Relative absorption areas of the Si-O-Si and Si-O-C ring link mode of the SiOC(-H) films prepared with and without UV irradiation.

of Si-O-Si bond decreased when UV irradiation. From these results, we know that the increasing of the relative area ratio (%) of Si-O-C ring link and open link film with UV irradiation are enhanced porosity as previously mentioned.

In the case of BTMSM and MTMS precursors, the relative area of the Si-O-C cage link of the SiOC(-H) films with and without UV irradiation increased with the rf power, but the relative area of the Si-O-C open link of the SiOC(-H) films with and without UV irradiation decreased. The relative

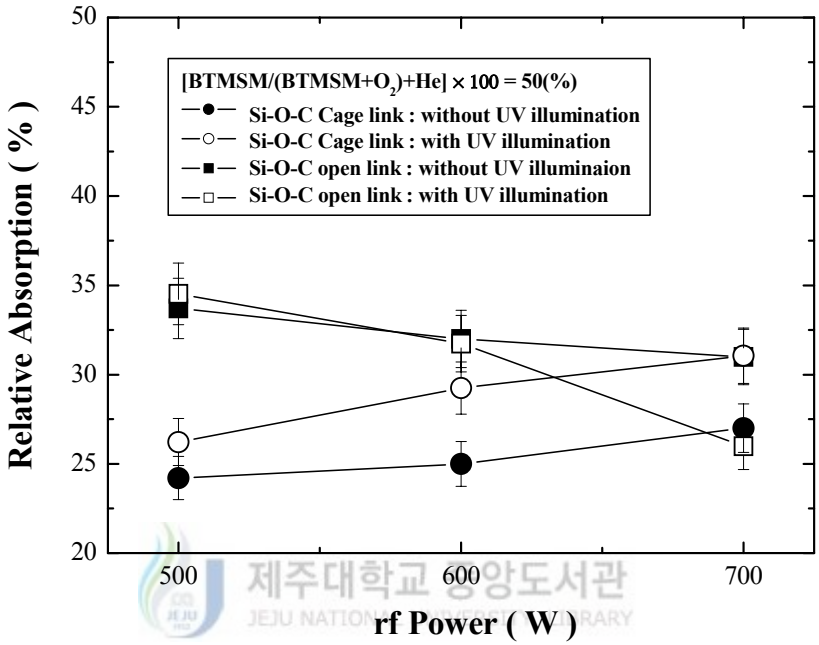

Fig. 62. Relative absorption areas of the open and cage link bonds of the Si-O-C bonding structure without and with UV irradiation using BTMSM+O_2+He mixture gases at rf powers of 500, 600 and 700 W.

area of the Si-O-C cage link of the SiOC(H) films with UV irradiation is greater than that without UV irradiation. For the Si-O-C open link, at an rf power of 700 W, the relative area of the film with UV irradiation was reduced to 22 ~ 33 % of that of the film without UV irradiation. These results show that the relative area of the cage link increases and the relative area of the open link of Si-O-C bonding mode in SiOC(H) film decreases with UV irradiation at an rf power of 700 W. This means that some of the

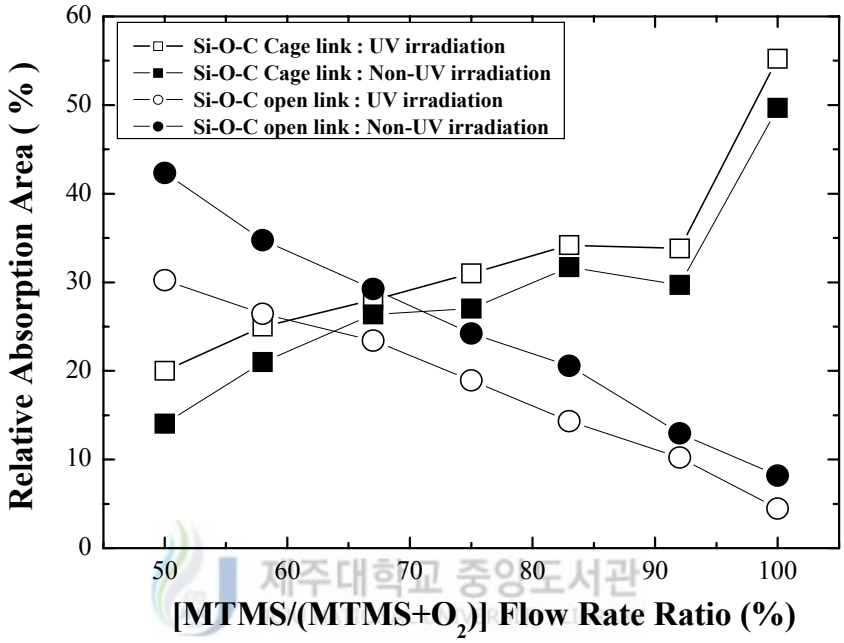

Fig. 63. Relative absorption areas of the open and cage link bonds of the Si-O-C bonding structure with and without UV irradiation as a function of [MTMS/(MTMS+O_2)] flow rate ratios.

Si-O-C open linked bonds change into cage links incorporating C atoms. Since the transformation of an open-linked to a cage-linked structure may have something to do with a reduction in OH groups, the chain of Si-O-Si links is broken, and spaces can form. Figure 63 shows the relative absorption areas of the open and cage-link bonds in SiOC(-H) films with and without UV irradiation as a function of MTMS flow rate ratios. The integrated absorption areas were calculated from the deconvolution using several

Gaussian peaks for FTIR spectra in the range from 900 to 1250 cm^{-1}. The relative area of the Si-O-C cage-link bond increased with flow rate ratio, while the relative area of the Si-O-C open-link bond decreased. The relative area of the Si-O-C cage-link bond in the SiOC(-H) films with UV irradiation was higher than that in the films without UV irradiation. The relative area of the Si-O-C open-link bonds in the film with UV irradiation decreased from 8 to 4% versus films without UV irradiation. These results indicate that some of the Si-O-C open-link bonds changed into cage links incorporating C atoms. The transformation of an open-linked to a cage-linked structure may have something to do with incorporation of CH_3 groups into the Si-O-Si chain structure forming void. Therefore, the increase in the relative area of Si-O-C cage-link bonds with UV irradiation enhances the porosity, as mentioned previously.

Consequently, when the bulk plasma is irradiated with UV light, the related CH_n or Si-C ions and the radicals are increased and the increase in CH_n groups on the SiOC(-H) film produces structural changes as a result of the bonding of -Si-CH_2-Si- and -O- Si-CH_3 bonds in -Si-O-Si- chain structure.

7.2.3. XPS analysis

Figure 64 shows the two high resolution C 1s spectra of the film with and without UV irradiation as 50 % of TMS flow rate. Each spectral region

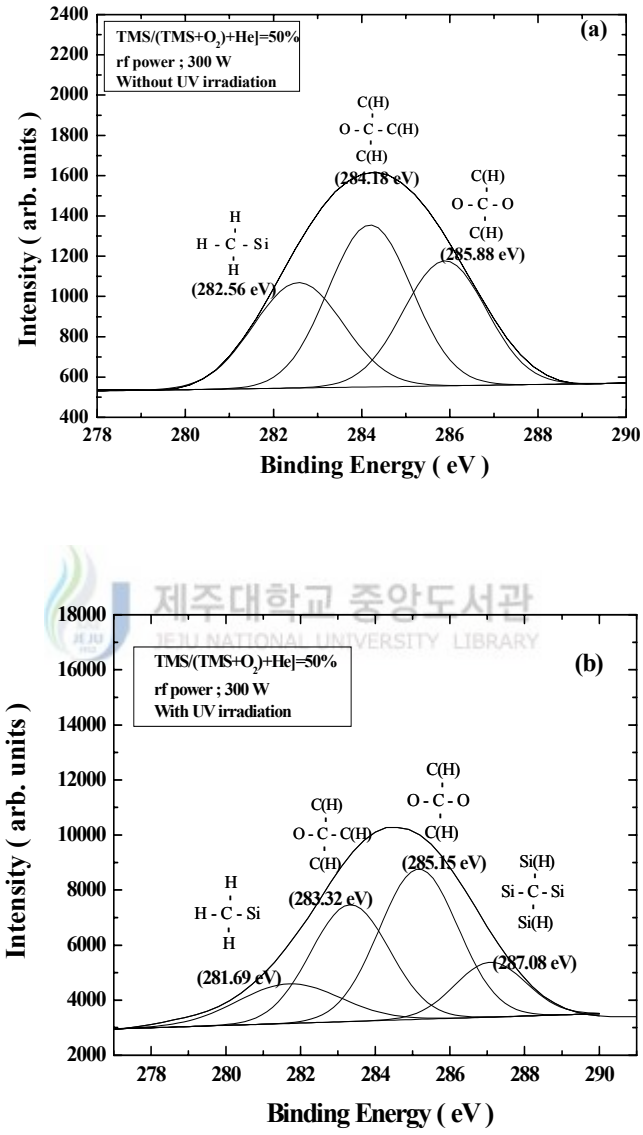

Fig. 64. C 1s spectra of (a) no UV irradiation SiOC(-H) film and (b) UV irradiation SiOC(-H) film as 50 % of TMS flow rate.

was deconvoluted into individual peak assuming all peaks to be perfectly Gaussian. The C 1s spectra were deconvoluted into three different modes such as CO_1 (285.88 eV), CO_2 (284.18 eV), Si-CH_3 (282.56 eV), respectively in Fig. 64 (a). The C 1s spectra were deconvoluted into four modes, Si_4C (287.08 eV), CO_1 (285.15 eV), CO_2 (283.32 eV), Si-CH_3 (281.69 eV), respectively in Fig. 64 (b). The majority of the C part is Si-CH_3 at 282.56 eV, which is in good agreement with the FTIR spectra. Since the major reaction during UV irradiation is increasing carbon contents C-Si, such binding energy changes can be easily explained by the carbon atoms. The electronegativity of the carbon atom is lower than that of oxygen atom. When carbon in O-Si is replaced by carbon-forming C-Si, therefore, the binding energy of C 1s is shifted to lower energy. It is reflected that the radical of carbon increase when a UV irradiation in plasma.

Figures 65, 66 and 67 show the high-resolution XPS Si 2p, C 1s and O 1s electron orbital spectra of the SiOC(-H) films with and without UV irradiation as 100 % of MTMS flow rate. Each spectral region was irradiation. Each spectral region was deconvoluted into individual peaks, with the assumption that all peaks were perfectly Gaussian. The fitted results for the SiOC(-H) films show that the Si 2p, O 1s and C 1s spectra consisted of major peaks centered at approximately 103 (Si-O), 534.4 (O-Si), and 285.9 (C-O/C-H) eV, respectively. In the SiOC(-H) films with UV irradiation, the spectra showed a chemical shift. The Si 2p electron orbital spectra of the films without UV irradiation consisted of two peaks (see Fig. 65) that were

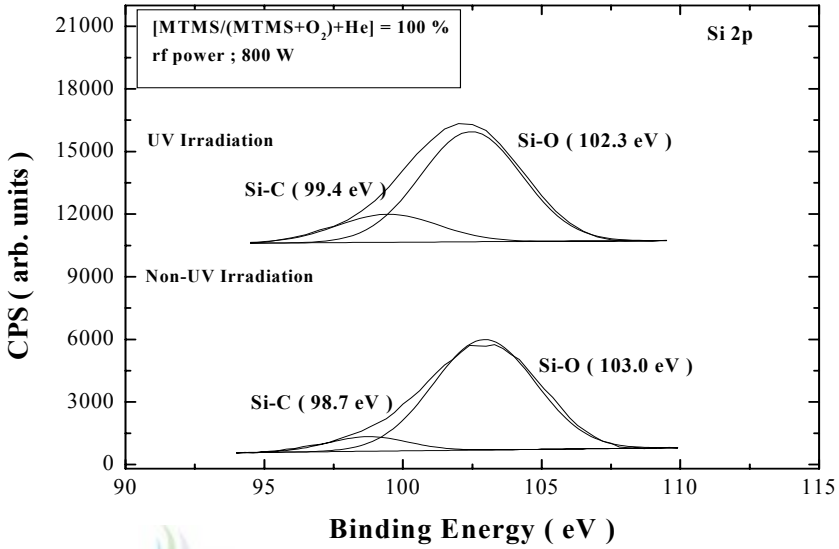

Fig. 65. Si 2p electron orbital XPS narrow scan spectra of SiOC(-H) films for [MTMS/(MTMS+O_2)] flow rate of 100 (%) with and without UV irradiation.

assigned to the Si-C (98.7 eV) and Si-O (103.0 eV) bonds. For the films with UV irradiation, the peaks of the Si-C and Si-O bonds were shifted chemically to higher and lower binding energies, respectively, of 0.7 eV. The electronegativity of the carbon atom is lower than that of oxygen atom. When the oxygen atom in O-Si bond is replaced with carbon, forming O-Si-C or Si-C bonds, and the binding energy of the Si-O bond is shifted to a lower energy, and that of the Si-C bond to a higher binding energy. The O 1s electron orbital spectrum is assigned to O-C and O-Si bonds, and the binding energy of the O-C and O-Si bonds of the films with UV irradiation

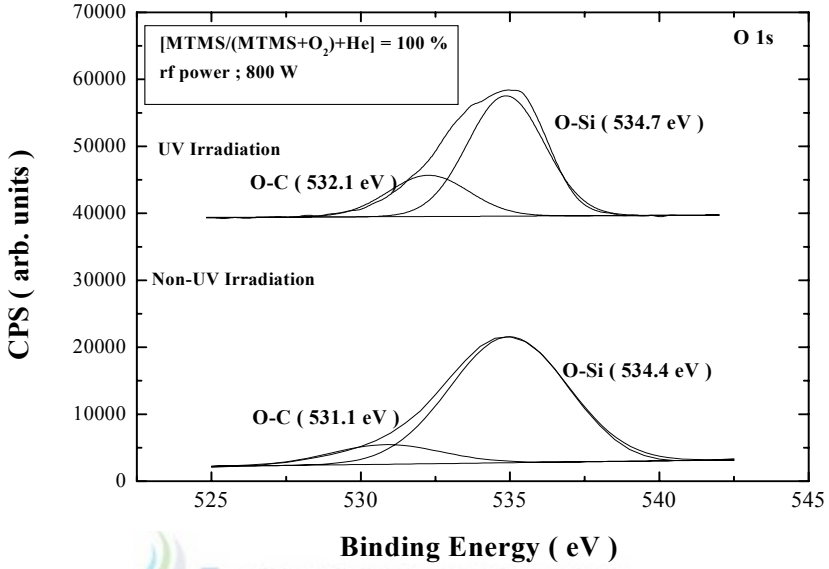

Fig. 66. O 1s electron orbital XPS narrow scan spectra of SiOC(-H) films for [MTMS/(MTMS+O_2)] flow rate of 100 (%) with and without UV irradiation.

is shifted to lower binding energies of 1.1 and 0.3 eV, respectively (see Fig. 66). The relative area of the O-C bond in the films with UV irradiation increased compared to the films without UV irradiation (from 12.7 to 26.4 %), while the relative area of the O-Si bond decreased from 87.3 to 76.3 %. These results suggested that the SiOC(H) film with UV irradiation contained more Si-O-C bonds. Figure 67 shows the C 1s electron orbital spectra consisting of two bond components; C-Si and C-O/C-H bonds. The binding energy of C-Si (282.0 eV) and C-O/C-H bonds (285.3 eV) in the films with UV

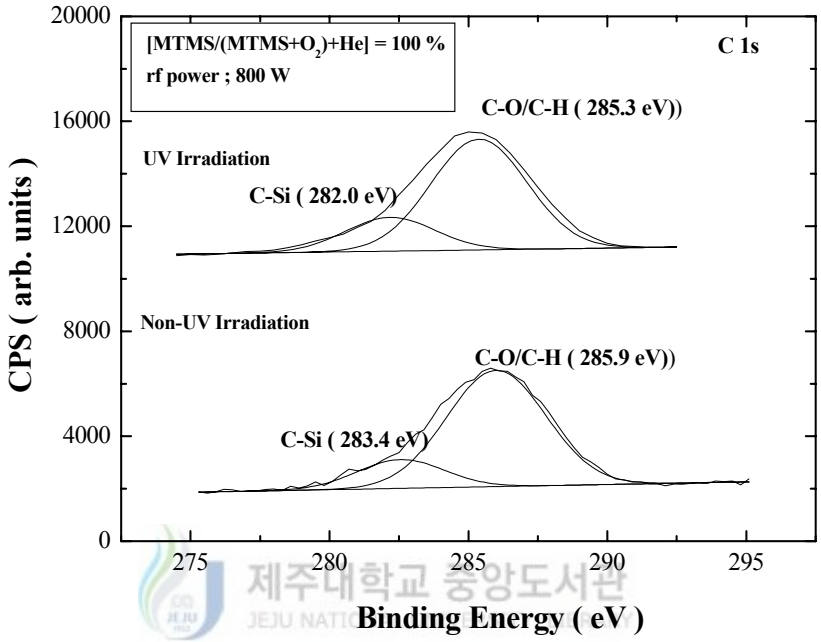

Fig. 67. C 1s electron orbital XPS narrow scan spectra of SiOC(-H) films for [MTMS/(MTMS+O_2)] flow rate of 100 (%) with and without UV irradiation.

irradiation was shifted to lower binding energies as 1.4 and 0.6 eV respectively. This shift to a lower binding energy resulted from the incorporation of many more carbon atoms in the Si-O-Si chain structure attached to CH_n group these carbon atoms are integrated into Si-O links to form Si-O-C links as UV irradiation of the bulk plasma produces more CH_n radicals. Figure 68 shows the atomic concentrations of the SiOC(-H) films with and without UV irradiation s a function of [MTMS/(MTMS+O_2)] flow rate ratios . The silicon

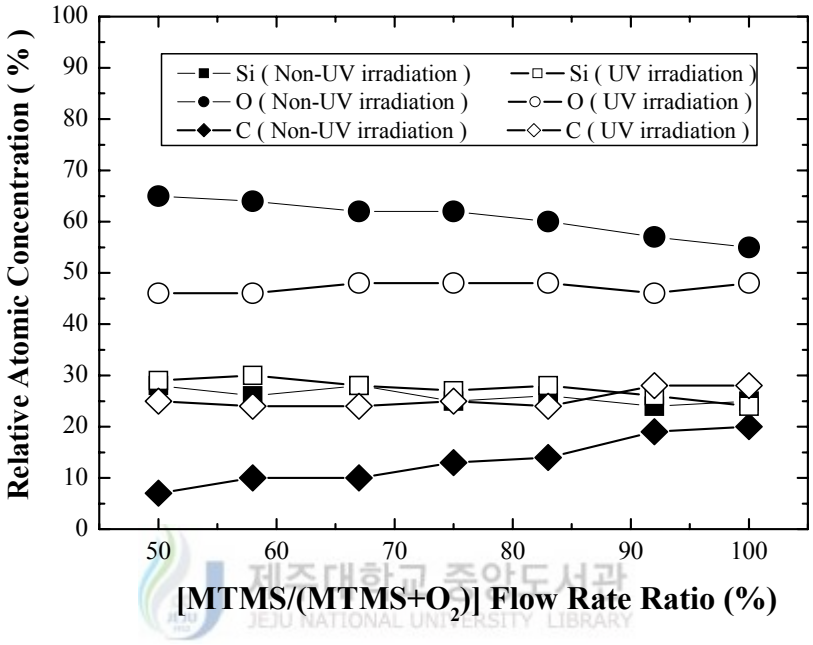

Fig. 68. Atomic concentration of SiOC(-H) films as a function of [MTMS/(MTMS+O_2)] flow rate ratios with and without UV irradiation.

atomic concentration remained similar, at about 28 %, for all flow rate ratios with and without UV irradiation. Without UV irradiation, the carbon concentration of the films increased and the oxygen atomic concentration decreased as a function of flow rate. With UV irradiation, the carbon atomic concentration increased and the oxygen atomic concentration decreased, relative to the non-UV-irradiated samples.

7.2.4. Dielectric constant

Figure 69 shows the dielectric constant of the films formed from several gas mixtures and the electron temperatures of the plasmas with and without the UV irradiation in the case of TMS precursor. When the UV light is not irradiated the electron temperatures of all of the mixtures are little above 8 eV and do not have much differences. The dielectric constant seems to be proportional to the electron temperature and their values are around 2.74 ~ 2.43. When the plasma is irradiated with UV light, the electron temperatures of

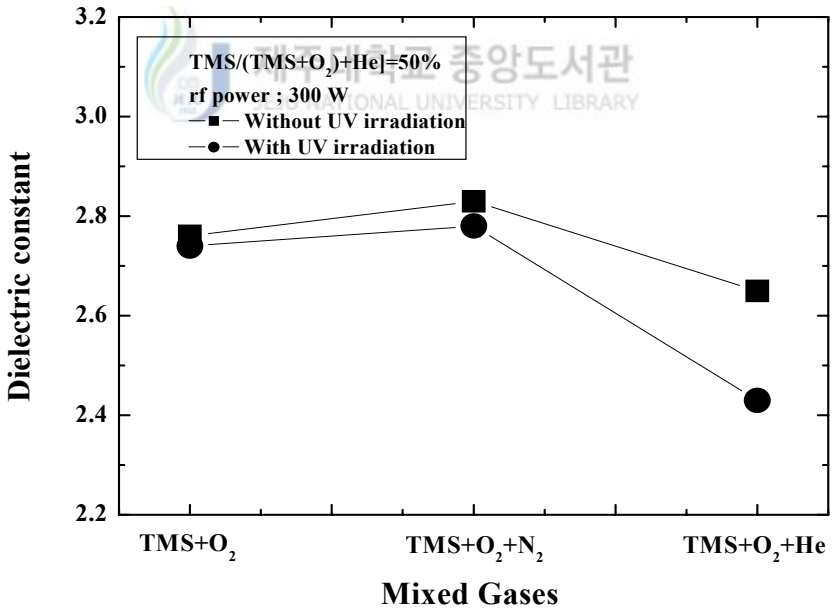

Fig. 69. The dielectric constant of the as-deposited SiOC(-H) films prepared with and without UV irradiation.

TMS+O_2, TMS+O_2+N_2, and TMS+O_2+He mixtures decrease to 4.33 eV, 4.72 eV and 3.21 eV, respectively from around 8 eV of unlighted case. The decrease of electron temperature is related to the increase of inelastic scattering and the increase of intra molecular excitation and dissociation. It is that the concentration of Si* and C* radicals increases when UV irradiation to the TMS/O_2/He mixtures. Thus the structure of the SiOC(-H) film or C concentration in the film seems to be changed by the energy of the ion.

Figure 70 shows the relative carbon content and dielectric constant of the

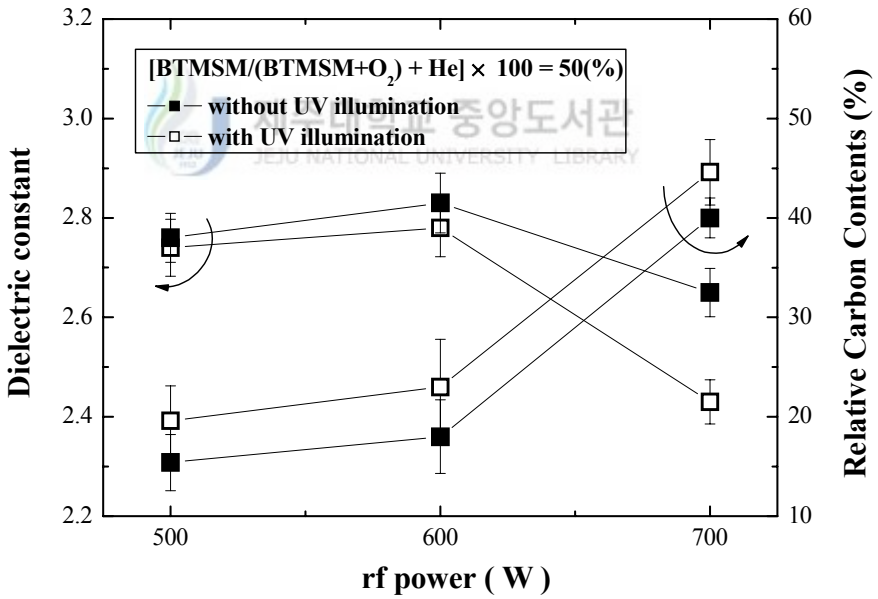

Fig 70. Relative carbon contents and dielectric constant of SiOC(-H) films with and without UV irradiation, which was deposited using a [BTMSM/(BTMSM+O_2)+He]100 flow rate ratio of 50% at rf powers of 500, 600 and 700 W.

SiOC(-H) films without and with UV irradiation, which is deposited with [BTMSM/(BTMSM+O_2)+He] flow rate ratio of 50% at rf powers of 500, 600 and 700 W. The relative carbon content of the SiOC(-H) films was calculated using: Relative carbon content (%) = [A_c/(A_0 + A_c)] × 100. This was normalized to the peak areas of the Si-O-C stretching vibration, where A_0 and Ac are the peak areas of the Si-O-C stretching vibration mode from 1000 to 1250 cm^{-1} and the Si-CH_3 stretching vibration mode from 889 to 1276 cm^{-1}, respectively. The relative carbon content increased with the rf power, and the relative carbon content of the film with UV irradiation is higher than that without UV irradiation. These results indicate that there are at least two methods of incorporating C atoms into SiOC(-H) films during deposition. The first method attaches CH_3 groups to Si atoms in Si-O-Si networks, and the other involves Si-O-C structures. The incorporation of CH_3 groups breaks the continuity of Si-O-Si networks and nano-pores are formed due to the repulsive force between the CH_3 group and other parts of the Si-O-Si links. The repulsive force between Si-O and Si-O bonds is smaller than that between Si-O and Si-C bonds in the [SiO_3C] tetrahedron since the electronegativity of the carbon atom (2.5) is lower than that of the oxygen atom (3.5).

Figure 71 shows the dielectric constant of SiOC(-H) films with and without UV irradiation in the case of MTMS precursor. The dielectric constant of the UV-irradiated samples was lower than that of films without UV irradiation. When flow rate ratio was 100%, the dielectric constant of the

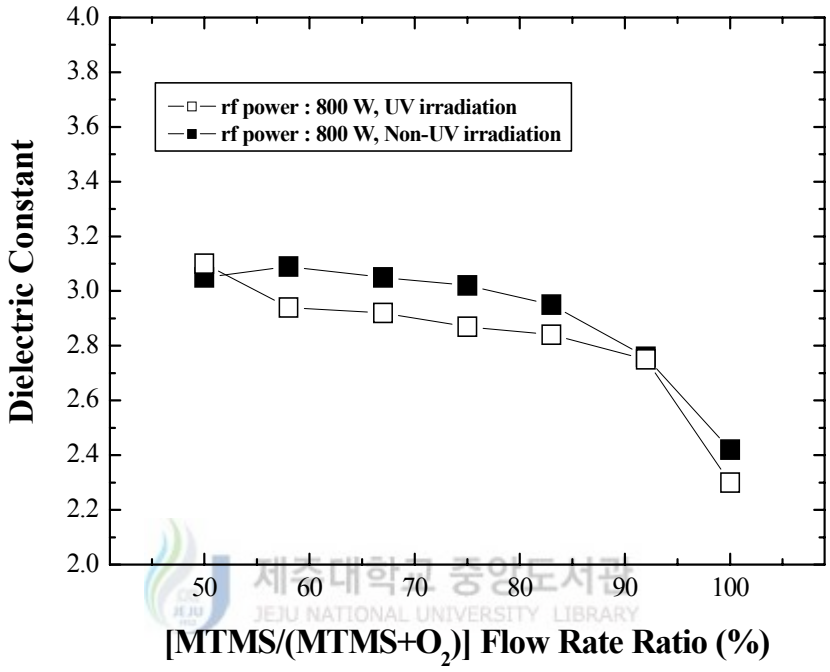

Fig. 71. Dielectric constant of SiOC(-H) films as a function of [MTMS/(MTMS+O_2)] flow rate ratios with and without UV irradiation.

SiOC(-H) films decreased consistently from 2.4±0.11 (without UV irradiation) to the lowest value of 2.3±0.11 (with UV irradiation). From these results, we assume that the irradiation of the [MTMS+O_2] plasma increased the carbon atomic concentration, because the UV irradiation can produce Si*, O*, -CH_3*, Si-C* or Si-O* radicals respectively. The dielectric constant of the SiOC(-H) film decreased as more CH_3 groups were incorporated into the films via a polymerization mechanism, and some of the Si-O-C open-link bonds changes

into cage- or ring-link bonds incorporating CH_3 [13]. Therefore, the SiOC(-H) film with a low dielectric constant have a cross-linked structure with nano-pores caused by the combination of Si-CH_n-Si bonds and the Si-O-Si network.

8. Discussion for Experimental Results

Characteristics of UV-assisted plasma

As shown Fig. 45, we found that a typical bi-Maxwellian distribution function with and without UV irradiation for Ar gas. Using the two-temperature model, we tried to resolve the measured non-Maxwellian EEPF into two Maxwellian EEPFs with the electron densities of n_{el} and n_{eh}, and electron temperature of T_{el} and T_{eh}, respectively, as follows :

$$f_p(\epsilon) = \frac{2}{\sqrt{\pi}} [n_{el} T_{el}^{-3/2} \exp(-\frac{\epsilon}{T_{el}}) + n_{eh} T_{eh}^{-3/2} \exp(-\frac{\epsilon}{T_{eh}})],$$

where, n_{el}, n_{eh}, T_{el}, and T_{eh} were obtained from a successive fitting procedure until the Chi-Square value reached a minimum value. We could determine, for example, that the EEPFs without UV irradiation consist of the low-energy group with $n_{el} = 4.2 \times 10^{10}$ cm^{-3} and $T_{el} \sim 1.42$ eV and the

high-energy tail with $n_{eh} = 2.0 \times 10^{10}$ cm^{-3} and $T_{eh} \sim 9.2$ eV, as shown in Fig. 45. The peak of the low energy electron group was gradually reduced with UV irradiation, and finally the distinction between the low-energy electron group and the high-energy electron group was completely ambiguous. Electron distribution with two energy group is common in rf argon discharges. This phenomena has been explained either by secondary electrons in capacitively coupled rf discharges or by a balance between the oscillation frequency and the momentum transfer collisional distribution. Analogous to the rf discharges, the formation of the low-energy group might have its origin in a balance between the angular frequency of electron oscillations and the frequency of the momentum transfer. The electron density of the plasmas without and with UV irradiation for Precursor+O_2+Ar(He) when the discharge power is increasing. The electron densities were about ~10^9 cm^3 and increased very slightly with the rf power. Therefore, we can infer that the efficient production and preservation of energetic electrons is important for a high degree of precursor ionization. The result in Figs. 47 and 49 shows that the electron density of the plasma with UV irradiation was higher than that without UV irradiation. This occurs because UV photons can excite the energy states of the precursors, increasing the number of radicals, including methyl (CH_n) groups with dissociative electrically excited states; abundant radicals and ions were generated in the presence of UV illumination. Therefore, more radicals form with UV irradiation. In the UV irradiated plasma, the electron temperature of the plasma with the Precursor + O_2 +

Ar(He) mixture decreased as the rf power increased than non UV irradiated. The electron temperature was much lower than that of conventional PECVD. Generally, the effective ionization threshold energy is a function of the electron temperature. From Figs. 48 and 50, the high electron temperature of O_2 plasma is due to the high ionization threshold energy of O_2 gas, rather than Ar(He) gas. This means that the electrons gain energy from UV light and the excited electrons collide with ions or radicals and energy transfer takes place. Electron energy involves inelastic collisions with excited radicals.

The emission intensity of OES for with and without UV irradiation are shown in Fig. 51 using MTMS precursor. From plasma emission data one cannot immediately and easily obtain information concerning the density of the species in their ground state; yet OES is one of the most common diagnostic techniques for plasma processes, because of its simple set-up and the easy identification of the emitting species. When the with UV irradiation, the intensity of CO_2^+, CH_n, CO species rapidly increase than that of without UV irradiation. In Fig. 51, the ratio of the CH species and CO intensities is shown as a function of the UV irradiation. This could mean that CO_2^+ is directly populated by electron impact of the CO_2 molecule, $CO_2 + e^- \rightarrow CO_2^{+*} + 2e^-$; therefore the OES trend evaluated by means of the CO_2^+ emission intensity is a fair approximation of the CO_2 concentration as a function of the feed gas composition. The CO_2 species are characterized by a profile with a maximum, which probably results from direct O atom oxidation of CO and of other C-related fragments. If the recombinative oxidation CO + O

+ M is contributing to carbon dioxide formation, the normalize plot of the actionometric product [CO]×[O] should lead to a profile close to that of CO_2. The emission intensity of CH/CO(O) increased as a increasing of MTMS flow rate with UV irradiation. According to emission intensity, each intensity ratio can be considered proportional to the ratio of the species densities, since the thresholds of the excitation energy of these radicals are similar. The UV irradiation and electron impact driven-dissociation paths occurs, it is commonly stated that the [MTMS]*, after electron impact, dissociates and eliminates methyl radicals. As shown Figs. 52 and 53, The dissociation of excited molecules by UV irradiation can hardly occur in the expanding plasma due to the low electron temperature; instead Ar^+ is responsible for initiating molecule activation, namely via a charge exchange reaction as follow:

$$Ar^+ (He^+) + UV + CH_3Si(OCH_3)_3 \rightarrow Ar + CH_3Si^+(OCH_3)_3 \quad \text{(a)}$$

$$Ar^+ (He^+)\ CH_3Si(OCH_3)_3 + UV \rightarrow Ar + CH_3Si^+(OCH_3)_2 + OCH_3 \quad \text{(b)}$$

The validity of the charge exchange reaction is supported by the MTMS molecule depletion as a function of the Ar^+ flow ratio rate and UV irradiation. The ion produced in (a) and (b) undergoes dissociative recombination with an electron, estimated to be at least 2 orders of

magnitude faster than 2. The possible reaction formed as follow:

$$CH_3Si^+(OCH_3)_3 \xrightarrow{e^-} CH_3Si^* + {}^*(OCH_3)_3 \quad \text{(c)}$$

$$CH_3Si^+(OCH_3)_3 \xrightarrow{e^-} CH_3Si^*(OCH_3)_2 + OCH_3 \quad \text{(d)}$$

$$CH_3Si^+(OCH_3)_3 \xrightarrow{e^-} CH_3Si(OCH_3)_2CH_2{}^* + OH \quad \text{(e)}$$

$$CH_3Si^+(OCH_3)_2 \xrightarrow{e^-} CH_3Si^* + O_2Si(CH_3)_2 \quad \text{(f)}$$

From this result, the reaction in Scheme 1 show the possible dissociation of MTMS molecules in the expanding thermal plasma : a charge exchange occurs between the He^+ and the MTMS molecules can dissociate at the Si-O, Si-C or C-H bond. The Si-O bond of the MTMS molecules is broken preferably, at least in conditions for which $[He^+]+UV \leqq [MTMS]$. The cleavage of the Si-O bond in the gas phase is not desirable as this bond represents the 'mechanical strong' backbone for the deposition of scratch-resistance $SiO_xC_yH_z$ films.

Deposition rate of UV-assisted PECVD

The deposition rates can be connected with the following parameters k_0,

k_1 and k_2. k_1 means the deposition rate (kg/m^2 · sec, mg/cm^2 · sec, etc) and k_2 is the thickness growth rate (m/sec, Å/sec, etc.). k_0 means the specific deposition rate, which is given by $k_0 = k_1/FM$, (m^{-2} or cm^{-2}), where F is the molar flow rate and M is the molecular weight of monomer, that is FM is the mass flow rate. The specific deposition rate k_0 is the only form of deposition rate that can be used to compare deposition characteristics of different monomers with different chemical structure and molecular weight under different discharge condition such as with UV irradiation or without UV irradiation. It has been well established that the plasma polymerization is primarily controlled by a composite power parameter, W/FM, where W is discharge power in watts. W/FM represents the energy input per unit mass of the monomer, which is given in J/kg. Based on W/FM, plasma polymerization can be divided into two regime; an energy deficient regime and a monomer deficient regime. In the energy deficient domain, ample monomer is available but the power input rate is not sufficient. In this domain, the deposition rate increases with the power addition. In the monomer deficient domain, sufficient discharge power is available but the monomer feed rate is the determining factor for the deposition.

As the power was added (at a given flow rate), the domain of plasma polymerization approaches the monomer deficient one, which can be recognized by the asymptotical approach of k_0 value to a horizontal line as the power addition. In the monomer deficient domain, the deposition rate will

increase as the power addition such as UV irradiation and shows a linear dependence on the discharge power feed-in rate at a given flow rate and the system pressure, i.e.

$$k_1 = k''(FM) \tag{f}$$

The relationship is given by f is valid in the flow rate deficient domain and UV irradiation. The further increase of the flow rate (FM) will eventually increase the deposition rate as the plasma polymerization changes to the energy deficient domain. The deposition rate is 310 nm/min for the mixture of TMS and O_2, and it is increased to 320 nm/min for the mixture of TMS/O_2 and He without UV irradiation. The deposition rate for the mixture of TMS, O_2 and N_2 is slightly less than that of TMS and O_2 in spite of the increased electron density. By the UV irradiation, the deposition rate increases about 10 to 15 %. In the case of MTMS precursor, the deposition rate of SiOC(-H) films for MTMS flow rate ratio with and without UV irradiation increased proportionally as a function of flow rate ratios. The deposition rate of the films with UV irradiation is higher about 10 to 15 % than that of films without UV irradiation. This is caused by change of input power k'' in f, it means that the increase in the deposition rate with a mixing ratio is mainly due to the large input power than non UV irradiation. From this result, we can infer that the electron density increase

and more radicals are produced when the UV light irradiates the bulk plasma. The silane (SiH_4) and methoxy (OCH_n) groups exist as dissociative electronically excited states and the UV irradiation generated abundant radicals and ions. The UV photon can excite the energy states of the precursors and the increase of radicals can occur. It means that the silane (SiH_4) and methyl group (CH_n) show dissociative electronically excited states and the abundant radicals and ions were generated UV irradiation.

Characteristics of SiOC(-H) film by UV-assisted PECVD

In the Figs. 56, 58, and 60, the characteristics features of the Si-O-Si and Si-O-C groups evident: asymmetric stretching and bending mode, around 1120 cm^{-1} and 780 cm^{-1}, respectively. The absorbtion bands at 2970 cm^{-1} and 1260 cm^{-1}, relative to the stretching of CH_n and the bending modes of methyl groups in $Si\text{-}CH_n$, as well, mark the presence of organic components in the film. It can be observed that at SiOC(-H) film condition of UV added plasma, the film infrared spectra show the clearly separated of characteristics features of Si-O-Si and caron-containing Si-O-C. This is in a good agreement with the results found in the plasma phase (see Figs. 52 and 53). The deposition precursors are mainly SiC_xH_y and CH_x radicals and partially oxidized radicals, and the film stoichiometry can be expressed as $SiC_xH_yO_z$. As UV irradiation and MTMS flow rate increased, the lower homogeneous oxidation efficiency produces more Si-O-C groups and the volatile molecule

CO_2 than Si and CH_x, leading to a marked inorganic character of the film (Si-O-Si functional group prevail over $Si(CH_3)_x$), thus the composition of film approaches SiOC(-H). The bonding angle of Si-O-Si(C) clearly increased with UV irradiation and precursor flow rate ratio. The Si-O-Si(C) bonding angle is increased with carbon contents, it means the Si-O network was broken and the inner size increased as the carbon included hydrogen atoms bonded with the silicon or oxygen atoms. Another point of view, the concentration of carbon and bonding angle is dependent as the flow rate ratio of BTMSM increase. XPS investigations on the films deposited as a function of MTMS flow rate and UV irradiation have shown that the silicon atomic concentration remained similar, at about 28%, for all flow rate ratios with and without UV irradiation. Without UV irradiation, the carbon concentration of the films increased and the oxygen atomic concentration decreased as a function of flow rate. With UV irradiation, the carbon atomic concentration increased and the oxygen atomic concentration decreased, relative to the non-UV-irradiated samples. XPS spectral region was deconvoluted into individual peaks, with the assumption that all peaks were perfectly Gaussian. The fitted results for the SiOC(-H) films show that the Si 2p, O 1s and C 1s spectra consisted of Si-O, Si-C, C-O/C-H, respectively. Each spectral region was deconvoluted into individual peak assuming all peaks to be perfectly Gaussian. The majority of the C part is $Si-CH_3$, which is in good agreement with the FTIR spectra. Since the major reaction during UV irradiation is increasing carbon contents C-Si, such binding energy changes can be easily explained by the carbon

atoms. The electronegativity of the carbon atom is lower than that of oxygen atom. When carbon in O-Si is replaced by carbon-forming C-Si, therefore, the binding energy of C 1s is shifted to lower energy. It is reflected that the radical of carbon increase when an UV irradiation in plasma. During the UV irradiation, the mixture of precursor and O_2 gases could be fully dissociated into more reactive ions and radicals such as Si*, -CH_3*, CH_n^+, O_2*, and O_2^- etc. Therefore, the oxidation mechanism became dominant during the growth of SiOC(-H) films growth as mentioned above. We can infer that the Si-O-C substructure was formed mainly by oxidation mechanism. The Si-CH_3 substructure was formed mainly by polymerization mechanism. The open-linked Si-O-C substructure was unstable and could be changed into ring-linked substructure by post-annealing. The dielectric constant decreased with UV irradiation and the increasing precursor flow rate ratio. The dielectric constant of the UV-irradiated samples was lower than that of films without UV irradiation. When MTMS flow rate ratio was 100 %, the dielectric constant of the SiOC(-H) films decreased consistently from 2.4±0.11 (without UV irradiation) to the lowest value of 2.3±0.11 (with UV irradiation). Considering the stable characteristic of Si-CH_3 and C-H groups in SiOC(-H) films under post-annealing, this decrease of dielectric constant must be caused by the transformation of open-linked Si-O-C to ring-linked Si-O-C substructure and the elimination of -OH groups during post-annealing procedure.

From these results, we assume that the irradiation of the [Precursor+O_2] plasma increased the carbon atomic concentration, because the UV irradiation can produce Si*, O*, -CH_3*, Si-C* or Si-O* radicals respectively. The dielectric constant of the SiOC(-H) film decreased as more CH_3 groups were incorporated into the films via a polymerization mechanism, and some of the Si-O-C open-link bonds changes into cage- or ring-link bonds incorporating CH_3. Therefore, the SiOC(-H) film with a low dielectric constant by UV-assisted PECVD have a cross-linked structure with nano-pores caused by the combination of Si-CH_n-Si bonds and the Si-O-Si network.

Chapter IV. Conclusion

According to International Technology Roadmap for Semiconductor 2002 (ITRS 2002), low dielectric constant (low-*k*) materials with *k* value less than 2.4 will be required for technology node 60 nm devices. Among low dielectric materials, SiOC(-H) film has many advantages as compared with other low dielectric materials since it has lower dielectric constant, higher thermal and mechanical stability.

In this study, SiOC(-H) films with low dielectric constant were deposited on *p*-type Si(100) substrate using PECVD and ultraviolet (UV)-assisted PECVD with a mixture of oxygen gas with precursors such as tri-methylsilane ($Si(CH_3)_3$, TMS), bis-trimethylsilylmethane (BTMSM: H_9C_3-Si-CH_2-Si-C_3H_9), Methlytrimethoxysilane (MTMS: $C_4H_{12}O_3Si$). FTIR spectroscopy performed in absorbance mode was used to determine the related Si-O and Si-CH_3 bonding configuration in the film, the bonding structure of the Si-O-C composite films were analyzed using XPS. The mechanical properties such as hardness (H) and elastic modulus (E) were measured by the nano-indentation method. The thickness and refractive index of the deposited Si-O-C composite films are measured by an ellipsometer. The dielectric constant at 1MHz was investigated with a metal insulator semiconductor (MIS, Al/SiOC(-H) film/*p*-Si) structure.

The bonding structure of SiOC(-H) film using BTMSM, TMS, and MTMS precursors consist of Si-O-Si, Si-O-C, Si-CH_n, CH_n and OH related bonds. In

the bonding structure of the SiOC(-H) film, clearly separated Si-O-Si and Si-O-C bonds and the Si-O-C bonds consist of ring, open and cage link. When the increasing of annealing temperature, the relative absorption area of Si-O-C ring link of the film and Si-O-C bonding angle increased and the Si-O-C open link of the film decreased. The reason of angle and structure variation is that the incorporation of CH_3 groups breaks the continuity of Si-O-Si networks and form the nano-pores by the aloof force between CH_3 group and other part of Si-O-Si links. Because the repulsive force between Si-O and Si-C bonds is smaller than those between Si-O and Si-C bonds in [SiO3C] tetrahedron due to electronegativity of carbon atom, which is lower than that of oxygen atom. The reason for the lower dielectric constant of the annealed SiOC(-H) films can be interpreted as a change of dipole moment, which depends on the bonding length between atoms. The bonding length of Si-C is shorter than the bonding length of Si-O in general because carbon atoms have smaller radius than oxygen atom. The carbon concentration increases as MTMS flow rate increased, which increased from 24 to 36 % and dielectric constant of annealed SiOC(-H) films decreased from 3.18 to 2.25 when the MTMS flow rate increases in steps from 50 to 100 %. Therefore, we define that the low-*k* values of SiOC(-H) film depend on the concentration of CH_n groups in the film. The dielectric constant and elastic modulus of SiOC(-H) film was influenced by the different precursors such as BTMSM and MTMS using PECVD. The dielectric constant varied from 3.6 to 2.1 for the annealed SiOC(-H) films as a function of BTMSM flow rate

ratios. In the case of MTMS, the variation of dielectric constant was measured from 3.05 to 2.39 for the annealed films. The elastic modulus of SiOC(-H) films varied from 7.42 to 3.98 GPa for the annealed SiOC(-H) films as a function of BTMSM flow rate ratios. In the case of MTMS, the variation of elastic modulus was measured from 9.89 to 7.12 GPa for the annealed films. The reason of this variation is that the structure of CH_n groups were different from BTMSM and MTMS. The different of BTMSM and MTMS is the structure of CH_n groups such as trimethyl[$(CH_3)_3$] and trimethoxy[$(OCH_3)_3$]. The methyl group can reduce for the dielectric constant more than the methoxy group. On the other hand, the methoxy group profits the mechanical properties such as hardness and elastic modulus than the methly group. From these results, we can infer that SiOC(-H) film using MTMS precursor is more suitable than BTMSM for low dielectric material on 60 nm device.

The quality of SiOC(-H) film is degraded by the damage from oxygen plasma ashing for photo-resist stripping. The surface treatment of plasma can effective improve the quality of SiOC(-H) film. In order to the control of electrical and structural unstability, the effects of the CH_4 plasma treatment for stabilizing low dielectric SiOC(-H) films were studied. The leakage current density of SiOC(-H) film was measured 7.3×10^{-5} A/cm^2, it is increased from 7.3×10^{-5} A/cm^2 to 1.8×10^{-3} A/cm^2 as a function of oxygen plasma ashing time. In the case of CH_4 plasma treated SiOC(-H) film, the variation of the leakage current density at 1 MV/cm^2 increased from 2.6×10^{-9}

A/cm^2 to 2.02×10^{-8} A/cm^2 during as a function of oxygen plasma ashing time. It means that the CH_4 plasma treatment provided additional hydrogen and carbon to surface dangling bonds of SiOC(-H) film. The dielectric constant of samples without CH_4 plasma treatment increased from 2.9 to 3.6 as oxygen plasma ashing time, and the dielectric constant of samples with CH_4 plasma treatment slightly increased from 2.9 to 3.3 as oxygen plasma ashing time. Therefore, CH_4 plasma treatment on SiOC(-H) film suggests that the carbon radical contributed to be react dangling bonds on the surface of SiOC(-H) and the hydrogen radical broken bonds, and the recombination of C and H atoms on the SiOC(-H) film is attributed to a structural change due to the formation of Si-H and Si-C bonds. From these results, we can infer that CH_4 plasma treatment is an effective method to improve the electrical stability.

UV-source can be controlled optimally, radical and ion production is improved by adjusting the energy of the UV irradiation. The electron temperature of the plasma with the BTMSM+O_2 mixture decreased from 7.0 to 6.4 eV as the rf power increased without UV irradiation, the electron temperature of the plasma with UV irradiation of BTMSM+O_2 decreased from 1.7 to 1.2 eV as the rf power increased. This means that the electrons gain energy from UV light and the excited electrons collide with radicals and energy transfer takes place. The UV irradiation of the bulk plasma with the Precursor+O_2+He(Ar) mixture caused the dissociation of ions that are more reactive and radicals, such as Si, -CH_3, CH_3^+, O_2, and O_2^-. This is due to the

increasing of ionization with excited precursors by UV irradiation. The reaction mechanism in the UV-assisted plasma, the possible dissociation of precursor molecules in the expanding thermal plasma : a charge exchange occurs between the He^+ and the precursor molecules can dissociate at the Si-O, Si-C or C-H bond. The Si-O bond of the precursor molecules is broken preferably, at least in conditions for which $[He^+ (Ar^+)]+UV \leqq$ [Precursor].

The deposition rate of the SiOC(-H) film increased proportionally as a function of MTMS flow rate ratios with UV irradiation. The deposition rate of the films with UV irradiation is higher about 10 to 15 % than that of films without UV irradiation. The silane (SiH_4) and methoxy (OCH_n) groups exist as dissociative electronically excited states and the UV irradiation generated abundant radicals and ions. From this result, we can infer that the electron density increase and more radicals are produced when the UV light irradiates the bulk plasma. The relative area of the Si-O-C cage-link bond in the SiOC(-H) films with UV irradiation was higher than that in the films without UV irradiation. The relative area of the Si-O-C open-link bonds in the film with UV irradiation decreased from 8 to 4% versus SiOC(-H) films without UV irradiation. These results indicate that some of the Si-O-C open-link bonds changed into cage links incorporating C atoms. The C 1s electron orbital spectra of SiOC(-H) film using UV-assisted PECVD consist of two bond components such as C-Si and C-O/C-H bonds. The binding energy of C-Si (282.0 eV) and C-O/C-H bonds (285.3 eV) in the films with

UV irradiation was shifted to lower binding energies as 1.4 and 0.6 eV respectively. This shift to a lower binding energy resulted from the incorporation of more carbon atoms than that of without UV irradiation in the Si-O-Si chain structure attached with CH_n groups and these carbon atoms are integrated into Si-O links to form Si-O-C links as UV irradiation of the bulk plasma produced more CH_n radicals. Therefore, we can infer that the SiOC(-H) film deposited by selectively radicals and ions with UV irradiation can be easily formed nano-pore structure for the inter-metal dielectric layer of the high density devices.

References

[1] P.V.Zant, "Microchip Fabrication : A Practical Guide to Semiconductor Processing", p.1, McGraw-Hill, New York, 2000.

[2] International Technology Roadmap for Semiconductors, Semiconductor Industry Association (2002).

[3] T.N.Thesis, IBM J.Res. Develop, 44, 379 (2000)

[4] M.Morgen, E.Todd, J.H.Zhao, C.Hu, T.Cho and P.S.Ho, Annu. Rev. Mater. Sci. 30, 651 (2000).

[5] S.P.Jeng, R.H.Havemann, M-C.Chang, Mater.Res.Soc.Symp.Proc, 337 (1994) 25.

[6] P.B.Ghate, C.R.Fuller, in : H.Huff, R.Kriegler, Y.Takeishi (Eds), Semiconductor Silicon-1981, Electrochemical Soc., Princeton, NJ, 1981, p.680

[7] A.K.Sinha, J.A.Cooper, Jr., H.J.Levinstein, Electron Device Lett. EDL-3 (1982) 90.

[8] K.Saraswat, F.Mohammadi, IEEE Trans. Electron Device ED-29 (1982) 4.

[9] S.P. Muraka, in IEEE-IEDM 1979, Tech. Digest, IEEE, New York, (1979). p.454

[10] C.P.Yuan, T.N.Trick, IEEE Electron Device Lett. EDL-3 (1982) 391.

[11] T.Sakurai, K.Tamaru, IEEE Trans, Electron Devices ED-30 (1983) 183.

[12] T.Sakurai, IEEE J. Solid State Circuits, SC-18 (1983) 418.

[13] H.B. Bakoglu, Circuits, Interconnections and Packing for VLSI, Addison-Wesley, Reading, MA, 1985.

[14] D.S. Gao, A.T. Yang, S. Kang, IEEE Trans. Circuit and Systems, SC-37 (1) (1990) 1.

[15] S. Sai-Halasz, IEEE ICCD, IEEE, New York, 1992, p.230.

[16] S. Oh, K. Chang, IEEE Circuits and Devices, 11 (1995) 16.

[17] B. Geuskens, K. Rose, paper presented at Microelectronic Manufacturing Conference '95, Austin, TX, 25-26 October 1995.

[18] M.T. Bohr, IEEE IEDM, 1995, Tech. Digest., IEEE, Piscataway, NJ, 1995. p.241.

[19] K. Rahmat, O.S. Nakagawa, S-Y. Oh, J. Moll, W.T. Lynch, IEEE IEDM, 1995, Tech. Digest., IEEE, Piscataway, NJ, 1995. p.245.

[20] M.E. Thomas, J.A. Sadat, S. Sekigahama, IEEE IEDM 1990, Techn. Digest. IEEE, Paisipanny, NJ, 1990, p.351.

[21] Von Hippl (Eds), Dielectric Materials & Applications, Artech House, Boston, 1995. p.5.

[22] C. Kittel, Introduction to Solid State Physics, McGraw-Hill, New York, 1976. p.399.

[23] R. A. Levi, Principle of Solid State Physics, Academic Press, New York, 1972. p.149.

[24] C. S. Yang, K. S. Oh and C. K. Choi, J. Korean Phys. Soc. Vol 44, No 5, May 2004, p. 1102.

[25] J. Y. Kim, M. S. Hwang, Y. H. Kim, H. J. Kim and Y. Lee, J. Appl.

Phys., 90, 2469 (2001).

[26] T. Homma, Materials Science and Engineering, R. 23, p.243 (1998).

[27] S. P. Murarka, Materials Science and Engineering, R 19, p.87 (1997).

[28] S. P. Murarka, Solid State Technol, 39, 83 (1996).

[29] M. J. Loboda and G. A. Toskey, Solid State Technol., p. 99, May (1998).

[30] E. Sabin and G. Albrecht, Electrochem. Soc. Proc., 97098, 136 (1997).

[31] M. J. Laboda, C. M. Grove, and R. F. Schmeider, J. Electrochem. Soc., 145, 2861 (1998).

[32] T. C. Chang, P. T. Liu, Y. J. Mei, Y. S. Mor, T. H. Perng, Y. L. Yang. and S. M. Sze, J. Vac. Sci. Techn., B17(5), 2325 (1999).

[33] W. C. Chen. and C. T. Yen., J. Vac. Sci. Techn., B18(1), 201 (2000).

[34] N. P. Hacker, MRS Bull. 22,33 (1993).

[35] R. J. Gutmann, W. N. Gill, T. M. Lu, J. F. McDonal, S. P. Murarka, and E. J. Rymaszeewski, Advanced Metallization Conference in 1996 (Materials Research Society, Pittsburgh, PA, 1997).

[36] E. T. Ryan, A. J. Mckerrow, J. Leu, and P. S. Ho, MRS bull. 22, 49 (1997).

[37] W. F. Goham, J. Polymer. Sci., Part A-1, 4, 3027(1966).

[38] S. Chow, W. Loeb, and C. J. Whit, J. Appl. Poly. Sci., 13, 2325(1969).

[39] S. S. Han, H. R. Kim, and B. S. Bae, J. Electrochemical. Soc., 146(9), 3383 (1999).

[40] E. Kondoh, T. Asano, H Arao, A Nakashima, and M. Komatsu, Jpn. J.

Appl. Phys., 39. 3919 (2000).

[41] K. Maex, M. R. Balkanov, D. Shamiryan, F. lacopi, S. H. Brongersma. and Z. S. Yanovitskay, J. Appl. Phys., 93, 8793 (2003).

[42] C. Y. Wang, Z. X. Shen, and J. Z. Zheng, Appl. Spectroscopy, 54(2), 209 (2000).

[43] C. S. Yang, K. S. Oh, J. Y. Ryu, D. C. Kim, J. S. Yong, C. K. Choi, H. J. Lee, S. H. Um. and H. Y. Chang, Thin Solid Films, 390, 113 (2001).

[44] X. Jun, C. S. Yang, H.R. Jang. and C.K.Choi, J. Electrochem. Soc., 150, F206 (2003).

[45] C. S. Yang, Y. H. Yu, K. M. Lee, H. J. Lee and C. K. Choi, Thin Solid Films, 435, 166 (2003).

[46] S. Y. Jing, C. K. Choi and H. J. Lee, J. Korea Phys. Soc., 39, S302 (2001).

[47] M. Kannan, C. S. Yang. and C. K. Choi, J. Korean. Phy. Soc., 45. 944 (2004).

[48] M. L. Wallach, J.Polym. Sci., part A:Polym. Chem., 26, 953 (1968).

[49] D. R. Cho, Polymer Sci. and Tech. (Korea), 6, 499 (1995).

[50] A. B. Weber, R. Pockelmann, and C. P. Klages, J. Vac. Sci. Tech., A16, 2120(1998).

[51] T. C. Chang, Y. S. Mor, S. M. Sze, Y. L. Yang, M. S. Feng, F. M. Pan, B. T. Dai and C. Y. Chang, J. Electrochem. Soc. 146 3802 (1999).

[52] P. N. Sen and M. F. Thrope, Phys. Rev. B15, 4030 (1997).

[53] M. Fryd, in "Polyimides", ed. by K. L. Mittal, p.377, Plenum, New York, (1984).

[54] B. C. Aumann, Proceedings of DUMIC, 295 (1995).

[55] R. M. Geffken, IEDM Technol Digest, 542 (1983).

[56] Y. K. Lee and M. fryd, " The Chemistry of the Semiconductor Industry", eds. by S. J, Moss and A. Ledwith, p.282. Chapman and Holl, New York, (1987).

[57] R. Sezi, G. Shmid, W. Radilk, D. Krabe and K. Buschick, 11th International Conference on Photo-Polymers, p.49. McAffee, NJ, (1997).

[58] M. Bruna, J. W. Fitch and P. E. Cassidy, J. Macromol. Sci. Rev. Macromol. Chem. Phys., C. 36, 137 (1990).

[59] J. G. Hilborn, J. W. Labadie and J. L. Hedrick, Macromlecules, 23, 2854 (1990).

[60] T^. Strunskus and M. Granze, "Polyimed", eds. by M. K. Ghosh and K. L. Mittal, p. 187, Marcel Dekker, (1996).

[61] G. Lucovsky, Philos. Mag. B39, 513 (1979).

[62] J. Xu, C. S. Yang, and C. K. Choi, J. Korean. Phys. Soc., 45, 1, 175 (2004).

[63] W. L. Wu and H. C. Liou, Thin Solid Films. 312, 73 (1998).

[64] J. H. Zhao, I. Malik, E. T. Ryan, E. T. Ogawa, P. S. Ho, W. Y. Shin, A. J. Mekerrow, and K. J. Taylor, Appl. Phys. Lett. 74, 944 (1999) .

[65] S. J. Martin, J. P. Godsehalx, M. E. Mills, E. O. Shaffer II, and P. H.

Townsend, Adv. Mater. 12, 1769 (2000).

[66] J. Im et al, ASME J. Electron. Packag. 122, 28 (2000).

[67] D. W. Gidley, W. E. Frieze, T. L. Dull, J. N. Sun, and A. F. Yee, Mater. Res. Soc. Symp. Proc. 612, D4.3.1 (2000).

[68] K. Oh, C. K. Choi, J. Korean. Phys. Soc., 45, S855 (2004).

[69] C. S. Yang, Y. H. Yu, H. J. Lee, K. M. Lee, C. K. Choi, Thin Solid Films, 475, 150 (2004).

국문초록

최근 반도체 소자가 고집적화 됨에 따라 초고속, 초저전력 그리고 높은 신뢰성에 요구됨으로서 Cu/Low-k 소자개발이 대두되고 있다. 이와같은 Cu/Low-k 소자 의 단위공정 기술 중 다층 금속배선과 층간 절연막 형성이 중요한 핵심기술이다. 현재 사용되어지고 있는 SiLK, SiO_2 박막은 평탄화 특성은 우수하지만 단차 피복성에 열악한 문제점과 불순물 잔류와 높은 유전상수로 인하여 0.1 ㎛급 이상 소자에서 배선간에 기생 정전용량이 생겨 배선물질의 저항과 층간 절연막의 정전용량으로 표현되는 RC 시정수가 증가하여 신호의 상호간섭과 잡음 등으로 소자의 고속화에 장애요인이 된다. 또한 배선폭의 미세화와 더불어 배선 간격을 완전하게 매설하는 것이 어렵게 된다. 이러한 문제점을 극복하기 위해서 현재 배선 금속으로 사용되고 있는 Al 보다 전도도가 높은 Cu를 배선으로 사용하는 공정이 개발되고 있으며 이때 사용될 수 있는 2.0 이하의 저유전상수를 갖는 층간절연 박막에 대한 연구 개발이 필수적이다. 다층 배선공정의 미세화의 가속으로 향후 개발될 65 nm급 Cu/Low-k 소자의 층간절연막은 유전상수가 2.0 정도로 요구되고 있다. 이와 같이 65nm 급 소자에서 기존의 저유전 박막중 SiLK와 SiOC(-H) 박막을 층간절연막으로 사용할 경우 소자의 동작속도를 저하시키는 문제가 발생한다. 향후 개발될 65 nm 급 Cu/Low-k 소자에서는 나노-기공을 함유하는 저유전 박막을 층간 절연막으로 적용하려고 많은 연구자들이 연구개발 중에 있다.

본 논문에서는 차세대 65 nm 급 Cu/Low-k 소자의 층간 절연막으로 적용될 저유전 물질중 SiOC(-H) 박막에 대한 유전재료, 결합구조, 전기

적, 기계적 특성에 대하여 연구하였다. 또한, 현재 사용되어지고 있는 PECVD 법으로 증착한 low-k 박막의 표면중 일부는 플라즈마 내부에서 높은 에너지를 갖는 이온(ion)들 때문에 손상을 입을수 있다. 이러한 높은 에너지의 이온들은 박막형성 과정중에 탈착(desorption)과정의 중요한 요인으로 지적되어져 왔다. 이러한 이유로 낮은 인가전압에서 낮은 전자온도(electron temperature)를 갖는 Photo-assisted PECVD법이 대안으로 제시된다. Photo-assisted PECVD법은 박막 형성시 열에너지뿐만 아니라 광에너지에 의한 광화학 반응을 이용하므로 박막형성 온도를 큰 폭으로 저하시킬수 있으며, 또 광에너지 자체가 반응가스를 분해시킬수 있으나 이온을 발생시킬 만큼 크지 않으므로 이온이 존재하지 않는 공정으로서 양질의 low-k 박막을 형성시킬수 있기 때문에 주목받고 있다. 이러한 Photo-assisted PECVD 방법에 의해 증착된 SiOC(-H) 박막의 물성에 대해서도 연구하였다.

SiOC(-H) 박막은 precursor의 유량이 증가 할수록, 박막내부에 C 원자의 농도가 증가한다. 이러한 C 원자의 농도의 증가는 O-Si-O network link와 결합하면서 O-Si-C ring link와 O-Si-C open link 구조를 만든다. O-Si-O network link가 Si-CH_n bond로 변화하는 것은 ionic에 의한 유전상수를 낮추게 하는 역할을 한다. 그리고, 많은 C 원자의 농도는 electronic과 ionic에 의한 유전상의 기여도를 낮추게 한다. 또한 C 원자의 농도가 증가할수록 Si-O bond와 Si-C bond 사이의 결합각이 커진다. 즉, O-Si-C bonding angle의 변화는 -CH_n group이 O-Si-O network link와 결합되면서 변화하는 것을 의미한다. O-Si-C 사이의 결합각이 커지면 dipole moment는 작아진다. 또한 C 원자의 농도가 증가하면 SiOC(-H) 박막의 밀

도는 감소한다. 박막의 밀도가 감소하면 유전상수는 낮아진다. 또한 증착한 SiOC(-H) 박막의 구조는 비정질이므로 orientation에 의한 유전상수의 기여는 무시할만하다. 이상의 반응기작에 의해 SiOC(-H) 박막은 기존의 SiO_2 보다 낮은 유전상수를 갖게 되며, 그 외의 물리·화학적 특징은 구조적으로 SiO_2와 유사하므로 비슷한 특징을 나타낸다.

CH_4 플라즈마로 표면 처리한 시료에 대한 O_2 ashing 공정을 수행한 결과 누수 전류 밀도의 변화는 CH_4 플라즈마로 표면 처리 하지 않은 경우와 유사하게 나타난다. 그러나 누수 전류 밀도의 변화 폭은 아주 작은데, 1 MV/cm 의 전기장에서 2.6×10^{-9} A/cm_2에서 2.02×10^{-8} A/cm^2으로 변화하였다. 특히, 누수 전류 밀도의 값의 차수(order)는 최대 ~ 10^{-6} A/cm^2 으로 측정되었다. 이러한 결과는 CH_4 플라즈마로 표면 처리를 하면 플라즈마 내부의 C과 H 성분에 의해서 SiOC(-H) 박막의 표면상태가 소수성에 가까워져 O_2 ashing 공정중에서 발생 할 수 있는 누수 전류 밀도의 변화폭을 크게 감소시키는 것이다. 이러한 결과로서 CH_4 플라즈마로 SiOC(-H) 박막의 표면을 처리하는 경우에 소수성의 증가로 인하여 O_2 ashing 공정에서 발생할 수 있는 친수성, 누수 전류 밀도의 증가등의 문제를 방지할 수 있다.

UV-assisted PECVD 방법은 UV를 조하하지 않은 경우의 전자온도와 비교하면 10 ~ 20 % 낮게 측정되었다. 일반적으로 비활성 기체를 반응 기체와 같이 혼합하여 방전 시킬 경우 비활성 기체 내부의 전자들이 자유전자가 되고, 그러한 자유전자들은 반응기체의 이온화를 촉진시킨다. PECVD 방법에 의해 박막을 증착하는 공정시 박막형성에 관여하는 입자들은 활성종과 이온들이다. 그러나 박막 형성시 전자온도가 높아지면 이

온들의 에너지가 높아지므로 이로 인한 기판의 손상을 가져올수 있다. 그러므로, 증착하고자 하는 박막이 이온들에 의한 손상(혹은 탈착)을 방지하려면 낮은 전자 온도에서 증착하는 것이 필요하다. 이러한 변화는 UV를 조사하지 않은 경우와 비교 하였을때 그 변화폭이 그다지 크지는 않다. 그러나 He 가스를 혼합한 경우에는 전자밀도가 그렇지 않은 경우에 비해서 다소 증가한다. He 가스는 이온화 단면적에 비해서 비교적 큰 비탄성 충돌 단면적을 가지고 있기 때문에 혼합한 precursor와의 충돌에 의해서 들뜬 전자(energetic electron)을 보다 많이 생성시키고 이러한 전자들은 또다시 precursor들과의 충돌에 의해 전자들을 생성하게 된다. 이러한 반등이 계속적으로 일어나게 됨으로서 전자밀도는 He 가스를 혼합하지 않은 경우에 비해서 다소 증가하게 된다.

본 연구에 결과를 종합해보면, SiOC(-H) 박막은 ULSI 소자의 층간절연막으로 사용할수 있는 매우 우수한 유전물질임을 알수 있었다.

CURRICULUM VITAE

◎ Personal Information

• Name : Yang Chang Sil

• Date of Birth : July 14, 1972

• Place of Birth : Cheju, Republic of Korea

• E-mail Address : nrl2001@naver.com

◎ Education

• B. S. in Physics (1993-1999) Cheju National University Jeju, Korea

• M. S. in Physics (1999-2001) Cheju National University Jeju, Korea

"*A study formation and Characteristics of FAC Thin Film by ICP-CVD*"

Supervisor : Prof. Chi Kyu Choi

• Ph. D. in Physics (2002-2006) Cheju National University Jeju, Korea

"*Investigations of Low Dielectric Constant SiOC(-H) Thin Films for Inter-layerDielectrics in Cu/Low-k Microelectronic Device Applications*"

Supervisor : Prof. Chi Kyu Choi

◎ Experiences

• 2001. 7 - Present : **Research Assistant**, Department of Physics, Cheju National University, Supervisor : Prof. Chi Kyu Choi

I am versed in National Research Laboratory(NRL) program from Ministry of Science and Technology. I performed all steps of the experiment from fabrication to measurement and data analysis about low dielectric materials such as carbon doped silicon oxide film.

• 2004. 6 - 2004. 12. : **Research Assistant**, Samsung Advanced Institute of Technology, Supervisor : Ph.D Hyun Dam Chung

I helped to deposit and analyze the precursor from Samsung Advanced Institute of Technology.

• 1999. 7 - 2001. 8. : **Research Assistant**, Department of Physics, Cheju National University, Supervisor : Prof. Chi Kyu Choi

I helped to deposit and analyze from Korea Science and Engineering Foundation. I performed all steps of the experiment from fabrication to measurement and data analysis about low dielectric fluorinated amorphous carbon thin film.

• 2004. 3 - 2004. 6. : **Teaching Assistant**, the premedical course, Cheju National University Teaching assistant for Experiment Physics.

◎ Publication Lists

1. **Chang Sil Yang**, Young Hun Yu, Heon-Ju Lee, Kwang-Man Lee, Chi Kyu Choi, " *The effect of the CH_4 plasma treatment on deposited SiOC(-H)*

films with low dielectric constant prepared by using TMS/O_2 PECVD ", Thin Solid Films, Vol. 475, 150-154(March 2005), Elsevier.

2. **Chang Sil Yang**, Chang Young Kim, Young Hun Yu, Kwang-Man Lee and Chi Kyu Choi, " *Investigation of Low Dielectric Carbon Doped Silicon Oxide Films Prepared by PECVD using Methyltrimethoxysilane Precursor* ", Thin Solid Films, In Press, Elsevier.
3. **Chang Sil Yang** and Chi Kyu Choi, " *The Characteristics of Carbon Doped Silicon Oxide Films with Nano-pore Structure Deposited by UV-source Assisted PECVD*", Thin Solid Films, In Press, Elsevier.
4. **Chang Sil Yang**, Meera Kannan and Chi Kyu Choi, " *Studies on the Low Dielectric SiOC(-H) Thin Films Deposited Using MTMS and Oxygen as Precursors by UV Source Assisted PECVD* ", Surface & Coating Technology, Vol 200, 1624-1628(2005), Elsevier.
5. **Chang Sil Yang**, and Chi Kyu Choi, " *Mechanical Property of the Low Dielectric Carbon Doped Silicon Oxide Thin Film grown from MTMS/O_2 Source* ", Current Applied Physics, In Press, Korean Physical Society.
6. **Chang Sil Yang**, Heon Ju Lee and Chi Kyu Choi, " *Formation and Characteristics of the Low Dielectric Carbon Doped Silicon Oxide Thin Film deposited by MTMS/O_2 ICPCVD*" Solid State Phenomena, Vol 107, 103-106 (October 2005), Trans Tech Publication.
7. Jun Xu, **Chang Shil Yang** Chi Kyu Choi, " *Annealing on the Structural and Electrical Properties of SiOC(-H) Films with Low Dielectric Constant prepared by Plasma-Enhanced Chemical Vapor Deposition* ", J. of the

Korean Physical Society. Vol. 45, No. 1, 175-179 (July, 2004), Korean Physical Society.

8. **Chang Sil Yang** and Chi Kyu Choi, *" Effect of Thermal Treatment on SiOC(-H) Films with Low Dielectric Constant*", J. of the Korean Physical Society, Vol. 45, S642-S646(2004, December), Korean Physical Society.
9. Meera Kannan, **Chang Sil Yang** and Chi Kyu Choi, *" Study on the Bonding Structures of Nano-Pore SiOC(-H) Films Deposited by UV-Source Assisted PECVD*", J. of the Korean Physical Society, Vol.45, S944-S948(2004, December), Korean Physical Society.
10. **Chang Sil Yang**, Kyung Suk Oh, Chi Kyu Choi, " *A Study on the Dielectric Components of SiOC(-H) composite Films Deposited by Using BTMSM/O_2-ICPCVD* ", J. of the Korean Physical Society. Vol. 44, No.5 1102-1107 (May, 2004), Korean Physical Society.
11. Young Hun Yu, Sang Chill Lee, **Chang Sil Yang**, Chi Kyu Choi, "*Mobility, Energy Gap and Dielectric Constant in SiOC films* ", J. of the Korean Physical Society. Vol. 42, No. 5 682-685 (May 2003) Korean Physical Society.
12. **Chang Sil Yang**, Young Hun Yu, Kwang Man Lee, Heon Ju Lee, Chi Kyu Choi, *" The influence of carbon content in carbon-doped silicon oxide film by thermal treatment* ", Thin Solid Films, Vol. 435/1-2,165-169(May 2003), Elsevier.

13. Heon-Ju Lee, **Chang Sil Yang**, Chi Kyu Choi, " *Effect of UV illumination on deposition of low-k SiOC(-H) films by PECVD* ", Materials Science Forum. Vol . 449-452, (June 2003), Trans Tech Publication.

14. Xu Jun, **Chang Sil Yang**, Hae Rim and Chi Kyu Choi, " *ChemicalStructure Evolution of SiOC(-H) Films with Low Dielectric Constant during PECVD and Post annealing* ", J. of The Electrochemical Society, Vol. 150(12), F206-F210 (December, 2003), The Electrochemical Society.

15. **Chang Sil Yang**, Kyoung Suk Oh, Jai Yon Ryu, Doo Chul Kim, Jing Shou-Yong, Chi Kyu Choi, Heon-Ju Lee, Se Hun Um, Hong Yong Chang, *" A study on the formation and characteristics of the Si-O-C-H composite thin films with low dielectric constant for advanced semiconductor devices* ", Thin Solid Films, Vol. 390, 113-118(July, 2001, Elsevier).

16. Min Sung Kang, **Chang Sil Yang**, Won Bong Jung, and Chi Kyu Choi, " *A study on the plasma parameters and characteristics of carbon doped silicon oxide film using MTMS/O_2 and He plasma*", Thin Solid Films, Submitted, Elsevier.

17. Min Sung Kang, Won Bong Jung, **Chang Sil Yang**, and Chi Kyu Choi, " *Novel method for low dielectric thin film using UV-assisted plasma CVD* ", J. of the Korean Physical Society, Submitted, Korean Physical Society.

18. K. Meera, **C.S. Yang**, and C. K. Choi, " *Bonding Structure and Electrical Properties of SiOC(-H) Films Deposited with MTMS Precursor*

by TCPCVD", J. of the Korean Physical Society, Submitted, Korean Physical Society.

19. **Chang Sil Yang** and Chi Kyu Choi, " *Low Dielectric Constant Materials for Cu Integration* " (**Review Article**), Sae Mulli, Vol 51, No 1, 1-22(July, 2005), Korean Physical Society.
20. Hyeon-Jin Shin, Hyun-Dam Jeong, Jong-Beak Seon, Jong-Min Kim, **Chang Sil Yang,** Chang Young Kim and Chi Kyu Choi, " *High-Performance, Low Dielectric Constant Thin Film from a Dual Organo Siloxane Precursor* ", SAMSUNG Journalof Innovative Technology, Vol 1, No 1, 231-238(Aug, 2005), SAMSUNG Advanced Institute of Technology.

◎ Awards

1. **Best Poster Award** - *12th Seoul International Symposium on the Physics of Semiconductors and Applications*.

2. **Award for Outstanding Young Researcher** - *4th International Symposiums on Pulse Power and Plasma Applications*.

◎ Technical Transfer to Industry

1. " *Technology of surface treatment using CH_4 plasma on the low dielectric SiOC(-H) thin film* ", JUSUNG ENGINEERING Co., Ltd, 2005.5.30

2. " *Formation technology of low dielectric thin film using UV-assisted PECVD* ", JUSUNG ENGINEERING Co., Ltd, 2005.5.30

3. " *Formation and Characteristics of low dielectric SiOC(-H) film with nano-pore structure using MTMS precursor* ", JUSUNG ENGNEERING Co., Ltd, 2005.5.30

4. " *Manufacturing equipment for semiconductor using low energy plasma* ", NexSo Co,. Ltd, 2002. 2. 1

◎ Conference Activities

• International Presentation

1. **C. S. Yang**, Y. H. Yu, H. J. Lee, K. M. Lee and C. K. Choi, " *The effect of the Plasma Treatment on SiOC(-H) Films with Low Dielectric Constant*", The 12th Seoul International Symposium on the Physics of Semiconductors and Applications- 2004.
2. K. Meera, K. S. Oh, **C. S. Yang**, H. J. Ko and C. K. Choi, " *Study of the Bonding Structure due to Post Annealing of Nano-pore SiOC(-H) Films Deposited by UV-Source Assisted PECVD* ", The 12th Seoul International Symposium on the Physics of Semiconductors and Applications- 2004.

3. **C. S. Yang**, Y. H. Yu, K. M. Lee and C. K. Choi, " *The structural and dielectric properties of hybrid-type SiOC(-H) films with low dielectric constant deposited by MTMS/O_2-ICPCVD*" 7th APCPST, 2004.
4. K. Meera, **C. S. Yang** and C. K. Choi, " *Bonding structure of SiOC(-H) Thin Films Deposited Using MTMS and Oxygen as Precursors by Plasma Enhanced Chemical Vapor Deposition* ", 3rd International Symposium on Practical Sur4face Analysis, and 5th Korea-Japan International Symposium on Surface Analysis, 2004.
5. **Chang Sil Yang** and Chi Kyu Choi, " *Characterization of Methly-doped Silicon Oxide Films deposited using MTMS by Chemical Vapor Deposition* ", ISPP-2004 Proceedings of the 5th International Symposium on Pulsed Power and Plasma Applications, 2004.
6. Kyoung Suk Oh, **Chang Sil Yang**, Heon Ju Lee and Chi Kyu Choi, " *The mechanical properties of the SiOC(-H) composite thin films as annealing process* ", ISPP-2004 Proceedings of the 5th International Symposium on Pulsed Power and Plasma Applications, 2004.
7. K.Meera, **C.S. Yang** and Chi Kyu Choi, " *Bonding Structure of SiOC(-H) Thin Films Deposited using MTMS and Oxygen as Precursors by Plasma Enhanced Chemical Vapor Deposition* ", 3rd International Symposium on Practical Surface Analysis and 5th Korea-Japan International Symposium on Surface Analysis, 2004.
8. K. Meera, **C. S. Yang** and C. K. Choi, " *Study on the Properties of Hybrid type SiOC(-H) Films with Nano-pore Structure Deposited by*

UV-source assisted PECVD", The Second International Workshop on Particle Beams & Plasma Interaction on Material and The Second Asia Symposium on Ion & Plasma Surface Finishing, 2004.

9. **Chang Sil Yang**, Young Hun Yu, Chi Kyu Choi, " *The Characteristics of Dielectric Properties of SiOC Film with the Variation of Bonding Angle on the Si-O-C Structure* ", The 30th International Conference on Plasma Science, 2003.
10. **Chang Sil Yang**, Heon Ju Lee, Kwang Man Lee and Chi Kyu Choi, " *The Characteristics of Dielectric Properties of SiOC(-H) film with the Variation of Dielectric Components on Si-O-C Structure* ", 2003 Korea-Japan Workshop on Advanced Semiconductor Processes and Equipments, 2003.
11. Chi Kyu Choi, Young Hun Yu, **Chang Sil Yang**, Kwang Man Lee and Heon Ju Lee, " *Low-k Films with Nano-pore Structure Deposited with various Precursors in a Plasma Enhanced Chemical Vapor* ", The 4th Asian-European International Conference on Plasma Surface Engineering, 2003.
12. **Chang Sil Yang**, Young Hun Yu, Kwang Man Lee, Heon Ju Lee and Chi Kyu Choi, " *Effects of He-Plasma Treatment on SiOC(-H) Films with Low Dielectric Constant Prepared by Using VTMS/O_2-PECVD*", The 4th Asian-European International Conference on Plasma Surface Engineering, 2003.

13. Young Hun Yu, **Chang Sil Yang** and Chi Kyu Choi, " *Effects of He-Plasma Treatment on SiOC(-H) Films with Low Dielectric Constant Prepared by Using TMS/O_2-PECVD* ", The 4th Asian-European International Conference on Plasma Surface Engineering, 2003.
14. **Chang Sil Yang** and Chi Kyu Choi, " *The Characteristics of Dielectric Properties of SiOC Film with Gas Flow Rate Ratio and Thermal Treatment on the Si-O-C Structure* ", 11th Asia-Pacific Conference on Non-Destructive Testing, 2003.
15. **Chang Sil Yang**, Young Hun Yu, Heon Ju Lee, Kwang Man Lee and Chi Kyu Choi, " *The Effect of the Post Plasma treatment on deposited SiOC(-H) Films with Low Dielectric Constant Prepared by Using BTMSM/O_2 PECVD*", The 3rd International Conference on Advanced materials and Devices, 2003.
16. Kyung Suk Oh, **Chang Sil Yang**, Chi Kyu Choi, " *A Study on the Formation and Characteristics of the Si-O-C Films with Nano-pore Structure by High Density Plasma Chemical Vapor Deposition* ", 12th Gaseous Electronics Meeting, 2002.
17. **Chang Sil Yang**, Kyoung Suk Oh and Chi Kyu Choi, " *The chemical bond structure investigation on the Si-O-C composite films with low dielectric constant deposited by high density plasma chemical vapor deposition*", 2002 IEEE international Conference on Plasma Science, 2002.
18. **Chang Sil Yang**, Kwang-ManLee, Heon-Ju Lee and Chi Kyu Choi, " *A study on the Influence of Carbon Contents in Carbon Doped Silicon Oxide*

Films after Thermal and Plasma Treatment ", Joint International Plasma Symposium of 6th APCPST, 15thSPSM, OS2002 & 11th KAPRA, 2002.

19. **Chang Sil Yang**, Kwang-Man Lee Heon-Ju Lee and Chi Kyu Choi, " *A study on the Influence of Carbon Contents in Si-O-C composite Films with nano-pore structure* ", The 11th Seoul International Symposium on the Physics of Semiconductors and Applications, 2002.
20. Ho Jeong Ko, **Chang Sil Yang**, Heon Ju Lee, Kwang man Lee, Young Hun Yu, Chi Kyu Choi, " *A study of structural characteristic of Low Dielectric Constant Thin Film by Inductively Coupled Plasma CVD Method* ", The 3rd International Mesostructured Materials Symposium, 2002.
21. **Chang Sil Yang**, Young Hun Yu, Kwang Man Lee, Heon Hu Lee, Chi Kyu Choi, " *The influence of carbon contents in carbon doped silicon oxide film by thermal treatment* ", The 3rd Japan-Korea Joint Workshop on Advanced Semiconductor, Processes and Equipment, 2002.
22. Kyung Suk Oh, **Chang Sil Yang**, Gun Sam Kang, Chi Kyu Choi, "*Low-k Organic-Inorganic materials Composite Films deposited by Inductively Coupled Plasma Chemical Vapor Deposition* ", The 1st international Symposium on Advanced Plasma Surface technology, 2001.
23. Kyung Suk Oh, **Chang Sil Yang**, Heon Ju Lee, Chi Kyu Choi, "*Low Dielectric constant films as an IMD by CF_4/CH_4-ICPCVD* ", The 2nd International Symposium on Pulsed Power and Plasma Applications, 2001.

24. S. Y. Jing, K. S. Oh, **C. S. Yang**, C. K. Choi, " *A Study on the Formation of the Low Dielectric constant Materials by High Density Plasma CVD method* ", The 3rd International Symposium on the Advanced Functional Materials in the North-East Region, 2000.

25. Jai, Yon Ryu, Doo Chul Kim, Kyoung Suk Oh, Min Sung Kang, **Chang Shil Yang**, Shou Yong Jing, Chi Kyu Choi, Se Hun Um, Hong Young Chang, " *Study on the Formation and Characteristics of the Black-diamond Thin Film with low dielectric constant by BTMSM/O_2-ICPCVD* ", The 5th Asia-Pacific Conference on Plasma Science & Technology, 2000.

26. Kyoung Suk Oh, Min Sung Kang, **Chang Shil Yang**, Shou Yong Jing,Heon Ju Lee, Chi Kyu Choi, Se Hun Um, Hong Young Chang, " *A Study on the Formation and Characteristics of the Fluorinated amorphous Carbon Film deposited by CF_4/CH_4-ICPCVD*", 5th Asia-Pacific Conference on Plasma Science & Technology, 2000.

27. Shou Yong Jing, Kyoung Suk Oh, **Chang Shil Yang**, Chi Kyu Choi, " *A Study on the Formation and Characteristics of the Organic-inorganic material with low-k dielectric constant deposited by High Density Plasma Chemical Vapor* ", The 10th Seoul International Symposium on the Physics of Semiconductors and Applications, 2000.

28. Kyoung Suk Oh, **Chang Shil Yang**, Shou Yong Jing, Min Sung Kang,Heon Ju Lee, Chi Kyu Choi, Se Hun Um, Hong Young Chang, " *Thermal Stability of Fluorinated amorphous carbon Films with a*

Low-Dielectric Constant deposited by CF_4/CH_4-ICPCVD ", The 10th Seoul International Symposium on the Physics of Semiconductors and Applications, 2000.

29. Kyoung Suk Oh, **Chang Shil Yang**, Chi Kyu Choi, " A Study on the Formation and Characteristics of Low Dielectric Materials for Advanced Semiconductor Devices" , The Sino-Korean International Symposium on Thin film Materials, 2000.
30. K. S. Oh, **C. S. Yang**, C. K. Choi, " A Study on the Formation of theLow Dielectric Materials by High Density Plasma Chemical Vapor Deposition ", The meeting of the Int'l. Conf. on Advanced Materials and Devices'99, 1999.

• **Domestic Presentation**

1. 김창영, **양창실**, 김승현, 이광만, 최치규, " *TCPCVD 방법에 의한 SiOC(-H) 박막의 형성과 특성에 관한 연구* ", 제 28회 한국진공회 학술발표회, 2005.
2. Kannan Meera, **Yang Chang Shil**, Choi Chi Kyu, " *Deposition of SiOC(-H) Films of Low Dielectric Constant using MTMS/O_2 by ICP-CVD and Its Characterization*", Bulletin of The Korean Physical Society, 2004.
3. **Yang Chang Shil**, Choi Chi Kyu, " *Low Dielectric Carbon Doped Silicon Oxide Thin Film Deposited by MTMS/O_2 and He Plasma*", Bulletin of The Korean Physical Society, 2004.

4. 김태언, Xu Jun, 오경숙, 고호정, **양창실**, 강권삼, 최치규, " *ICPCVD 방법으로 형성한 저유전 SiOC(H) 박막의 특성에 관한 분석* ", 2003년도 한국물리학회 학술논문발표회, 2003.
5. **양창실**, Xu Jun, 오경숙, 고호정, 고성범, 강권삼, 김태언, 최치규, " *A study on the influence of carbon doped silicon oxide films by thermal treatment* ", 2003년도 한국물리학회 학술논문발표회, 2003.
6. 최치규, 고호정, **양창실**, 강권삼, 김태언, " *Electrical and Optical Properties of Dielectric thin film by Plasma Enhanced Chemical Vapor Deposition* ", 2003년도 한국물리학회 학술논문발표회, 2003.
7. 오경숙, **양창실**, 유영훈, 이헌주, 이광만, 최치규, " *A Study on the Formation and Characteristics of the Si-O-C Films with Nano-pore Structure by ICPCVD* ", 2002년도 한국물리학회 학술논문발표회, 2002.
8. **양창실**, 오경숙, 최치규, " *HDP-CVD 방법으로 증착한 Si-O-C(-H) 박막의 구조분석* ", 제 22회 학술발표회, 한국진공학회, 2002.
9. **양창실**, 강권삼, 최치규, 이광만, *" HDPCVD 방법에 의한FAC 박막의 형성과 특성에 관한 연구* ", 제 16회 한국통신학회, 한국전자공학회 학술발표대회, 1999.
10. 오대현, 강민성, 오경숙, **양창실**, 양두훈, 이광만, 변종철, 최치규, 김건호, " *ICP-CVD 방법에 의한 TiN Diffusion Barrier Thin Film 형성* ", 제 17회 한국진공학회 학술발표회, 1999.

감사의 글

6년 동안의 대학원 생활을 지내고 보니 참으로 많은 것을 배우고 느낀 소중한 시간이었습니다. 먼저, 대학원 생활과 학위논문을 무사히 마치도록 지도와 격려를 해주신 최치규 교수님께 감사드립니다. 교수님께서는 특유의 성실함으로 대학원 생활 내내 저를 이끌어 주셨습니다. 또한, 학위논문 심사위원이신 현남규 교수님, 유영훈 교수님, 한국과학기술원의 장홍영 교수님, 그리고 서울대학교의 김형준 교수님께 감사드립니다. 저에게 충고와 격려를 하여 주신 모든 교수님들께 진심으로 감사드립니다.

제가 졸업하기까지는 주위의 많은 분들의 도움이 있었으며 그 분들께 이글을 통하여 감사드립니다. 어렵고 힘들 때 힘이 되어준 실험실 선·후배 여러분들, 물리학과의 대학원생들, 그리고 저의 졸업을 누구보다도 기뻐하실 부모님과 장인·장모님과 누님, 매형, 그리고 동생에게 이 기쁨과 보람을 전하고 싶습니다. 매일 늦게 들어가고 짜증낼 때 묵묵히 곁에 있어준 사랑하는 제 아내와 그리고 예원이가 곁에 있어 너무 힘이 되었습니다. 고맙습니다. 저를 아는 모든 분들께 다시한번 감사의 말씀을 드립니다.

본 학위논문을 완성할 수 있게 지원해주신 일운장학재단의 황철주 회장님과 재단 이사진들께도 감사의 말씀을 드립니다.